การสังเคราะห์ในเฟสของเหลวของไนโอเบียมออกไซด์และซิงค์ออกไซด์

ที่มีการควบคุมสัณฐานวิทยา

นางสาวศิรชยา กุญชร ณ อยุธยา

วิทยานิพนธ์นี้เป็นส่วนหนึ่งของการศึกษาตามหลักสูตรปริญญาวิศวกรรมศาสตรดุษฎีบัณฑิต

สาขาวิชาวิศวกรรมเคมี   ภาควิชาวิศวกรรมเคมี

คณะวิศวกรรมศาสตร์ จุฬาลงกรณ์มหาวิทยาลัย

ปีการศึกษา 2550

LIQUID PHASE SYNTHESES OF NIOBIUM OXIDE AND ZINC OXIDE
WITH CONTROLLED MORPHOLOGY

Miss Sirachaya Kunjara Na Ayudhya

A Dissertation Submitted in Partial Fulfillment of the Requirements

for the Degree of Doctor of Engineering Program in Chemical Engineering

Department of Chemical Engineering

Faculty of Engineering

Chulalongkorn University

Academic Year 2007

Thesis Title   LIQUID PHASE SYNTHESES OF NIOBIUM OXIDE AND
                 ZINC OXIDE WITH CONTROLLED MORPHOLOGY
By   Miss Sirachaya Kunjara Na Ayudhya
Field of Study   Chemical Engineering
Thesis Advisor   Professor Piyasan Praserthdam, Dr.Ing.
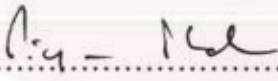Thesis Co-Advisor Professor Gabor A. Somorjai, Ph.D.

Accepted by the Faculty of Engineering, Chulalongkorn University in Partial Fulfillment of the Requirements for the Doctoral Degree

....Dean of the Faculty of Engineering

(Associate Professor Boonsom Lerdhirunwong, Dr.Ing.)

THESIS COMMITTEE

.... Chairman

(Associate Professor Chairit Satayaprasert, Dr.Ing)

.... Thesis Advisor

(Professor Piyasan Praserthdam, Dr.Ing.)

.... Thesis Co-Advisor

(Professor Gabor A. Somorjai, Ph.D.)

.... Member

(Assistant Professor Somchai Ratanathammaphan, D.Eng.)

.... Member

(Assistant Professor Okorn Mekasuwandamrong, D.Eng.)

.... Member

(Akawat Sirisuk, Ph.D.)

ศิรชยา กุญชร ณ อยุธยา: การสังเคราะห์ในเฟสของเหลวของไนโอเบียมออกไซด์และซิงค์ออกไซด์ที่มี
การควบคุมสัณฐานวิทยา (LIQUID PHASE SYNTHESES OF NIOBIUM OXIDE AND ZINC
OXIDE WITH CONTROLLED MORPHOLOGY)   อ. ที่ปรึกษา: ศ.ดร. ปิยะสาร ประเสริฐธรรม,
อ. ที่ปรึกษาร่วม: PROF. GABOR A. SOMORJAI, 163 หน้า.

การพัฒนาวิธีการสังเคราะห์สารในระดับนาโนเมตร โดยให้มีการควบคุมสัณฐานวิทยา (morphology)
จะช่วยส่งเสริมการสร้างวัสดุที่มีสมบัติที่น่าสนใจสำหรับการประยุกต์ใช้ในอนาคต งานวิจัยนี้มีเป้าหมายในการ
ควบคุมลักษณะของรูพรุนระดับเมโซพอร์ (mesopores) และการควบคุมรูปร่างของสารโลหะออกไซด์
ไนโอเบียมออกไซด์ (niobium oxide) ที่มีรูพรุนระดับเมโซพอร์และผลึกซิงค์ออกไซด์ (nanocrystalline zinc
oxide) ที่มีรูปร่างไม่สมมาตรแบบทิศเดี่ยว (anisotropic shape) จะเป็นตัวแทนในการศึกษาโดยวิธีสังเคราะห์แบบ
เปียก เมื่อใช้อุณหภูมิสูงในการทำให้สารแห้ง การใช้พอลิเมอร์ชนิดสามบล็อก (triblock copolymer) ที่มีส่วนของ
เอทิลีนออกไซด์ (ethylene oxide) ที่ยาวจะช่วยให้ได้โครงสร้างเมโซพอร์ของไนโอเบียมออกไซด์ที่มีระเบียบ ซึ่ง
เมื่อเผาพอลิเมอร์ออกแล้ว รูพรุนที่ได้ก็จะมีลักษณะเป็นระเบียบด้วย การบ่มสารระบบปิด (hydrothermal aging)
ที่อุณหภูมิ 110 องศาเซลเซียส ช่วยเพิ่มขนาดรูพรุนและพื้นที่ผิวของสาร รวมถึงเปลี่ยนแปลงโครงสร้างภายในตัว
ไนโอเบียมโดยคาดว่าจะมีสมบัติให้ความเป็นกรดลิวอิส (Lewis acidity) ที่มากขึ้น ผลดังกล่าวขึ้นอยู่กับปริมาณ
ของน้ำในระบบด้วย โดยหากปริมาณน้ำมากไปหรือไม่มีเลยจะทำให้ไม่พบผลของโครงสร้างที่มีสมบัติดังกล่าว
อีกทั้งพื้นที่ผิวและขนาดรูพรุนก็ต่ำลง การควบคุมขนาดรูพรุนแบบละเอียดในช่วง 3-7 นาโนเมตรสามารถทำโดย
วิธีไดอะไลซิส (dialysis) วิธีนี้จะให้สารออกไซด์ในสภาพตกตะกอน (precipitates) ซึ่งย่นระยะเวลาการทำให้แห้ง
ที่ยาวนานของวิธีปกติลง หลังจากเผาที่อุณหภูมิ 500 องศาเซลเซียส สารไนโอเบียมออกไซด์ที่มีรูพรุนจะมีพื้นที่
ผิวอยู่ในช่วง 120-170 ตารางเมตรต่อกรัม ภายใต้ภาวะที่ศึกษา กลยุทธ์สำหรับการปรับสมบัติเชิงพื้นผิว (textural
properties) ของสารรูพรุนนี้คือการปรับไมเซลล์ (micelles) ของพอลิเมอร์และปรับภาวะทางเคมีในโซลเจล (sol-
gel chemistry) ของสารไนโอเบียม ในการสังเคราะห์ผลึกซิงค์ออกไซด์ วิธีโซลโวเทอร์มอล (solvothermal) โดย
ปราศจากหมู่ไฮดรอกซิล (hydroxyl group) ให้ค่าสัดส่วนความยาวต่อเส้นผ่านศูนย์กลาง (aspect ratio) ของแท่ง
ผลึกที่มีค่ามากที่สุด รูปร่างผลึกมีความเกี่ยวเนื่องกับค่าคงที่ไดอิเล็กทริก (dielectric constant) ของสารละลาย
(solvent) และ การเกิดของนิวคลิไอ (nuclei) กับการโตของผลึก (crystal growth) มีผลกระทบมาจากสารที่ใช้
เริ่มต้น

ภาควิชา..... วิศวกรรมเคมี.............	ลายมือชื่อนิสิต................................	
สาขาวิชา.......วิศวกรรมเคมี..............	ลายมือชื่ออาจารย์ที่ปรึกษา.................	
ปีการศึกษา.... 2550..................	ลายมือชื่ออาจารย์ที่ปรึกษาร่วม..............	

##4771827121: MAJOR CHEMICAL ENGINEERING

KEYWORD: SYNTHESIS / NIOBIUM OXIDE / ZINC OXIDE / SOL-GEL METHOD / SOLVOTHERMAL METHOD / TRIBLOCK COPOLYMER / MESOPOROUS / SELF-ASSEMBLY / EISA / ASPECT RATIO / MORPHOLOGY / DIALYSIS

SIRACHAYA KUNJARA NA AYUDHYA: LIQUID PHASE SYNTHESES OF NIOBIUM OXIDE AND ZINC OXIDE WITH CONTROLLED MORPHOLOGY. THESIS ADVISOR: PROF. PIYASAN PRASERTHDAM, Dr.Ing., THESIS CO-ADVISOR: PROF. GABOR A. SOMORJAI, Ph.D., 163 pp.

Development on the synthesis approaches for controlling morphology of nanomaterials would implement to new advanced materials for many interesting applications in the future. Two main synthesis goals presented in this research were controlling mesoporosity and shape of metal oxide. Niobium oxide with mesoporosity and nanocrystalline zinc oxide with anisotropic shape were representatives for each synthesis goal and the syntheses were based on wet chemistry. Using high drying temperature, the longer ethylene oxide chain of the triblock copolymer enhanced the well organization of the mesostructure and the mesoporous niobium oxides obtained after template removal were well-organized. The hydrothermal aging at 110°C showed significantly enlarged mesoporous size and surface area, with distinct structural development pathway of niobium skeleton which showed potentially enhanced Lewis acidity. An amount of water in the system was also found to affect the properties observed. Too large or an absence of water did not give the distinct observations and the surface area and pore sizes were lower. Fine tuning of the pore sizes in the range of 3-7 nm was attained by making use of dialysis process. The procedure gave precipitates form of mesostructured oxide and shortened the long drying time required in the normally non-dialyzed method. The mesoporous niobium oxide, after calcinations at 500°C, possessed surface area in the range of 120-170 m^2/g under the concentrations employed. The strategy to the adjusted textural properties of all the mesoporous niobium oxide samples were mainly based on the modification of the triblock copolymer micelles and the intrinsic sol-gel chemistry of the niobium moieties. In nanocrystalline zinc oxide syntheses, solvothermal process in the absence of hydroxyl group gave highest aspect ratio of 1-dimensional nanorod. The morphology of the products was related to dielectric constant of the solvents and the nuclei formation and growth rate of crystal were affected by the reagents.

Department........Chemical Engineering….. Student's signature..........................

Field of study....Chemical Engineering….. Advisor's signature.........................

Academic year...2007……………….... Co-advisor's signature ....

ACKNOWLEDGEMENTS

The author would like to first grant her utm ost acknowledgement to Professor Piyasan Praserthdam, advisor, for acc epting her as his advisee with a provided scholars hip and opening great opportunity for her to learn both scientific knowledge and gratitude of life throughout the graduate study. The author would like to express her highest gratitude to Professor Gabor A. Somorjai from Department of Chem istry, University of California, Berkeley, for his kindness in allowing her to experience life abroad. The appreciation is also given to Professor Michael C. Williams, Prof essor Emeritus, from Chemical and Materials Engineering Department, University of Alberta, Canada, for his t houghtfulness in having the author on his business an d introducing her to Profe ssor Somorjai. The author could never have a chance to such great experience without both professors. The Thailand Research Fund (TRF) is also thanked for its funding of all the needs in Thailand and abroad. The dissertation committees and advicers in the Research Center on Cataly sis and Cataly tic Reaction Engineering Laboratory all deserve the author's appreciation as well.

In addition, the author acknowledges to all fellows who worked or helped the author in any way. In particular, Dr. Apinan Soo ttitantawat has alway s been supportive and helped the author in some characterizations and screening or comments on the paper works. Michael E. Grass, from University of California, Berkel ey, has also sacri ficed his valuable time fo r corrections and comme nts on the paper works. Assistant Professor Okorn Mekasuwandamrong and Assistant Professor Varon g Pavarajarn have also granted valuable help to nanocry stalline project. Alex ander mastroianni, from University of California, Berkeley, has been helpf ul on the experi ments in which he g ains expertise and al ways expressed caring during the author's stay in Berk eley. Many thanks are also given to the members of the Research Center on Catalysis and Catalytic Reaction Engineering Laboratory. Mostly of them have sense of hum or which makes the laboratory environment out o f boredom. Other people such as Inger Coble, Kimani A. Stancil and his wif e, Guillermo Zetina, Simon Humphrey, Becky Grass, Rachel K. Smith, Diana Philip, Jonathan Owen and other friends also deserve t hanks from the author for their friendship during the author' s life in Berkeley.

Finally, the author would like to devote her deepest gratitude to her parents who have always been the source of support and encouragement throughout all difficulties.

CONTENTS

LIST OF TABLES

LIST OF FIGURES

CHAPTER I

INTRODUCTION

Among the most active trends in modern materials chemistry nowadays, the development of the synthetic routes to synthesize inorganic materials having mesopores and to control the size and shape of the densed inorganic in the nanometer regime have been realized of their significant research interests because there are many potential applications in using these new developed materials.

Researches on mesoporous materials formation in the presence of surfactant molecules as templating agents have been paid attention especially since the development of silica-based M41S materials [1, 2]. Generally, the preparation of these mesoporous materials involves an organic template assembly such as cetyltrimethylammonium bromide (CTAB) or non-ionic polyethylene oxide surfactants [3-5]. These mesoporous materials have potential applications in the field of catalysis, separation, and can be used as a host material to encapsulate broad range of inorganic and organic guest species [6-8]. The transition metal oxides have many interesting properties not found in the silica-based materials such as the various oxidation states and the electrochemical, optical, or electrical properties. The silica-based synthesis procedures has also been extended to apply for the transition metal (TM) based systems [9-11] because it was suggested, on the basis of mechanistic ideas, that it should be possible to synthesize non-siliceous materials following similar pathways [10-12].

However, in the field of non-siliceous mesoporous materials, slow developments, compared to that of mesoporous silica, have been found on their synthesis researches. The reasons may rely on the fact that many of the research groups have their origins in zeolite chemistry and are active in the field of mesoporous materials of silicon and aluminum, but are not very familiar to the chemistry of other elements. To synthesis the material of new composition, some adaptation of the procedures would be required, depending on the chemistry of the system and the transition metal (TM) based systems are different from Si-based

system in many aspects such as in reaction kinetics such as hydrolysis reaction, redox reactions, phase transitions and Coordination aspects. For example, the tendency of silicon to form amorphous silica networks favors the formation of mesoporous materials while some of the non-siliceous species have a high tendency to form a stable crystalline structure with high lattice energy that leads to phase separation of the inorganic species from the templating surfactant. Thus, the condition of mesostructure formation can't be obtained. The presence of crystalline materials can in most cases not accommodate the curvatures formed by the organic template in the mesostructure and most of the mesoporous materials reported so far have amorphous wall structures [10, 11].

On the other hand, synthesis of the inorganic nanocrystals (nanocrystalline materials) has been focused on the method for controlling size and shape. Architecture of nanocrystals can be classified into zero-dimensional (0D) quantum dots including nanospheres, cubes and tetrahedrons, one-dimensional (1D) structure such as nanorods and wires, and two-dimensional (2D) structure such as nanodiscs, and plates, and other advanced shapes such as multipods and nanostars. Among these possible structures, one-dimensional (1D) structure is of current interest in materials chemistry because of its dimensional anisotropy. For example, the semiconductor nanorods could provide efficient electron conduction along the long axis of the nanorods. Also some properties such as optical properties of nanocrystals also depend on the length-to-diameter (aspect ratio) of the nanorods. The potential applications of one-dimensional (1D) nanostructures include light-emitting diodes (LEDs), single-electron transistors, field-effect transistors (FETs), biological and chemical sensors, photodetectors, electron emitters, ultraviolet nanolasers, and as active components or interconnects in fabricating other nanoscale devices [13-18]. The fact that fundamental properties can be various with aspect ratio and many of their potential applications make semiconducting oxides the most attractive classes of materials for functional nanodevices and various means have been reported for the synthesis of one-dimensional semiconducting materials [19-22].

Regarding the above rational, the research here would divide into two topics, both dealing with the controlled synthesis. First, the work would aim to the synthesis to get the mesoporous of a transition metal oxide, which has an amorphous nature

formation, using the organic agent as the mesostructure directing agent. The second part of the work would deal with the synthesis of the nanocrystalline metal oxide and trying to control the shape or the aspect ratio or to understand the possible mechanism of the parameter having large impact on the shape of the oxide.

For the first part of the work, niobium oxide would be the transition metal oxide of interest to get the mesoporous structure.

Niobia or niobium oxide has been a transition metal oxide interested for applications in catalysis due to its strong metal support interaction (SMSI) and redox potential. Its function in catalysis includes promoter or active phase, support, solid acid catalyst, or redox material. Niobia has been used for various types of reactions such as NO reduction, hydrogenolysis, disproportionation of hydrocarbons (methathesis), hydrogenation of CO, oxidation and ammoxidation, dehydrogenation, or other acid-catalyzed reactions and photocatalytic reactions [23]. Niobium oxide is also a dielectric material and a promising candidate as new high capacitance devices for the future electronic devices [24]. Nanoporous structure of niobium oxide is, therefore, one of transition metal oxides expected to exhibit novel properties in catalysis, photocatalysis, electronic, sensing devices, and biotechnology [25-32].

Among important properties, high surface area are crucial for catalyst supports, photocatalysts [25, 33-35] while large pore size is also crucial for applications as adsorbents and sensors [26]. Hence, high surface area and controllable pore size are an interesting issue concerned in the development of the synthesis pathway for future material, especially for catalysis and sensor applications [11, 36].

Synthesizing niobium oxide without surfactant generally resulted in low surface area oxide [37-42] while higher surface area niobium oxides were obtained by adding surfactant template in the synthesis processes [28, 34, 43].

Triblock copolymers of the type PEO-PPO-PEO (EO = ethylene oxide, PO = propylene oxide) have been extensively employed as surfactant template for the synthesis of mesoporous transition niobium oxide [28, 34, 43, 44] and the procedures have generally been based on the evaporation-induced self-assembly (EISA) gel

drying method [28, 43-46] with an aim to produce well-ordered porous structure [28, 43, 44, 47, 48].

However, to obtain the ordered mesoporous feature often creates problems concerned with reproducibility [11]. Some parameters, such as water concentration, drying humidity and evaporation temperatures, may show a significant influence on the final materials properties and on the required drying time which could be over a week [49-53]. High temperature drying usually be avoided to prevent the possibility of losing self-aggregation of the block copolymer or macroscopic (inorganic-organic) phase separation [48].

To date, well-ordered mesoporous niobium oxides syntheses based on the EISA process using the triblock copolymers have been dried at low temperature (40°C) [28, 43, 44, 47]. An incomplete condensation of the niobia network at this low temperature also resulted in flexibility of the mesostructure hybrid [54]. The niobium(V) chloride, usually employed as the niobium precursors [28, 34, 43-46, 55] in the syntheses with triblock copolymer, also generates hydrochloric acid (HCl) *in situ*, which retard condensation to form dense metal-oxo network [10, 56, 57]. Therefore, to obtain an ordered organization of the structure could be irreproducible as the mesostructure rearrangement is involved along the drying process of an EISA method [11].

One objective in this work is, therefore, an investigation of the method to appropriately provide well-ordered mesoporous niobium oxide with reproducible results. An idea was started with high temperature drying in order to evade the effect from unpredictable humidity and versatile movement of the mesostructure at low temperature process.

Nevertheless, the well-ordered mesoporous niobium oxides reported so far is also recognized of its relatively low stability to high thermal treatment [58]. The thermal treatments (calcination) to remove the template and create the mesoporosity have been mostly done at 450°C to the maximum [28, 43, 44, 47]. Increasing temperature to 500°C resulted in loss of surface area, pore volume and deterioration of the mesostructure due to the growth of an inorganic phase in the crystallization

process [34]. The inability to withstand high temperature is a serious limitation for most catalysis applications [52]. Also, the performance of the well-ordered structured materials reported may or may not be better than the disordered structure [49] and the high effort needed to get the well organization of the pores may not be justified, compared with other important properties such as surface area, and pore size [11, 25].

In order to obtain high surface area and porous properties at higher thermal treatment, aging is the process in consideration. Aging could permit a better consolidation of the inorganic walls [52] and give greater pore size and pore volume of the dried gel [59]. If the as-prepared mesostructured hybrid prior to calcinations is aged, template shape and size is also affected; hence the pore size, surface area and porosity of the final products could be changed or improved. While information on the effect of aging on the silica based system has been widely reported, relatively little investigation has been performed on the aging effect for the case of transition metal oxide [19].

The properties of the mesoporous transition metal oxide could also be influenced by other factors; for instances, amount of water in the solution, type and concentration of the triblock copolymer, the presence or concentration of mineral acid such as HCl. These can have an impact on both the reaction of niobium precursor and on the behavior of triblock copolymer [37, 58, 60].

These lead to the second objective of this work; the investigation of aging effect on the properties of the mesoporous niobium oxide. The results observed also lead to another investigation on the effect of water under the best condition of aging previously obtained.

The other objective arose from the difficulty encountered from the gel drying method and from the niobium(V) chloride used as niobium precursor. The time needed for the viscous gel to dry is long. Large amount of the hydrochloric acid (HCl) is also generated *in situ* when the chloride precursor is mixed with alcohol or water [57].

Although there have been some syntheses of mesoporous niobium oxide using niobium(V) ethoxide as precursor [52, 61-63], this type of precursor is known for fast condensation reaction, which leads to an uncontrolled phase separation of the oxide precipitates without interacting with the templating micelle [64]. Niobium(V) chloride, on the other hand, has been widely used in the syntheses with triblock copolymer [28, 34, 43-46]. However, as HCl act as condensation inhibitors and prevent precipitation of the oxide [56], a precipitation form of niobium oxide synthesized from its chloride precursor has rarely been investigated. Compared to the gel drying method, the precipitate-based method produces a solid product within the reaction solution within shorter times and can be separated by filtration or centrifugation.

Therefore, the last objective of the work about niobium oxide synthesis is to apply the dialysis process to allow for the release of HCl from the initial sol. The concentration of HCl was varied by varying the dialysis time. The concentration and length of block copolymer employed were also varied in the syntheses to investigate their effect on textural properties [52, 65, 66] under the dialysis processes. It was expected that the precipitate form of mesoporous niobium oxide should be beneficial for large scale synthesis and for applications like catalyst or catalyst support.

The second part deals with the nanocrystalline metal oxide synthesis. Zinc oxide (ZnO) is a polar inorganic crystalline material of an n-type semiconductor with direct band gap of 3.37 eV. It has many applications mostly as electronic and photonic materials [67]. They are, for examples, UV photodetection, transparent electronics, humidity sensor, gas and chemical sensor, microlasers, memory arrays, coatings, catalysts, and biomedical applications [21, 68-70]. For these applications, it is preferred that the size and shape of ZnO particles are controlled [71-75].

Zinc oxide would be the target material to be worked on the shape controlled synthesis study. The effort to understand how its aspect ratio could be controlled should provide a way to tune its properties. The work employed the solvothermal process to synthesize ZnO nanoparticles. Effects of properties of solvent on aspect ratio and crystallization mechanism of ZnO were investigated.

   To summarize, this dissertation presents two main parts of the syntheses and preliminary test of properties for materials applications. The first syntheses part is about mesoporous niobium oxide syntheses with four objectives; firstly, an investigation of the method for reproducibly obtain well-ordered mesoporous niobium oxide; secondly and thirdly, an investigation of aging effect and effect of water under the best condition of aging previously obtained; lastly, an investigation of dialysis process applied to reduce HCl concentration. The other syntheses part is about the shape controlled synthesis of zinc oxide (non-porous) by solvothermal method. Finally, the last part is the test of dielectric properties of niobium oxide, and the photoluminescence spectra of zinc oxide. Both niobium oxide and zinc oxide were also tested in photocatalytic decomposition of ethylene.

   This dissertation has been organized by chapters. Chapter 2 introduces the related theory of the syntheses strategies employed in this dissertation. Chapter 3 presents reviews of the works in the literatures linked to the objectives and experiments present in this dissertation. Chapter 4 presents the experimental sections that describe techniques and characterizations used throughout the course of this dissertation. Chapter 5 presents the results and discussion of the experiments. Main story of the chapter is comprised of four parts of niobium oxide syntheses and one part of zinc oxide synthesis. For the niobium oxide syntheses, the first part is 'High temperature evaporation-induced self-assembly of ordered niobium oxide'. The second part is 'Effect of aging on the properties of mesoporous niobium oxide synthesized with triblock copolymer F127'. The third part is 'Water effect on the properties of niobium oxide synthesized with triblock copolymer F127 under aging'. The forth part is 'Influence of dialysis on the formation and structure of mesoporous niobium oxide from niobium(V) chloride'. The zinc oxide synthesis part is presented under the title 'Solvothermal synthesis of ZnO with various aspect ratios using organic solvents'. The last part in this chapter presents a preliminary investigation of some selected properties interested for applications; dielectric property of niobium oxide, and luminescence property of zinc oxide. Photocatalytic activities of selected niobium oxide and zinc oxide samples were also preliminary investigated. Chapter 6 is the conclusions and recommendations on the work.

CHAPTER II

RELATED THEORY

2.1 Sol-Gel Chemistry [76, 77]

2.1.1 Fundamentals

In the sol-gel process, a solution, typically a solution of metal-organic compounds or a "sol", a suspension of very fine particles in a liquid, is converted into a "gel", a highly viscous mass.

The gelation phenomenon may be regarded as a phenomenon, in which sols (or solutions) with fluidity are converted to solids without fluidity. The gelation point is judged by visual observation and determined as the point where the sol (or solution) does not flow on tilting the container. The presence of absence of the flow under gravity depends not only on the viscosity but also on the rheological behavior of the sol (or solution). Rapid increases of the viscosity with time are general for sol-to-gel conversion.

If a "sol" is used, the gelled material consists of identifiable colloidal particles (1 to 1000 nm) that have been joined together by surface forces to form a network. If a solution is used, the gelled material may consist of a network of polymer chains formed by hydrolysis and condensation reactions without particles larger than 1 nm.

Basic flow chars of a sol-gel processing starting from a suspension of fine particles (particulate or colloidal gel) and a solution (polymeric gel) is shown in Figure 2.1.1 while the structure of the corresponding gel is shown in Figure 2.1.2.

In many cases, the distinction between a particulate and a polymeric system may not be very clear, particularly when the particle size approaches the lower limit of the colloidal size range.
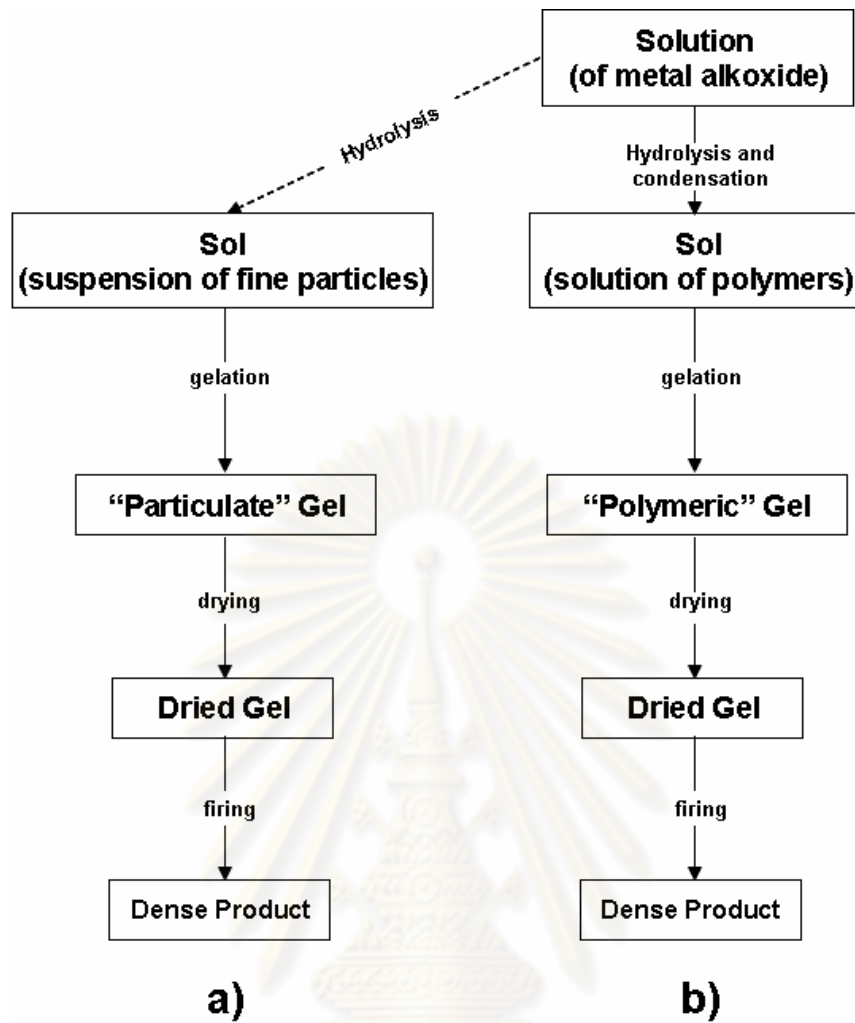
Figure 2.1.1 Basic flow charts for sol-gel processing using (a) a suspension of
fine particles and (b) a solution, from Ref. [77]
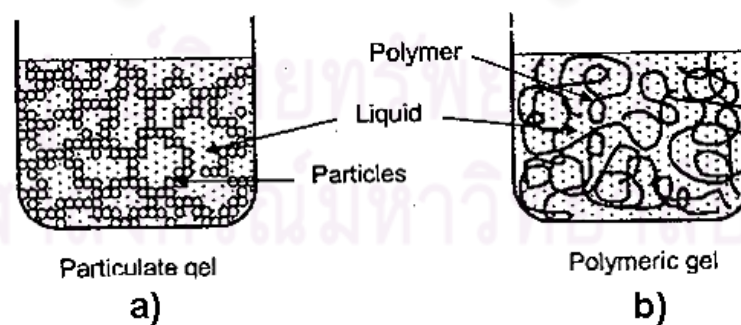
Figure 2.1.2 Schematic diagram of the structure of (a) a particulate gel formed
from a suspension of fine particles and (b) a polymeric gel from a
solution, from Ref. [77]

The pores in polymeric gels are normally much finer than those in particulate gel, whose pore sizes are relatively large compared with the size of the particles (i.e. the average pore size is about 1-5 times the particle size).

In particulate gels, the attractive van der Waals forces dominate, and the particles get in touch with one another, forming a skeletal network. Polymeric gels consisting of a skeletal network of entanglement and cross-linking of growing polymer chains or clusters in solution could provide much better chemical mixing at a molecular level than at the colloidal level. Hence, the polymeric gel route commonly provides exceptional chemical homogeneity.

The structure of the polymer chains in a polymeric gel can vary considerably, depending on the preparation conditions. Different extent of branching of a skeletal network can be affected by parameters such as water concentration. The gel consisting of a weak amorphous solid structure and an interconnected network of very fine pores filled with liquid could be 'frozen' at the point of gelling, where a sharp increase in the viscosity occurs. The frozen structure can change appreciably during subsequent aging or drying of the gel. The aging gel can shrink considerably while expelling liquid while removal of the liquid by evaporation can collapse the weak polymer network and result in additional cross-linking of the polymer structure. Cross-linking and collapse of the gel continues until the structure can withstand the compressive action of the capillary stresses of the very fine pores in the gel. During the firing or calcination process, the gel structure will change to become more highly cross-linked with a corresponding reduction in its free volume and its surface area. The solid skeletal phase that makes up the dried gel may not be identical to the corresponding bulk amorphous solid produced. In contrast, the structure of the particles in particulate gels normally corresponds to that of the bulk solid with the same composition.

In colloidal chemistry, controlling for appropriate surface charges or species adsorbed on surfaces of particles is required so that the gelation could occur by particle whose sizes small enough to obtain homogeneous colloidal sol without coagulation and precipitation. The solution chemistry should be more easily to be controlled than colloidal chemistry using colloids as starting materials.

In general cases, the reactions occurred in the sol-gel chemistry are the hydrolysis, equation <2.1>, and condensation (inorganic polymerization) reaction, equation <2.3> and <2.4>. It is not necessarily restricted to an aqueous system, but aqueous reactions have been known for a long time.

Hydrolysis reaction:

$$\equiv\text{M-X} \quad + \quad \text{H}_2\text{O} \quad \rightarrow \quad \equiv\text{M-OH} \quad + \quad \text{HX} \quad <2.1>$$

Condensation reaction:

$$\equiv\text{M-OH} \quad + \quad \text{X-M}\equiv \quad \rightarrow \quad \equiv\text{M-O-M}\equiv \quad + \quad \text{HX} \quad <2.2>$$
$$\equiv\text{M-OH} \quad + \quad \text{HO-M}\equiv \quad \rightarrow \quad \equiv\text{M-O-M}\equiv \quad + \quad \text{H}_2\text{O} \quad <2.3>$$
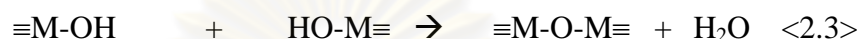
where M = metal; X = reactive ligand like halogen, (OR)group.

The chemical reactions which occur during the conversion of the metal precursor solution to the gel have a significant influence on the structure and chemical homogeneity of the gel. Foreign species such as counter ions, solvent molecules or chemical additives are often involved in the sol-gel chemistry. Complexation by these species plays an important role in the formation of condensed phases. The rates of the chemical reactions are controlled by the processing variables such as chemical composition of the precursor, concentration of reactants, pH of the solution, and temperature. When the hydrolysis rate is of the same order of magnitude, or lower, than the condensation rate, precipitates or colloidal gels are usually obtained. High concentration of the precursor can also lead to precipitation [78].

2.1.2 Inorganic Precursors [76, 77]

The starting compounds for the preparation of the sol are inorganic salts (precursors). Few general requirements are required for the metal precursors used in sol-gel process; they have to be soluble in the reaction media, and they have to be reactive enough to participate in the gel forming process. The reactivity of a precursor depends on its chemical nature and also on the applied reaction conditions.

Precursors such as nitrates, or acetates salts, oxides, hydroxides, complexe chelated precursors, amines, and alkoxides can be used if soluble. Among these,

metal alkoxides are the most common sol-gel precursors, due to their commercial availability for the most important elements, and their well know basic chemistry.

However, metal alkoxides are generally very reactive species for hydrolysis, condensation or chemical modification reactions, probably due to the presence of electronegative alkoxy groups that make the positively charged metal atoms highly prone to nucleophilic attack. Highly electronegative ligands such as halides increase the electrophilic character of the metal atom.

Chlroalkoxides are considered as chemical modifications of alkoxides. They can be obtained through the reaction of metal chlorides with alcohols. Chloroalkoxides offer a good compromise between inorganic and metal organic precursor. They seem to be very convenient molecular precursors for sol-gel polymerization since they are cheap and easy to synthesize from the metal chlorides which are more available than the alkoxides [76, 79].

The reactivity of metal chlorides towards alcohols decreases with increasing electropositive charge of the metal. The reaction of $SiCl_4$ with ethanol can be pushed to completion with the formation of $Si(OEt)_4$, while those of $TiCl_4$ and $ZrCl_4$ can undergo only partial substitution and form $TiCl_2(OEt) \cdot 2EtOH$ and $ZrCl_3(OEt) \cdot EtOH$ [76].

2.1.3 Nonhydrolytic sol-gel routes to oxides [79]

Generally, nonhydrolytic sol-gel route could provide an interesting method to control the fast reaction rates of the metal alkoxides by improved controlling over the reaction mechanisms. It is also an alternative for better homogeneity in multicomponent oxides. The chemistry of hydroxylation and condensation reactions proposed in this nonaqueous route are shown in equation <2.4> and <2.5>.

$$MX_4 + R\text{-}\bar{O}\text{-}R \longrightarrow \begin{array}{c} R \\ R \end{array}\!\!\bar{O}\cdots M\!\!-\!\!X \longrightarrow RO\text{-}MX_3 + RX \qquad <2.4>$$

$$MX_4 + R\text{-}\bar{O}\text{-}MX_3 \longrightarrow \begin{array}{c} R\text{-}\bar{O}\text{-}M \\ M\text{-}X \\ X \end{array} \longrightarrow M\text{-}\bar{O}\text{-}M + RX \qquad <2.5>$$
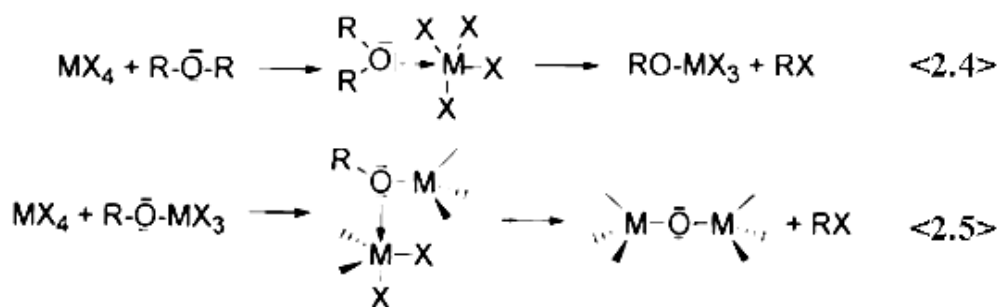
where, R stands for alkyl group or hydrogen, X for halides, and M for metal.

Equation <2.4> is reaction of alcohols on halides, while the condensation between alkoxide and halide functions is outlined in equation <2.5>. A nonhydrolytic method for the formation of an oxo bridge is provided by the condensation reaction between two different functional groups bonded to two different metal centers by eliminating a small organic molecule like alkyl halide. Alkyl halide elimination can occur in the temperature range from room temperature to about 100°C, depending on the reagents involved.

2.1.4 Drying of gel [77]

The gel contains a large amount of liquid in the fine interconnected channels, typically ~2-50 nm in diameter, and it must be dried before conversion to a useful material. Two main consequences in removal of the liquid by evaporation are: development of large capillary stresses, and shrinkage of the gel under the action of the capillary stress. If the pore channels in the gel are simplified as a set of parallel cylinders of radius a, then the maximum capillary stress exerted on the solid network of the gel, p, is as in equation <2.6>

$$p = (2(\gamma_{l/v})\cos\theta)/a \qquad <2.6>$$

where $(\gamma_{l/v})$ is the specific surface energy of the liquid/vapor interface and θ is the contact angle.

The pores in polymeric gels are normally much finer than those in colloidal gels and the capillary pressure can be quite large in the polymeric gel, causing warping and cracking of the gel. Drying by evaporation under normal conditions, the resulting dried gel is called a xerogel.

2.2 Principle of Self-Organization [80]

In chemistry, self-organization is a phenomenon when well-defined structures result spontaneously from the components of a system by noncovalent forces, for example, in liquid crystals, micelles. The principle of self-organization is based on attractive/repulsive pairs of forces. When both long range repulsive and short range attractive forces exist at the same time (shown in schematic in Figure 2.2.1), ordered structures can be built up.
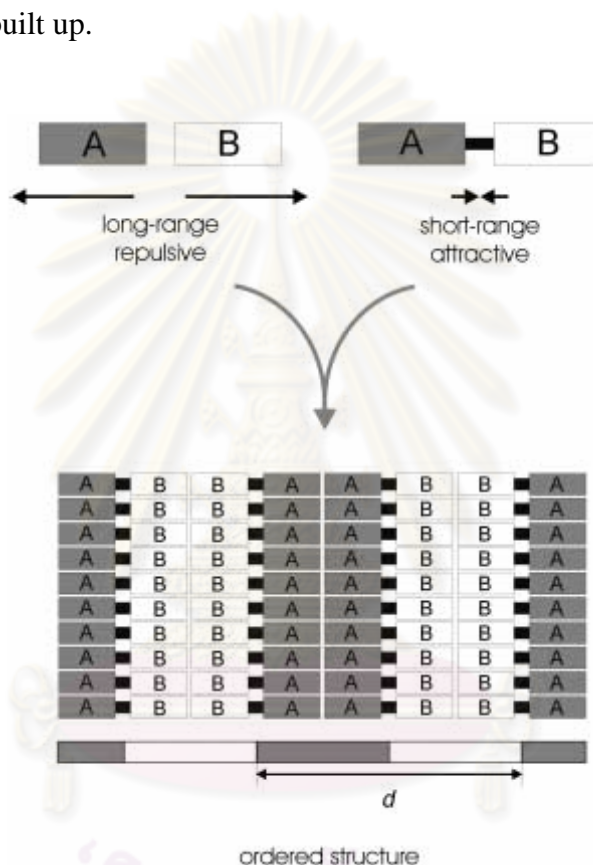
Figure 2.2.1 Illustration of an ordered structure built by self-organization as a result of long-range repulsive and short-range attractive forces (d is the periodic length of the structure), from Ref. [80]

Table 2.2.1 shows examples of pairs of forces which are important for the formation of ordered materials.

Table 2.2.1 Examples of pair of forces which can lead to self-organization, from Ref. [80]

Long-Rang Repulsion	Short-Range Attraction
Hydrophilic/Hydrophobic	Covalent Binding
Incompatibility	Covalent Binding
Coulombic Repulsion	Electroneutrality
Excluded Volume	Minimum Space Required
Electric Dipole Field	Electric Dipole Interaction
Magnetic Field	Magnetic Dipole Interaction

When the molecules subject to the interaction of the pair of forces join other molecules, domains and interfaces are formed in the way that reflects the shape of the molecules. As seen in Figure 2.2.2, the A and B domains are separated from each other by the interface (dotted line). When the A and B are stretched in shapes, planar interfaces are formed and stripe or lamellar domains result. When the domain of A is larger than that of B, curved interfaces result and the bend is characterized by the curvature radius R. The right hand picture in Figure 2.2.2 represents application of the model to block copolymers.
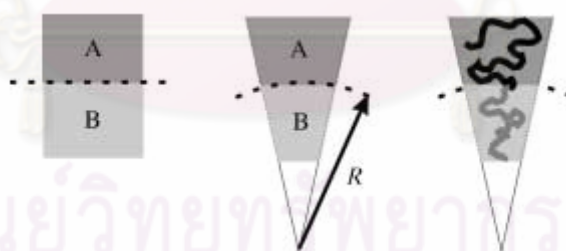
Figure 2.2.2 Local geometry and the curvature of domains and interfaces
formed when molecules subject to the interaction of the pair of
forces join one another. The curvature of the interface is R. The
application of the model to block copolymers is shown by the
right hand one, from Ref. [80]

Using the given curvature and domain size, it is possible to predict the symmetries and topologies/structures of the organized systems. Self-organization structures of block copolymers and surfactants and be varied from the spherical

micelles, cylindrical micelles in dilute solutions to lamellae or other complicated structures in higher concentrations, as shown in Figure 2.2.3.
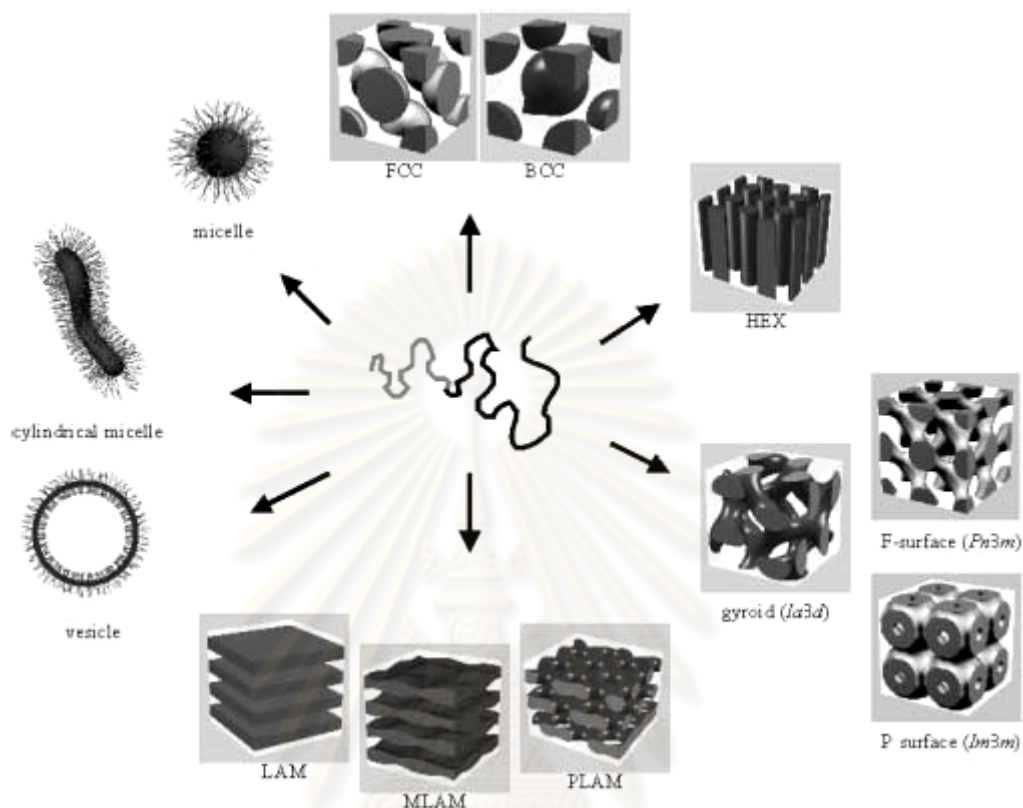
Figure 2.2.3 Self-organization structures of block copolymers and surfactants: spherical micelles, cylindrical micelles, vesicles, fcc- and bcc-packed spheres (FCC, BCC), hexagonally packed cylinders (HEX), various minimal surfaces (gyroid, F surface, P surface), simple lamellae (LAM), as well as modulated and perforated lamellae (MLAM, PLAM), from Ref. [80]

2.3 Block Copolymers

Block copolymers are supramolecules that are hazard-free and industrial available [58]. These polymers consist of two or more segments (blocks) of polymers joined in certain arrangements. These block copolymers are classified by the number of blocks per one molecule; block copolymers with two, three, and more blocks are called diblock, triblock, and multiblock copolymers respectively. For instance, ABC linear triblock copolymer (also called terpolymer) consists of three different

monomers, while an ABA linear triblock copolymer has two monomer, A and B types [81].

These block copolymer molecules can be regarded as surfactants since they have a tendency to accumulate at the boundary of two phases [82]. They are nonionic surfactants that are different from cationic and anionic surfactants in the way that the molecules of block copolymer are actually uncharged and the hydrophilic groups are made up of water-soluble moieties, rather than charged head groups [49]. In aqueous solution, block copolymer molecules orientate themselves in the way that the hydrophobic blocks are removed from the aqueous or polar environment in order to achieve a state of minimum free energy. As the concentration of the polymer in solution is increased, the free energy of the system begins to rise due to unfavorable interactions between water molecules and the hydrophobic region of the polymer resulting in structuring of the surrounding water and a subsequent decrease in entropy. At a specific concentration range, several molecules of these polymers will self-assemble into colloidal-sized particles, called 'micelles' and the critical concentration is termed the 'critical micelle concentration (CMC)'. The formation of micelles effectively minimizes unfavorable interactions between the surrounding water molecules and its hydrophobic portion. Although micelles are classified as colloids, they are not solid particles. Many experiments indicate that the individual molecules or unimers that make up the micelle are in a dynamic equilibrium with the unimers in the bulk. When the concentration is diluted below the CMC, micelles can disassemble with the rate of disassembly being largely dependent on the structure of the molecule and interactions between the chains. In some cases where there are physical interactions among chains in the micelle core, disassembly can be resisted. If the concentration of the polymer in solution is maintained above the CMC, micelles are thermodynamically stabilized against disassembly. Dynamic equilibrium of aggregated copolymers with unimers is shown in Figure 2.3.1. [82]
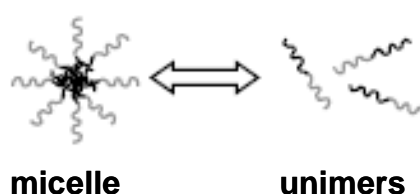
micelle   **unimers**

Figure 2.3.1 Aggregated copolymers in dynamic equilibrium with unimers, from Ref. [82]

Typically, micelles have diameters ranging from 10 to 100 nm and are characterized by a core-shell architecture in which the hydrophobic portions form an inner core surrounded by a corona composed of the hydrophilic portions of the copolymer molecules [82].

An interesting class of block copolymers is the poly(ethylene oxide)-poly(propylene oxide)-poly(ethylene oxide), PEO-PPO-PEO triblock copolymers with structure shown below. They are sold under the trade name Pluronics® (BASF), and also known by other names such as Proxanols, Synperonics, Poloxamers, etc [81].

$$HO-(CH_2-CH_2-O)_n-(CH_2-CH-O)_m-(CH_2-CH_2-O)_n-H$$
$$CH_3$$
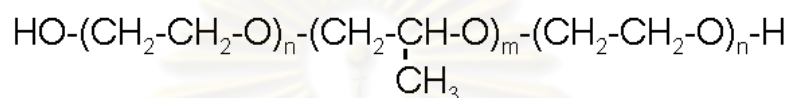
For the Pluronics® (BASF) block copolymers, the alphabetical designation explains the physical form of the product: 'L' for liquids, 'P' for pastes, 'F' for solid forms. The first digit (two digits in a three-digit number) in the numerical designation, multiplied by 300, indicates the approximate molecular weight of the hydrophobic PO moieties. The last digit, when multiplied by 10, indicates the approximate total EO content in the molecule. For example, Pluronic F68 is a solid material. The molecular weight of the hydrophobe is approximately 1,800 (6x300). The hydrophile (EO moieties) represents approximately 80% of the molecule, by weight, (8x10). Pluronic F127 is a solid with approximately PO of 3,600 (12x300) molecular weight, and the EO content in the molecule of about 70% (7x10) of the molecule [83].

Micellization of PEO-PPO-PEO in aqueous solutions has been studied by several methods such as surface tension, viscosity measurement, cryo-TEM, light scattering, and fluorescence, dye-solubilization technique etc. [81]. The core-shell micelles are formed by hydrophobic middle PPO block forming a core surrounded by an outer shell of the hydrated hydrophilic PEO end blocks [81]. Proper micellization then requires folding behavior of the polymer chain, as shown in Figure 2.3.2.
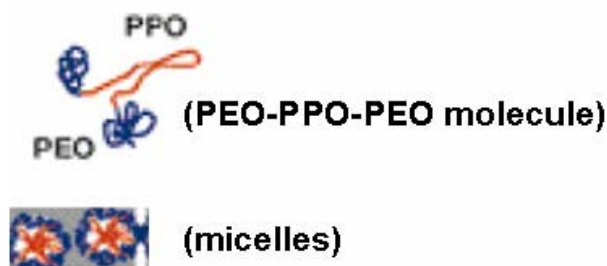
Figure 2.3.2 Micellization of triblock copolymer of the type (PEO-PPO-PEO), from Ref. [56]

Critical micellization concentrations for Pluronic copolymer aqueous solutions as a function of solution temperature has been reported by Alexandridis et al. [84], and the data is shown in Table 2.3.1.

Table 2.3.1 Critical micellization concentrations for Pluronic copolymer aqueous solutions as a function of solution temperature, from Ref [84]
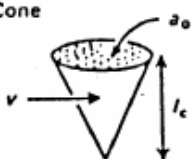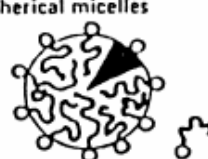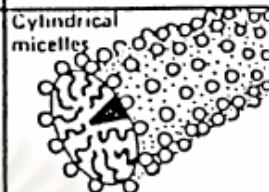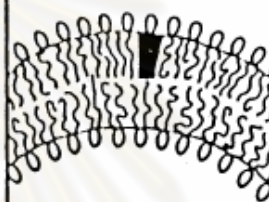
temp, °C	L64 % w/v	mM	P65 % w/v	mM	F68 % w/v	mM	P84 % w/v	mM	P85 % w/v	mM	F88 % w/v	mM
20	–		–		–		–		–		–	
25	–		–		–		2.6	6.190	4	8.695	–	
30	1.5	5.172	4	11.76	–		0.6	1.428	0.9	1.956	–	
35	0.4	1.379	1	2.941	–		0.15	0.357	0.2	0.434	1.7	1.491
40	0.1	0.344	0.35	1.029	7	8.333	0.04	0.095	0.05	0.108	0.6	0.526
45	0.02	0.069	0.1	0.294	3	3.571	0.013	0.031	0.014	0.030	0.24	0.210
50	–		0.04	0.117	0.9	1.071	–		–		0.09	0.079
55	–		–		0.3	0.357	–		–		0.04	0.035

temp, °C	P103 % w/v	mM	P104 % w/v	mM	P105 % w/v	mM	F108 % w/v	mM	P123 % w/v	mM	F127 % w/v	mM
20	0.7	1.414	2	3.389	2.2	3.384	–		0.18	0.313	4	3.174
25	0.07	0.141	0.3	0.508	0.3	0.461	4.5	3.082	0.03	0.052	0.7	0.555
30	0.01	0.020	0.04	0.067	0.025	0.038	0.8	0.547	0.005	0.009	0.1	0.079
35	0.002	0.004	0.008	0.013	0.005	0.007	0.15	0.103	0.001	0.002	0.025	0.019
40	–		0.002	0.003	0.001	0.001	0.04	0.027	–		0.008	0.006
45	–		–		–		0.008	0.005	–		–	
50	–		–		–		–		–		–	
55	–		–		–		–		–		–	

2.4 Micellar Geometry

Micellar aggregates can organize to different shapes. The architecture of the molecule and the head group charge play important roles in deciding the micellar shape. It can be shown that micellar shape depends on the packing factor (P) which is a relative value of the chain length (l), chain volume (v) and the head group area (a) of the molecule; $P = v/a \cdot l$. The packing factor increases along the developed shape from spheres to cylinders micelles, to bilayer, as shown in Figure 2.4.1 [52, 85].

Critical packing parameter $v/a_o l_c$	Critical packing shape	Structures formed
< 1/3	Cone	Spherical micelles
1/3-1/2	Truncated cone	Cylindrical micelles
1/2-1	Truncated cone	Flexible bilayers, vesicles
~1	Cylinder	Planar bilayers

Figure 2.4.1 The packing factor (parameter) of a surfactant molecule and the various structures they form in aqueous solutions, from Ref. [85]

The packing factor for geometric explanation of the amphiphilic block copolymers like Pluronics is simply described by the ratio of the effective cross-sectional area of the tail (hydrophobic) group, a_T, to that of the head (hydrophilic) group, a_H; $P = a_T/a_H$ [86]. The packing factor, P, determines the curvature of the micelle and therefore the micelle shape. For example, when P<1/3, highly surface curvature micelles, i.e., spherical micelles are form. When 1/3<P<1/2, less surface curvature micelles would form and the micellar shape is usually cylinder. The schematic diagram showing the effective cross-sectional area and micellar shape of the PEO-PPO-PEO block copolymer is shown in Figure 2.4.2 [86].
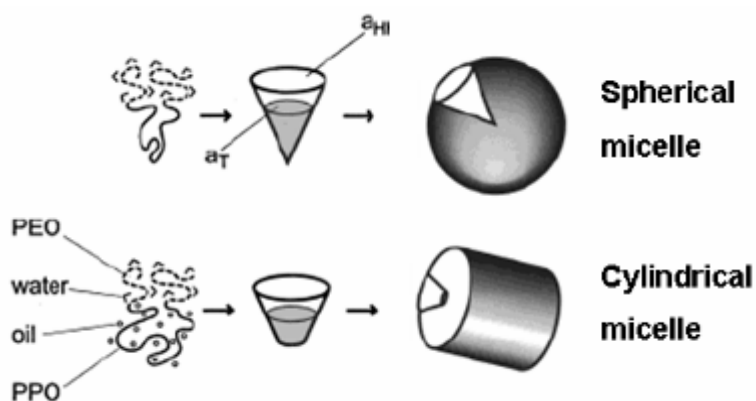
Figure 2.4.2 Schematic diagram of effective cross-sectional area and micellar shape of the PEO-PPO-PEO block copolymer, from Ref. [86]

2.5 Mesoporous Oxide Formation by Block Copolymer Template [58]

Two main processes can be acknowledged in the formation of the mesophases: a) The self-assembly property of the organic template which results in microphase separation into hydrophobic and hydrophilic domains, and b) the formation of inorganic components by the sol-gel chemistry of the inorganic precursor; the growth of an inorganic network is extended through the organic-inorganic hybrid network by the condensation reaction [58].

There are three main components involved in the synthesis to form a mesostructured hybrid: an organic template, an inorganic species, and solvent. The interactions both of among or between the components at the hybrid interface will control the final obtained structure (see Figure 2.5.1). For example, inorganic condensation is often controlled by the solvent. The solvent also correlates to the phase diagram of an organic template [58]. The inorganic can interact and modify the self-assembly behavior of an organic template [56]. The inorganic condensation can 'freeze' a mesostructure, even a metastable one [58].
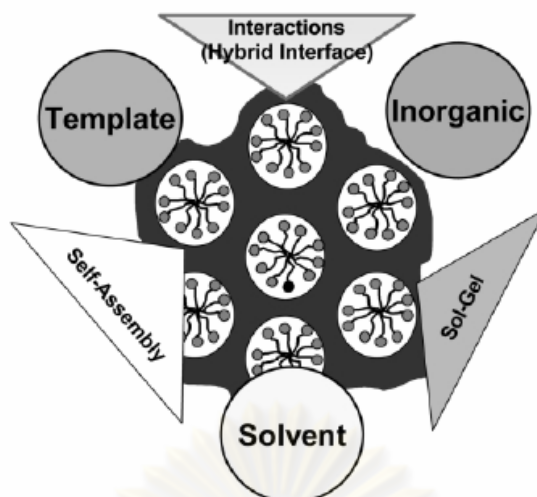
Figure 2.5.1 Scheme of the main interactions at the hybrid interface between
the solvent, organic template, and inorganic species, from Ref. [58]

The organic-inorganic interaction is particularly important in block
copolymer-metal oxide hybrids, especially in PEO-PPO based ones. Three possible
structures at the interface, having different strength of interaction between a nonionic
block copolymer template and an inorganic framework are shown in Figure 2.5.2.
Two strong interactions can disrupt the formation of an organized mesophase, leading
to no ordered structure of the final mesoporous materials.
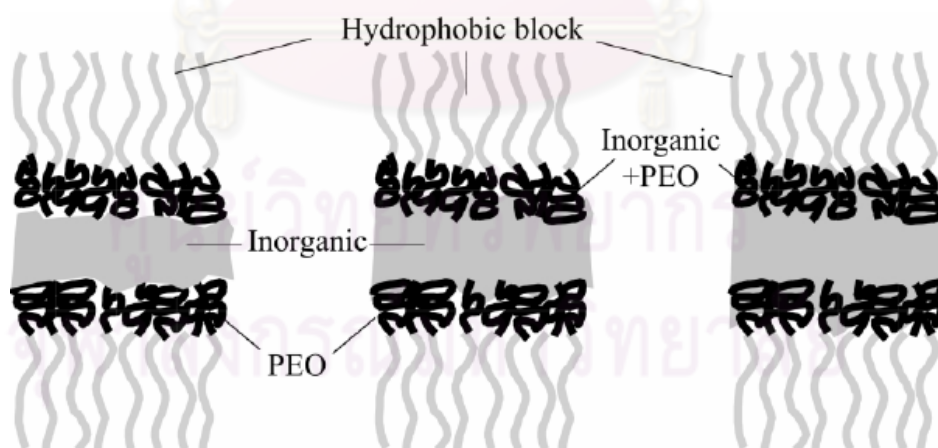
Figure 2.5.2 Three possible structures of a hybrid interface composed of a
nonionic polymer and an inorganic framework: the PEO block is
completely segregated from the inorganic phase (left); a fraction of
PEO is free (middle); the inorganic phase is completely integrated into
the PEO block (right), from Ref. [58]

The balance between two competitive processes: organization of the template vs. inorganic polymerization should determine the formation of an organized hybrid mesostructure.

After the mesostructured hybrid of the organic-inorganic is formed, the step to consolidate the mesostructure might be necessary to enhance the inorganic wall integrity before the organic template is removed (usually by burning out in a calcinations process). The steps leading to a mesoporous oxide network as presented in Figure 2.5.3.
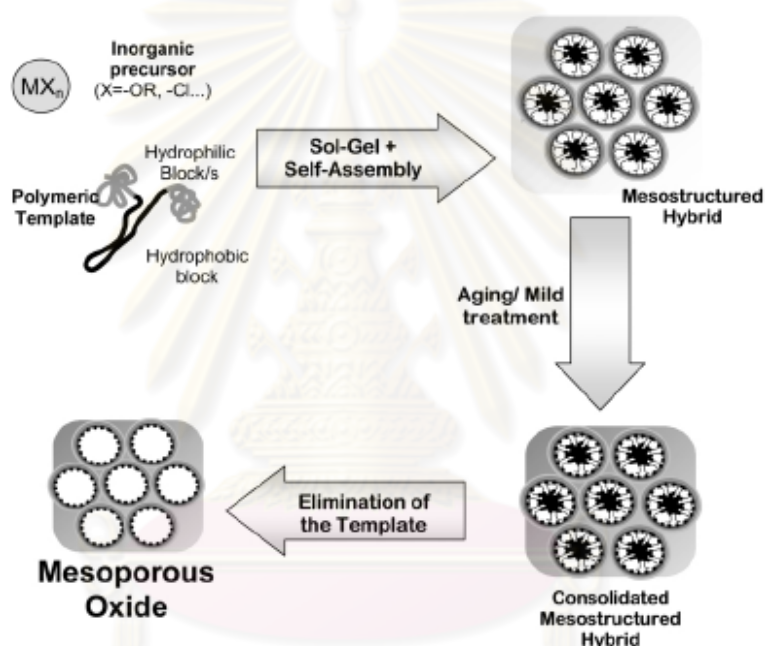
Figure 2.5.3 Schematic view of the steps leading to a mesoporous oxide network, starting from a solution, from Ref. [58]

Most of the works of well-organized mesostructures have been performed on PEO-based templated silica and derived from the precipitation-based synthesis. Depending on the synthesis conditions such as pH value, or anion concentration, an optimized precipitation conditions yielding excellent organization has been reported [87]. Other form of synthesis conditions such as films or xerogels have also been reported, especially in non-silica systems. The film thickness is approximately 100-300 nm for a thin film, and 100-1,000 μm for a xerogel. However, external humidity and solvent evaporation rate is crucial for obtaining ordered mesostructures, as the as-

prepared hybrid mesophases are still flexible and flux of components exchange to or from the film can trigger the mesophase formation. Therefore, not only the chemical parameters but also the processing conditions are of paramount importance to obtain robust and reproducible systems [58].

2.6 Evaporation-Induced Self-Assembly (EISA) [10, 49, 58, 88]

The evaporation-induced self-assembly method is the synthesis strategy mostly applied to obtain ordered hybrid mesophases of the non-silica system in the form of thin films and xerogels. The method starts from dilute solutions and the progressive surfactant concentration upon solvent evaporation drives self-organization of micelles into periodic hexagonal, cubic, or lamellar mesophases.

Within a short period, complex mechanism involving parallel competitive processes are developed (Figure 2.6.1);

- Solvent (ethanol/water) evaporation
- Auto-assembly and segregation at the nanometer scale of organic and inorganic phases
- Formation of a hybrid mesostructure
- Further hydrolysis/condensation reactions, aided by evaporation of HCl (condensation inhibitor), and water diffusion into the system.
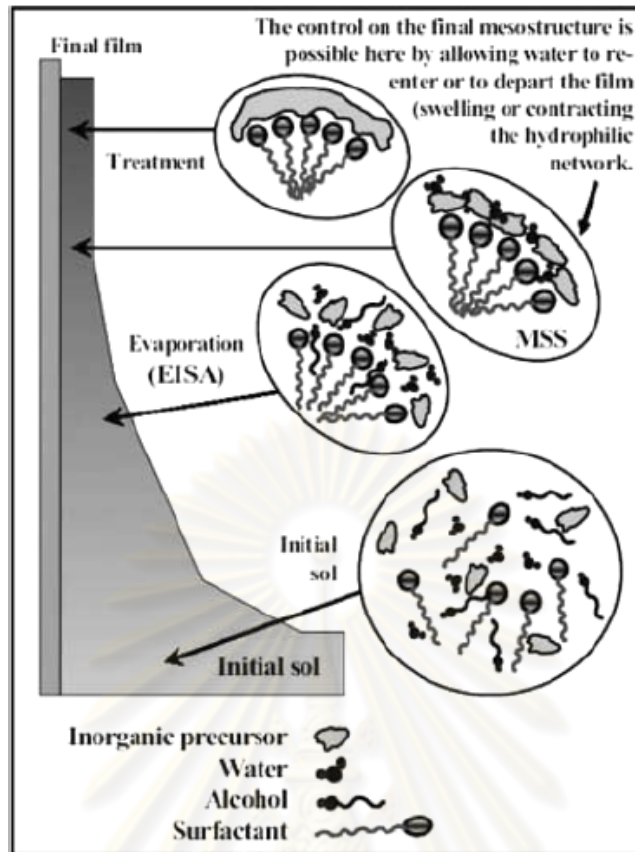
Figure 2.6.1 Mesostructure formation by the EISA strategy, from Ref. [49]

Depending on variation in processing conditions, different composition is triggered along the evaporation-driven pathway, before arrival of final mesostructures. Thus, different mesophases can be possibly obtained.

2.7 Growth Mechanism and Shape Control Strategy of Oxide Crystals [19, 89, 90]

It has been assumed that, for the crystal growth mechanism, the main mechanisms are the formation of the growth units and the incorporation of growth units into the crystal lattice at the interface making the formation of the nuclei of the oxide crystal. After forming the nuclei the crystal begins to grow and the growth habit of crystals is related to the relative growth rate of various crystal faces.

In order to control the crystal growth, the surface energy of each crystal faces needs to be controlled by the way such as using mixtures of different surfactants that bind differently to the different crystallographic faces. An isotropic growth forming CdSe nanorods is shown in Figure 2.7.1 as an example of crystal growth control based on the surfactant assisted condition.
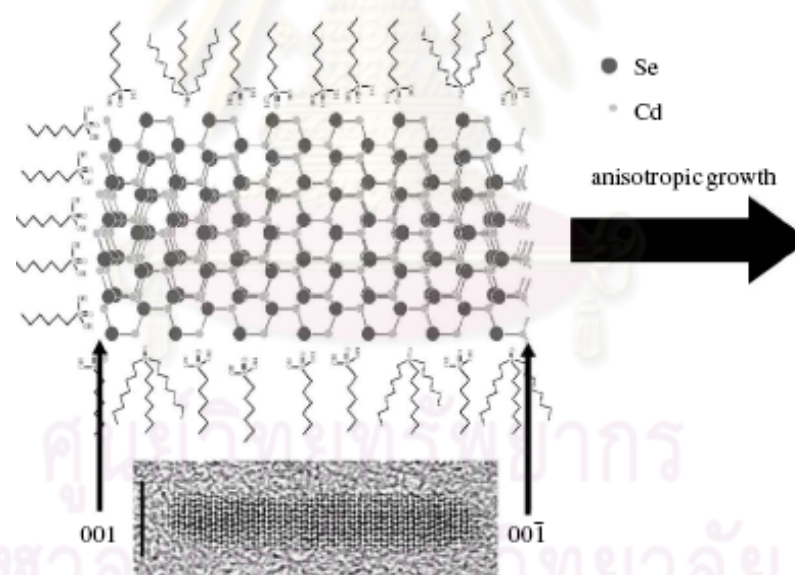
Figure 2.7.1 Proposed growth mechanism for CdSe nanorods, from Ref. [19]

It could be seen that the organic surfactants cannot coat one face of the nanocrystal, making this face have a high energy and rapid growth is allowed. So the rod shape could be formed. It should be noted here for the CdSe crystal that although both the (001) and (00 $\bar{1}$) faces have layer of Cd and Se atoms, their bonding

characters are different which makes differences of the abilility to be passivated by the surfactant and end up with only the (001) face being the fastest growing face.

The hypothesis was introduced for the oxide formed by the hydrothermal process that the growth unit is the complex formed by the attraction of cation and hydroxyl (OH$^-$) ions, whose coordination numbers is equal to that of the cation in the crystal to be formed. For the ZnO crystal, the growth units hypothesized was believed to be the complex $Zn(OH)^{2-}_4$. In the supersaturation condition, growth units $Zn(OH)^{2-}_4$ are bonded together through dehydration reaction and by sharing of the elements, stacking order of the coordination polyhedron forms the ZnO crystal.

In the interior of the crystal, coordination polyhedra are connected together by sharing O^{2-} while the OH$^-$ ligand presents at the interface of crystal. The idealized interface structure is shown in Figure 2.7.2 below:
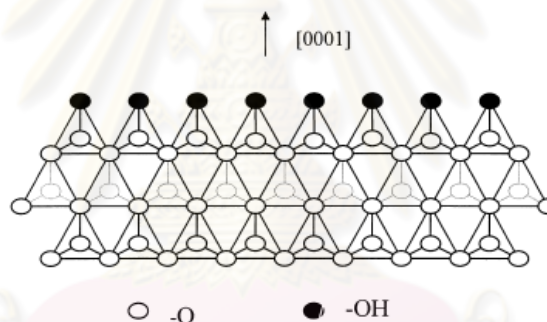
Figure 2.7.2 Idealized interface structure image of ZnO crystal in [0001] direction, from Ref. [91]

The different growth rate among various crystal faces resulted in the growth habit observed for that crystal. From the coordination structure of the oxide crystal, it can be found that the fastest growth rate is the direction of the crystal face with the corner of the coordination polyhedron present at the interface. For the ZnO crystal, the observed maximal crystal growth velocity is fixed in the <0001> direction followed by the <01 $\bar{1}$0> and the <000 $\bar{1}$> direction. The crystal planes of the ZnO crystal and its idealized growth habit is shown in Figure 2.7.3.
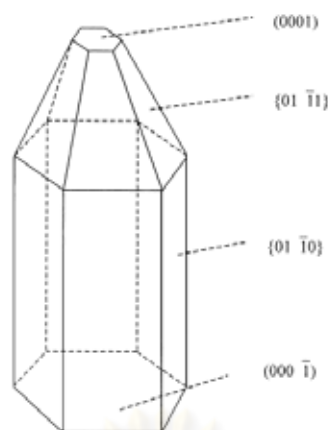
Figure 2.7.3 Cystal planes and idealized growth habit of the ZnO crystal, from Ref. [91]

2.8 Solvothermal / Hydrothermal Method [92]

The 'solvothermal method' involves using a solvent well-above its boiling point by heating the solvent in a sealed vessel (autoclave, bomb, etc.), so that the autogeneous pressure far exceeds the ambient pressure which will automatically raises the effective boiling point of the solvent. Such a technique is indeed extensively used in the preparation of inorganic solids, particularly the synthesis of zeolite materials [93]. If the solvent being water, the technique is often called 'hydrothermal method'.

The solvothermal process can be considered to have three main synthesis routes according to the nature of the solute (liquid or solid), and the chemical reaction involved during the process [94]:

(1) The solvothermal precipitation - the solute and the solvent are in the same phase (liquid).

(2) The solvothermal decomposition - the solute (the material precursor) is insoluble in the solvent. The critical temperature is adjusted to the decomposition of the precursor.

(3) The solvothermal recrystallization - the chemical composition of the material precursor is the same as the final material, but is amorphous or poorly crystallized.

The physico-chemical nature of the material precursor and of the solvent can exert an effect on the morphology and size of the microcrystallite particles [94].

CHAPTER III

LITERATURE REVIEWS

3.1 Syntheses Reviews

3.1.1 Niobium oxide syntheses reviews

3.1.1.1 Syntheses without surfactant

Amorphous niobium oxide could be synthesized by simply calcining niobic acid and hydrolyzing niobium(V) chloride ($NbCl_5$) or niobium(V) ethoxide and low specific surface areas of the products were usually observed after calcination.

For example, calcination of niobic acid ($Nb_2O_5.nH_2O$) in the work of da Silva et al. [39] obtained Nb_2O_5 support having specific surface area of 108 m^2/g after calcination at 450°C for 3 hours, while the value of 65 m^2/g were observed by Passos et al. [41, 42] for the niobic acid calcined at 500°C for 2 hours.

When niobium (V) chloride was mixed with methanol with pH raised to 6-6.5 by ammonium hydroxide, white precipitate of the Nb_2O_5 with surface area ranging from 18 to 39 m^2/g was obtained but the surface area dropped to only 10 m^2/g after calcination at 520°C [40]. By hydrolyzing niobium(V) chloride and washed in a boiling 50% aqueous solution of nitric acid for 48 hours, an amorphous niobium oxide was obtained with the BET surface area of lower than 10 m^2/g after being heated at 380°C for 3hours under reduced pressure [38].

In the V-Nb oxide systems, non-hydrolytic sol-gel condensation of $NbCl_5$ gave $NbVO_5$ with surface areas ranging from 1-3 m^2/g for all samples after calcinations at 550°C for 5 hours [95]. In the preparation of cobalt-niobia catalysts by the colloidal sol-gel technique, niobium (V) chloride was mixed with ethanol and

CCl_4 and gave the sample with surface area of 57 m^2/g after subjected to 550°C for 8 hours under hydrogen [96].

By using niobium(V) ethoxide as a niobium precursor and mixing with methanol ,HNO$_3$ acid, and water solution, xerogel niobium oxide possessing specific surface area of only 26 m^2/g and pore volume of only 0.03 cm^3/g was obtained after calcination at 500°C for 2 hours [37].

Other method such as thermal reaction of niobium(V) ethoxide in n-butoxide or toluene in an autoclaved heated to 300°C for 2 hours resulted in amorphous niobia with surface area of 135-155 m^2/g after calcinations at 500°C but the pore diameters were not reported [97]. Pore diameter of more than 10 nm. with BET surface area up to 205 m^2/g after calcinations at 500°C was reported in the work of Suh and Park, in which the aerogel niobium oxide was synthesized from niobium(V) ethoxide under supercritical condition [37]. Applying supercritical carbon dioxide in the synthesis using niobium(V) ethoxide in s-butyl alcohol mixed with water and nitric acid gave an amorphous niobia with higher surface area up to 190 m^2/g and pore volume of 1.280 cm^3/g after calcination at 500°C; though, the pore sizes were distributed in the range of 2-10 nm [98]. These supercritical conditions need high pressure and specific equipment. The xerogel obtained from the same system without super critical condition showed a crystallized niobia TT-structure with surface area of 100 m^2/g, pore volume of 0.184 cm^3/g and widely dispersed pore sizes from 2 to 20 nm [98].

The crystallized phase of niobia usually resulted in an uncontrolled pore size distribution of which the sizes become large and widely distributed. This is probably arisen from interparticle voids of crystalline particles. Also, the surface areas obtained were not large. These may be disadvantageous to the applications that need high selectivity of the adsorption such as adsorbents, catalysts and chemical/biological sensors [11, 55].

The synthesis techniques that carry out the reaction mixture of niobium precursor in heated vessel usually resulted in nanocrystalline niobia products at the temperature used for the synthesis. For example, the reaction mixture of niobium(V) ethoxide and benzyl alcohol inside an autoclave at 220°C for 4 days resulted in

crystalline niobia nanoparticle [99]. Spherical crystalline niobia was obtained

after 15 minutes heating at low temperature of 300°C, in the niobium(v) ethoxide -

diethylene glycol-water system [100]. Different morphology of niobia nanocrystals

having surface area of 79-327 m^2/g were obtained after treated at 140°C and 120°C,

respectively, in the hydrothermal treatment of niobium peroxo complex. In this

method, an adequate precursor i.e. niobium peroxo complex was required and the step

to obtain the suitable precursor is needed prior to the hydrothermal treatment. The

pore diameter was 24.8 nm for the sample treated at 120°C while bimodal pore

diameters of 41 nm and 93 nm was observed after treatment at 140°C [101].

3.1.1.2 Syntheses with surfactant

The niobium oxides possessing high surface area with narrow

distribution of pore size in the range of 2-6 nm were obtained by using surfactant as a

template. The surfactant employed could be an ionic single chain molecule such as

tetradecylamine or a non-ionic surfactant of block copolymer type such as the triblock

copolymer of the type $EO_nPO_mEO_n$.

The single chain surfactant normally resulted in small pore sizes and the

synthesis process was complicated. For example, in the work of Antonelli and Ying

[55], niobium(V) ethoxide was mixed with tetradecylamine and the precipitation of a

white solid was observed after adding water. This material was further aged for

several steps at ambient temperature at 80°C, 100°C, and 180°C and followed by

washing by water, ethanol, and ether for several times and dried in vacuum oven at

110°C. The amine surfactant was removed from the product by treatment with 70%

nitric acid at pH 1-2 in ethanol for 1-12 hours at room temperature, followed by

stirring in ethanol for 12-24 hours. Finally, they obtained the niobium oxide with the

hexagonally packed pores with the specific surface area of 400-600 m^2/g and the pore

size of about 2.5 nm.

The application of nonionic triblock copolymer, polyethylene oxide (EO)-

polypropylene oxide (PO)-polyethylene oxide (EO), as the surfactant template for

mesoporous transition metal oxides, including niobium oxide, was first reported by

Yang et al. [28]. They mixed the ethanol solution of Pluronic P123 ($EO_{20}PO_{70}EO_{20}$)

with niobium(V) chloride precursor. The obtained gel was consequently dried on an open Petri dish at 40°C in air for 1-7 days and calcined at 400°C for 5 hours. This material had specific surface area of 196 m^2/g and the pore size of 4 -5 nm with a hexagonally packed pore structure.

After the success in obtaining mesoporous transition metal oxides with stable and well-ordered pore structure of this work, there has been effort on researches to replicate the method for further investigation on its potential novel properties. The attractive motivation of the syntheses by using surfactant template to obtain the well-defined mesopous structure is the expectation on its possibility to intentionally tailoring the pore size through varying surfactant chain lengths or other strategies which will offer increased selectivity in reactions involving large molecules or for easiness to introduce dopant [55]. However, it is not easy to reproducibly obtain such well-defined porous structure [11].

Lee et al. [43] also synthesized highly ordered mesoporous mesoporous niobium oxide starting from niobium(V) chloride and triblock copolymer P85 (EO$_{26}$PO$_{39}$EO$_{26}$) as the mesostructure directing template. They used propanol as the solvent and added the salt (Li$^+$, Mg$^+$, Ca$^+$, and Ba^{2+}) solution in the system. The final solution was applied onto glass plates and the gel product was dried at 40°C for one week and after calcinations at 450°C for 5 hours in air, the products possessed specific surface area of 210-220 m^2/g and pore size around 4-5 nm. It was stated that the concentration and the timing of the addition of cations affected the regularity of the pores and the poorly ordered mesostructure was observed instead of the well-ordering hexagonal pore structure.

Tian et al. [46] grouped the acidic and basic precursors and the mixture of 'acid-base' pair precursors was claimed to give highly ordered mesoporous or mesostructured composite materials including metal oxides such as niobium oxide. For example, the niobium(V) chloride was designated as a strong acidic precursor and niobium(V) ethoxide was grouped to the basic precursor and the mixture of both precursors resulted in stable mesoporous niobium oxide products. The work implied that in order to prepare stable and homogeneous mesoporous materials, one needs to consider the inorganic-organic interaction, and the inorganic-inorganic (precursors)

interaction to produce a homogeneous and solid inorganic wall. By using the mixture of niobium(V) chloride and niobium(V) ethoxide with the same surfactant and similar method to Yang et al. [28], Xu et al. [47] produced the niobium oxide thin film of hexagonal mesoporous structure having surface area of 190 m^2/g and the pore size at 6 nm after calcination temperature of 350°C. In their work, the relative humidity and temperature in the drying condition was precisely controlled.

It could be seen in those works reviewed above that mesoporous niobium oxide has been developed through the well-ordered structure which is a result of the self-assembly behavior of the surfactant templates employed. The triblock copolymer gave larger pore sizes than the amine surfactant and most of the works employing triblock copolymer used niobium(V) chloride as niobium precursor. The procedures based on gel drying of those works were actually known as an evaporation-induced self-assembly (EISA) method. They seem to require precise controlled conditions in the syntheses. This is consistent to the observations that some negligible parameters such as water concentration, processing humidity and evaporation temperatures, may show a significant influence on the final materials obtained from the EISA process [49, 50].

3.1.1.3 Factors influencing textural properties of the mesoporous metal oxide synthesized with organic surfactant

There are many factors influencing the ordered structure, surface area, pore volume and pore size of the final mesoporous product.

3.1.1.3.1 Influence of water

The synthesis media consisting of high and low water content also exerts the effect on the behavior of the mesostructure formation system. The function of water is critical to the formation of inorganic skeleton and the promotion of the polymer template folding, which is the important characteristic of the micelle formation for the block copolymer surfactants [56, 58].

The role of water is twofold: its high polarity helps promoting domain separation of the PEO and PPO blocks by accentuating the difference between them. The presence of water also leads to inorganic polymerization (condensation), which takes place ideally in the polar (aqueous or alcoholic-aqueous) phase. The amount of water in the systems could considerably differ the hydrolysis-polymerization of the transition metals [56].

In the initial solvent-rich systems (typically, surfactant: metal: ethanol ratios are on the order of 0.01-0.1: 1: 30), chelation of the polar head of the surfactants to the metallic centres could be blurred due to the masking effect from the presence of polar molecules like ethanol. Upon solvent evaporation, the bonding by the polar heads becomes more predominant. In the PEO-PPO copolymer systems, where both fragments are able to chelate the metal centres, the chelation of the metal moieties to the polymer could alter the micellization behavior due to modification of the relative solubility of the blocks.

Soler-Illia et al. [56] proposed reaction pathways of the two extremes of 'anhydrous' or 'aqueous' conditions. In the case of anhydrous, or low hydrolysis ratios (water-to-metal ratio, $h \leq 1$) system, the polymer unfolding could be pronounced due to strong chelating effect of metal on the surfactant by covalent coordinative bonds. In this anhydrous system, condensation of the metal moieties can occur through water provided by residual traces of the polymer templates or a non-fully dried solvent and from air moisture. In the case of $TiCl_4$ mixed with ethanol, the $TiCl_{n-x}(OEt)_x$ species are formed and can condense through normal condensation reactions from the trace supply water, coupled with nonhydrolytic processes to form $Ti_p(OH)_yO_z(OR)_q$ oligomers.

In the aqueous route, rapid condensation to form oxo-metal oligomers could be favored. In this case where $h > 2$, the oxo-metal oligomers are hydrophilic due to the presence of OH group from water. The eventual interaction between the metal subunits and the polymers should be H-bonding type interaction, which enhances, rather than blurs, the solubility of PEO-PPO blocks and promote microscopic segregation to form micelle. The co-condensation of the hydrophilic clusters around the micelles finally forms the inorganic network.

It can be realized that the inorganic-organic interaction plays a critical role in the mesostructure phase formation [46, 56]. An adequate control of an organization, hydrolysis-condensation reactions and the interaction is a key feature to obtain the desired mesophase. Nevertheless, ordinary phase diagrams of surfactant could ideally be used as a first hint to find the water-to-surfactant ratio of the right position and make the system attain the desired mesophase.

3.1.1.3.2 Influence of inorganic salts

Salts affect non-ionic surfactants in many ways. Ions can promote the ordering of surfactant aggregates through charging by adsorption in the case of non-ionic surfactants and the mesophase diagram could be altered in the presence of salts [102]. For example, Niez et al. [103] synthesized mesoporous alumina by varying the amounts of 37 wt% HCl added in the system of aluminium tri-*tert*-butoxide and found that the resulting products after the gels were dried and calcined possessed different mesostructural ordering, textural properties and pore size distribution. Only the appropriate amount of the acid gave the hexagonal structure of monomodal pore size distribution while the lesser or higher amount gave the pore sizes that wider distributed into two regions.

The addition of some salts could dehydrate the non-ionics containing ether groups. In the mesoporous silica SBA-15 synthesized using P123 and tetraorthosilicate (TEOS) under microwave-hydrothermal condition [104], the pore size could be reduced in the presence of salt owing to the self-hydration of the salt that the PEO blocks become more dehydrated and the hydrodynamic volume of micelles was reduced [104]. The presence of NaCl salt was shown to enhance micellization of the block copolymer to occur at lower concentrations than in water at ambient condition. The presence of NaCl salt could also induce stronger interaction between polymer moieties and silica in this system. The pore volume, pore size, and specific surface area were also affected. For example, when using TEOS as the silica source, the specific surface area dropped from 820 m^2/g in the no-salt synthesis to 345 m^2/g when the salt was added for 23.3 mmol per 10 mmol of Si [104].

Yu et al. [105] investigated the effect of addition of salts such as NaCl and NH_4Cl to the mesoporous silica synthesized in the system containing TEOS, CTAB (cetyltrimethylammoniumbromide), NaOH, and H_2O. They found that the mesostructure phase transformation from well-ordered hexagonal to amorphous (disordering) could occur upon the increase in NaCl/surfactant molar ratio or the addition of NH_4Cl. The surface area and pore size distribution also varied upon different amount of the added salts.

The effect from anions could be stronger than cations effect and most mesoporous synthesis procedures employ cationionic or non-ionic surfactatants as templates are stongly affected by anions [102]. Alexandridis and Holzwarth [106] found that the presence of certain ions (such as Cl^-) in the aqueous solution decreases the solubility of the EO block. The critical micelle concentration (cmc) of non-ionic surfactants could also be decreased by anions such as Cl^-. The attractive interactions between non-ionic micelles can be increased and the non-ionic templating in the presence of anions may not always be non-ionic [49, 102].

The effect of anions or inorganic acid also exerts on the chemistry of hydrolysis-condensation reactions of the inorganic precursor. While the increase of acid anion concentrations, such as Cl^- in the form of HCl, reduced the time required for the silica mesophase to precipitate [87], the presence of HCl can control the hydrolysis-condensation reactions of the transition metal alkoxide and the addition of condensation inhibitors such as mineral acids like HCl is often used to avoid precipitation or segregation of a nonporous dense oxidic phase [10].

The appearance of the sol-gel products could be varied depending on the various amount of mineral acid. For example, when various amount of nitric acid was introduced to the niobium(V) ethoxide alcoholic solution. Large acid content resulted in transparent polymeric gels whereas lesser acid content gave translucent gels which contained precipitates within the gel network. Under weaker acidic conditions, the solution became turbid from the formation and precipitation of particulate materials [37]. Soler-Illia et al. [78] added the HCl into the system of titanium iso-propoxide or titanium iso-butoxide and used ethanol or butanol as a solvent and obtained both xerogel and precipitate depending on the conditions.

Using transition metal chloride precursor, instead of alkoxide precursor, is a way to introduce large quantity of HCl *in situ*. Grosso et al. [107] mixed $TiCl_4$ with ethanol and added water into the mixture. This solution was very acidic and showed no precipitates or further changes for several weeks, even when the water to metal ratio was 10.

However, using metal chloride precursor could suffer from the large amount of this chloride and from the chloride existing as an impurity.

3.1.1.3.3 Chloride effects from the chloride precursor

Niobium(V) chloride strongly reacts with water giving gelatinious precipitates of $Nb(OH)_3Cl_2$ while HCl gas evolves. Nb_2O_5 colloidal solutions or gels are then quite difficult to obtain through peptisation of the precipitate [76]. However, when niobium(V) chloride is mixed with alcohol, a chloroalkoxide is formed [44, 57, 76, 108], as in equation <3.1>.

$$NbCl_5 + ROH \text{ (excess)} \rightarrow NbCl_{5-y}(OR)_y + yHCl \qquad ...<3.1>$$

After hydrolysis of the niobium chloroalkoxide, chlorine was shown to still be present even after all OR groups have been removed [76]. Some works on niobium(V) chloride hydrolysis also indicated the existence of chloride remaining in the structure. For example, Da Silva et al. [39] hydrolysed niobium(V) chloride, that was earlier sublimed with the alumina support, under a flow of synthetic air saturated with water vapour at 60°C for 5 hours and heated the product to 450°C for 5 hours under a pure oxygen flow. The XPS results showed a considerable contamination of the surface with chloride anion, indicating that the hydrolysis treatment used was not enough for complete chloride removal. The researchers pointed out that the niobium sub-halides are considerably more resistant to hydrolysis than the corresponding penta-halides.

Ikeya and Senna [38] prepared an amorphous niobium oxide by hydrolyzing niobium(V) chloride and washed in a boiling 50% aqueous solution of nitric acid for

48 hours. The washed and filtered material was subsequently heated at 380°C for 3 hours under reduced pressure. They stated that the chlorine was still contained in the sample, up to ~3wt % and could only be removed by heating at temperatures above 550°C, where the crystallization simultaneously occurred. Yang et al. [44] used the energy dispersive X-ray spectroscopy (EDX) measurements and quantitative elemental analysis and detected weak Cl signals in the walls of the calcined mesoporous niobium oxide samples.

Parvulescu et al. [96] investigated the strong metal support interaction (SMSI) effect of the cobalt-niobia catalysts in the butane hydrogenolysis reaction and supposed that the chloride content remained from using chloride precursor could influence the SMSI effect exerted by niobia. Therefore, the existence of chloride in the sample could exhibit negative effect in its practical applications.

The presence of chloride as a chloroalkoxide results in oligomer species of the type metal-oxy-chloride that have different ability in inorganic network formation under the environment of surfactant micelles; hence, different hybrid inorganic-organic properties, when compared to metal-oxo oligomers obtained through an alkoxide precursor [107].

3.1.1.3.4 Effect of aging

The hybrid inorganic-organic phases of the product as-synthesized from acidic aqueous solutions present a relatively low stability to thermal treatment, due to incomplete condensation of the inorganic network because of the low initial pH values. Detailed structural and in-situ characterization shows that the immediately formed mesostructured hybrids are composed of an incompletely condensed inorganic framework that can evolve upon aging [54]. Grosso et al. [107] carried out the thermogravimetric along with chemical analysis and Rutherford backscattering (RBS) of the titanium dioxide mesoporous film derived from $TiCl_4$ and demonstrated that the Cl^- anions (initially present in the hybrid mesostructure) were released, probably as HCl or chloroalkanes, upon heating at moderate temperatures around 150-300°C at which further condensation took place and resulted in mesostructure contraction.

In the work Lee et al. [48], porous niobium oxide synthesized by niobium(V) chloride was unstable at the as-synthesized stage at 40°C and the second aging step at 100°C also regarded as the step to help stabilizing the niobium wall. By drying the gel product at 100°C for 1-2 days before washing, they obtained the microporous size of around 1.7 nm which was unchanged after subjected to high temperature treatment at 500°C.

Bagshaw [109] found that the pore morphology and characteristics of mesoporous silicate were changed upon subjecting to treatment in water at 100°C under autogeneous pressure after the product was dried. This was attributed to an internal dissolution-redirection mechanism which the silica layer at the template interphase could dissolve at the elevated temperature of the treatment and reprecipitate into a more dense phase on the pore wall when it supersaturated.

A high temperature aging not only affects the sol-gel or hydrolysis-condensation of an inorganic phase but also affects properties of surfactants. Aging of silica precipitates in the mother liquor at 80°C also showed an increase in pore size of the mesoporous products due to increase hydrophobicity of the EO block moiety [87].

3.1.1.3.5 Types of template effect

It has been accepted that the block copolymer such as P123 ($EO_{20}PO_{70}EO_{20}$), F127 ($EO_{106}PO_{70}EO_{106}$) could provide bigger pore size, compared to the single chain surfactant such as CTAB [52, 58]. The pore sizes of the mesostructure materials could also be adjusted by using different types of polymer template. For example, in the work of Kriesel et al. [66] the mesopores radii of the $AlPO_4$ and $ZrO_2.4SiO_2$ materials were found to be correlated with the length of the block copolymer employed and the F127 gave bigger pore sizes when compared to P123.

3.1.1.4 Importance of the pore size

Xu et al. [26] applied the porous niobium pentoxides as a matrix for immobilization of biomolecules having diameters of about 3.3 nm and 4.8 nm and

suggested the importance of large pore size and surface area in applying porous niobium oxide materials as a biosensor. The matching of the pore size of the mesoporous adsorbent with the size of biomolecules was also mentioned to prevent undesired conformation of the biomolecules.

Shimizu et al. [110] applied the ordered mesoporous tin oxide powder, synthesized by using tin chloride and triblock copolymer, as a gas sensor and detected the H_2 response. The study showed relatively large H_2 response of the sample having small specific surface area while larger surface area of 305 m^2/g in another sample but having smaller pore size at ca. 1.6 nm could be inactive probably due to the limitation of gas diffusion into the inner surface of the mesoporous structure.

3.1.2 Zinc oxide synthesis reviews

ZnO is also a material interested for many applications, including catalysis and sensors. Certainly the porous structure is expected to be advantageous. However, its syntheses of mesoporous form have scarcely been reported, the reason of which is the zinc cation is sensitive to acidic or basic environments and precipitation often occurs ,causing difficulty in obtaining a homogeneous ZnO gel for the formation of ordered nanostructure [111]. Complexing agent such as diethanolamine or monoethanolamine has generally been used as complexing agent in preparing ZnO sol and the different pH as a result of different amine agents added also effect the gel stablility [112]. Optimal gelation condition was investigated in order to obtain a homogeneous gel without precipitation in the solution started from zinc acetate dehydrate and ammonia solution, using citric acid as complexing agent [113].

Using organic molecules as templates to help forming ZnO have also been carried out but the suitable conditions were also sensitive. For example, ZnO porous thin films prepared by sol-gel with polyethylene glycol (PEG) as template were shown to be influenced by the PEG content, sol treated temperature, and sol concentration and the porosity could disappear when the zinc oligomers formed rapidly before PEG self-assembling [114].

The preformed copolymer gel template soaked with zinc salt solution was one interesting method to let Zn moieties inside the gel and prevent precipitation and aggregation of zinc cation. However, the pores of the products after calcination at 450°C were a result of interconnected particulate ZnO particles and the pore size distributions were quite broad [111].

The triblock copolymers of the type $EO_nPO_mEO_n$ such as P123 and F127 were also used in the sol-gel ZnO synthesized from zinc acetate dihydrate, lithium hydroxide system [115]. The properties of the mesoporous ZnO samples were only reported for the as-prepared mesoporous precursor (pre-calcined state) and the calcinations for template removal showed crystalline ZnO [115].

By using amine surfactants as template and carried out the syntheses at 0°C in the work of Ning et al. [116], although the pore size of about 3.8 nm and BET surface area of 95 m^2/g were obtained these properties belonged to the ZnO at the as-synthesized state after washing without subjected to higher temperature than 120°C of the degass condition.

Some other methods have been done on synthesizing porous ZnO. There are porous bulk ZnO solids obtained by treating of ZnO powders under pressures, or porous ZnO arisen from small particles after heat treatment. For example, porous ZnO ribbons were synthesized by oxidation of ZnS ribbons at 700°C in air [117]. Porous ZnO bulk solids were prepared by solvothermal hot pressing ZnO nanoparticles in water or cetyltrimethyl ammonium bromide (CTAB) solution [118]. These porous structure are generally composed of nanoparticles forming pores or channels, not the pores inside the particle [111].

In the work of P.Yang to synthesize mesoporous metal oxides [44], gelation of $ZnCl_2$ and P123 ethanoic solution took more than 30 days and mesoporous ordering was not succeeded after calcination. Only recently that Wagner et al. [119] succeeded in synthesizing highly ordered mesoporous ZnO with very small crystal domains within the pore walls. However, the synthesis procedure, which needed two-step replication of silica SBA-15 and carbon CMK-3, is quite complicated.

In contrast to small amount of researches on porous ZnO, relatively large amount of approaches to preparing shape-controlled ZnO nanoparticles have been reported due to the wide direct bandgap property of ZnO which results in its variety in electronic and photonic applications [21].

Vapor-liquid-solid epitaxy is one of the common methods for achieving vertical alignment of ZnO nanowires on lattice-matched substrates [120, 121]. However, the main limitation of the epitaxial growth methods is that the crystals are attached to a substrate or embedded in a matrix, which limits the range of possible applications [22, 122]. Other methods for synthesizing one-dimensional (1D) ZnO nanostructures include liquid-phase syntheses such as hydrothermal synthesis, solvothermal synthesis, precipitation method, direct deposition in aqueous solution, and colloidal routes. The wet chemical routes provide a promising way for large-scale production [34, 67] and have long been used for 1D-ZnO syntheses. Among these liquid-phase syntheses, the hydrothermal method is popular to prepare metal oxide powders of high crystallinity and dispersity [91]. There have been many adaptations of this simple process for controlling the size and shape of nanoparticles, such as the emulsion/surfactant assisted method and changes in precursors and reaction conditions. For example, Wei et al. [123] employed hydrothermal synthesis and used zinc acetate dehydrate and sodium hydroxide to synthesize ZnO nanorods having diameter in the range of 60-120 nm and the length in the range of 200-400 nm, which corresponds to aspect ratio of no more than 7. Ni et al. [124] obtained the rod-like ZnO products with the mean size of about 50 nm x 250 nm by hydrothermal method assisted by the cetyltrimethylammonium bromide (CTAB) as a growth directing agent. Most of these methods failed to produce rods with diameters less than 100 nm or with aspect ratio of more than 40 [18, 70, 125-129].

Li et al. [91] introduced the hypothesis of the growth unit of ZnO using zinc acetate solution. Many works also used zinc acetate as zinc precursor. It has been reported that anhydrous zinc acetate, can undergo decomposition and form ZnO nuclei within zinc acetate particles without forming any intermediates [130-132]. Nevertheless, the thermal stability of zinc acetate has been reported to depend on its interaction with the surrounding solvent [105, 130]. For example, Yang et al. [130] coated zinc acetate by different organic additives and investigated their roles on the

thermal decomposition process of the precursor. It was found that β-cyclodextrin coated zinc acetate had much higher decomposition temperature than the uncoated zinc acetate and this was explained by the interaction between the pair. The decomposition of zinc acetate has also been reported to be enhanced by increasing the content of water, in the system [131].

The presence of organic guest species in the zinc acetate precursor has also shown to effect on the growth of ZnO nanoparticles in the direct decomposition process of zinc acetate. The coating organics which formed weak coordinations to the zinc ions resulted in a non-homogeneous and bigger ZnO particle size compared to the system having an organic coating specie that could form strong interaction to the zinc acetate precursor [130].

A solvothermal process is a useful wet chemical route. In solvothermal synthesis, a solvent acts as a reaction medium that allows the relatively high temperature required for crystallization of inorganic materials to be achieved [133]. Patzke et al. [134] surveyed publications on the synthesis of oxide nanotubes and nanorods and concluded that solvothermal synthesis is one of the most powerful tools for providing distinct morphologies of nanomaterials.

Properties of the solvent, such as viscosity, saturated vapor pressure, and molecular structure leading to the steric hindrance effect have been proposed to be key parameters controlling nanoparticle formation [135, 136]. In the work of Lee and Choi [135], the shape and size of the nanocrystalline indium tin oxide (ITO) particles prepared under solvothermal process showed strong influences from the solvent viscosity; the increasing solvent viscosity increased the ITO size and the particle shape became more square. Hu et al. [137] have synthesized ZnO nanoparticles by using zinc acetate dehydrate and sodium hydroxide in various alcohol solvents varying from ethanol to 1-hexanol. The nanoparticle ZnO products obtained were quite spherical and the sizes increased with time and increasing temperature. The results suggested that the surface energy increases with increasing chain length of the solvent and the nucleation and growth of ZnO are faster in the longer chain length alcohols.

Zhang et al. [136] have reported that the polarity of the solvent affects not only the nucleus formation and preferential direction of crystal growth but also the amalgamation of crystals. Polarity compatibility between the reactant and the solvent led to homogeneous dispersion of the reactant in the mixture. Consequently, the growth of the crystal was less confined to the boiling droplet of solvent in the reaction system and resulted in a crystal with a flowerlike morphology.

The effects of solvents on ZnO nanoparticle synthesis, i.e., both nucleus formation and crystal growth, were indeed complex and many work dealing about morphological control synthesis of ZnO dealt with a solvent having hydroxyl group (OH$^-$) and this group was proposed to be a key factor for ZnO nucleus formation in the hydrothermal method [89, 136, 138]. However, solvothermal reaction in a medium that lacks a hydroxyl group, such as n-alkanes and aromatic compounds, has been rarely reported.

3.2 Reviews on Properties Related to Applications

3.2.1 Dielectric property of niobium oxide

Nb_2O_5 is a dielectric material having excellent chemical stability and are expected to be applicable in many electronic devices such as chemical sensors and biosensing technology [26, 27, 139-141].

In fact, previously, Ta_2O_5 having higher dielectric permittivity (dielectric constant) than the conventional silicon nitride-silicon dioxide structure has been employed as an corrosion resistant material, antireflection coating, insulating layer, and sensitive layer in various components, circuits and sensors. It has also been used in the applications like mobile phones and be of interest in the EDP (electronic data processing) power section applications, and all limiting space applications like hard disk drives, laptops or PDA's (personal digital assistant). Niobium belongs to the same group in the periodic system of elements and its chemical properties are very similar to tantalum. However, the niobium pentoxide Nb_2O_5, has a dielectric constant

of about 41, higher than the value of 27 of Ta_2O_5 and this makes niobium-based capacitors promising candidates as new high capacitance devices for the future [24].

Arshak et al.[142] developed a real time pressure monitoring system using an oxide dielectric layer to form thick film capacitors. The results showed that capacitors with an Nb_2O_5 layer were most sensitive, compared to those of titanium dioxide and cerium dioxide.

The process to form the dielectric niobium pentoxide could be similar to the tantalum case. However, by oxidizing the niobium, not only the dielectric Nb_2O_5, but also other suboxides like the metallic conducting NbO and the semiconducting NbO_2 also present. The presence of these suboxides could lead to a potential risk of higher leakage current or even failures in a capacitor [24, 143, 144].

However, from the observations, the niobium pentoxide dielectric material produced from the solution method such as sol-gel route or hydrothermal method mostly yielded the Nb_2O_5 phase without the presence of oxidation states other than Nb(V) and the niobium oxide prepared from these methods with the subsequent crystallization showed Nb_2O_5 crystalline structure, and not the NbO or NbO_2 structure [32, 97, 145, 146].

There are many factors that can influence the dielectric property of the material. For example, the low porosity [147, 148], the presence of hydroxyl group (or water) [149], high crystallinity [13, 150] and the larger particle size [151] could increase the dielectric constant.

In the work of Pignolet et al. [13], niobium pentoxide thin films have been deposited on substrates by reactive magnetron sputtering and the dielectric studies were made from the metal-insulator-metal (MIM) configuration of the films. It was found that the dielectric constant was improved with increasing oxygen partial pressure in the sputtering of the amorphous film. This was suggested to be a result of better stoichiometry in the high oxygen pressure condition which lead to a better structure and a better insulating nature of the film. The properties of the polycrystalline niobium pentoxide films resulting from the high temperature

annealing were also investigated and the results showed the improvement of the dielectric constant at 100 Hz from 32 of the amorphous films to 90 for the films annealed at 800°C which had the T phase Nb_2O_5 crystalline structure. The improvement of the dielectric constant upon crystallization was also observed for the Ta_2O_5 case of which its amorphous exhibit the value in the range of 22-28, while the values up to 40 could be detected when it's crystallized [150].

The dielectric measurement of the powder could be carried out in the form of pellets. Mohammed and Mekkawy [152] pelletized the zeolite powders into pellets of 10 mm in diameter and 0.5 mm of thickness with the hydraulic pressure of 5.0×10^3 kg/cm^2. By having the pellets tightly interfaced with polished silver disks in the Cu electrode holder, they conducted the measurements by varying the applied frequency.

Balkus and Kinsel [153] applied mesoporous niobium pentoxide (Nb_2O_5) thin film as capacitive type chemical sensors and found the enhancement of the capacitance response due to the high surface area of the mesoporous structure.

3.2.2 Applications of powder in a thick film sensor

The material in the powder form could be applied in the electronic applications such as sensors through the screen printing technology in which the powder would be blended with a binder to make a paste suitable for screen printing. The thick film technology produced by the method of screen printing has long been used as devices of measuring parameters such as humidity, gas vapours, radiation, strain and pressure. The film produced in this way can withstand many harsh environments and allow low-cost production with good reproducibility provided that the starting materials are very well controlled [142, 154, 155]. The use of nanosized powders in the fabrication of gas sensors by screen-printing technology also significantly enhances the sensor sensitivity [156]. In the capacitive sensors, the capacitance change is determined by comparison with the capacitance of a reference capacitor and the change could result from the absorption of an analyte into a polymer-coated layer leading to the change in its relative dielectric constant and resulting in a capacitance change [157]. In order to design an efficient capacitor

while minimize its dimensions, one needs a high dielectric constant material which can support the realistic working voltage applied on that device.

3.2.3 Photocatalytic property of niobium oxide

Niobia (Nb_2O_5) has been used as photocatalysts. It was shown to have higher selectivity but lower conversions than TiO_2 in liquid phase photooxidation of alcohols [35].

Niobia was tested for photocatalytic activity in the liquid-phase oxidative dehydrogenation of 2-propanol to acetone and mesoporous niobia material showed very poor photoactivity compared to a crystalline sample. The low activity was attributed to surface defects over amorphous mesoporous materials after surfactant removal [25]. However, porous nanostructures of materials such as ZnS showed a very high photocatalytic activity [158]. Chen et al. [34] used the EISA method similar to the work of Yang et al. [44] with two-step calcinations process and obtained well-ordered mesoporous niobia having surface area of 143 m^2/g after calcinations at 450°C. The sample showed superiority in photocatalytic activity in the hydrogen production from methanol, compared with the low activity of the more crystallized Nb_2O_5 powder obtained after calcinations at 500°C which showed surface area of 84 m^2/g.

3.2.4 Photoluminescence and photocatalytic properties of zinc oxide

Zinc oxide (ZnO) have also been used as photocatalysts and was shown to have similar photocatalytic activity with niobium oxide; having higher selectivity but lower conversions than TiO_2 in liquid phase photooxidation of alcohols [35].

For semiconductor material like zinc oxide, it has been reported that the photoluminescence (PL) spectrum can provide a quick evaluation of the photocatalytic activity of semiconductor samples [159]. The PL intensity could reflect the content of surface oxygen vacancies and defects and the higher the intensity, the higher the photocatalytic activity could possibly be [159]. The PL intensity could be affected by the nanoparticles size as the increasing ZnO particle size decreases the PL intensity [159]. The relative intensity ratio of the green

emission to the UV emission in the PL spectra was also observed to relate to the diameter of ZnO nanowire as the decrease of diameter size gave increase of the intensity ratio [160].

In the work of Li and Haneda [161], ZnO were synthesized from various methods (alkali precipitation, spray pyrolysis, and organo-zinc hydrolysis) and were tested for photocatalytic decomposition of acetaldehyde. Different morphology, e.g. rod-like particles, spherical particles, intertwined needle-like, or ellipsoidal aggregates, was indirectly presumed to have different exposed crystal faces which exerted an effect on different photoactivities.

CHAPTER IV

EXPERIMENTS

4.1 Mesoporous Niobium Oxide Syntheses

4.1.1 Syntheses of niobium-polymer solution

All syntheses began with the preparation of a niobium ethanoic solution by adding absolute ethanol (>99.9%, Merck) into niobium(V) chloride (99%, Aldrich) with a Nb: ethanol molar ratio of 1: 32.75. This was done under argon atmosphere using Schlenk line to evade the contamination of water from the air humidity. The solution of triblock copolymer of the type poly (ethylene oxide)-poly (propylene oxide)-poly (ethylene oxide), or $EO_nPO_mEO_n$, was made by dissolving F127 ($EO_{106}PO_{70}EO_{106}$; Aldrich) or P123 ($EO_{20}PO_{70}EO_{20}$; BASF) in absolute ethanol (with or without water). The polymer solution was added to the niobium solution to obtain a final molar ratio of (Nb: water (if present): ethanol: F127 or P123) of concentration as indicated in the Table 4.1.1. The mixture was stirred overnight (>15 hours) to ensure complete mixing of the niobium-polymer solution. The preparation was performed at room temperature (25-30°C).

The concentration of F127 or P123 in the polymer solution could be varied (from concentration c1 to c2, or c3) for an investigation of the effect of triblock copolymer concentration.

The amount of water added to the polymer (F127) solution could be reduced for an investigation of water effect. The presence of water in the polymer solution helps dissolving polymer, especially F127. When water was absent, the F127 ethanoic solution was heated to 45±5°C for better dissolution.

The niobium-polymer solution could be further added with water to investigate the effect of larger amount of water in the system. The water addition was done by a syringe pump at a rate of about 19.4 ml/min (if not specified otherwise).

The variation in the components was summarized into various code of concentrations and indicated in Table 4.1.1.

4.1.2 Dialysis of the niobium-polymer solution

If the solution was dialyzed, it was placed in a dialyzing membrane (Spectrum Companies, Gardena, CA, Spectra/Por 3, MWCO: 3,500). The dialyzing membrane of about 15 cm long was used per an aliquot of the solution containing 4 mmol of Nb and the solution was dialyzed against distilled water (75 ml per an aliquot of solution containing 4mmol of Nb), which was changed every 24 hours. The dialysis was carried out at room temperature (27-30°C). After the desired dialysis time (2 hours, 6 hours or 2 days), the material was hydrothermally aged in a closed vessel at conditions as indicated in Table 4.1.1. Then, the liquid was decanted following centrifugation at 3,000 rpm for 15 minutes before drying.

4.1.3 Aging the solution

If the niobium-polymer solution was aged, the aging process was done before drying. There are aging on a Petri dish (in an open air) at 40°C and hydrothermal aging.

For the hydrothermally aged conditions, the solution containing 8 mmol of niobium was put into a closed vessel (100 ml PTFE bottle) and heated (autogenious pressure) at desired temperatures and periods. The normal hydrothermal aging condition is 110ºC for 24 hours. Other conditions done for various samples were as indicated in Table 4.1.1.

4.1.4 Drying the solution

If the niobium-polymer solution was not aged, an aliquot of the solution was placed on a Petri dish to dry in an oven at 110°C (±5°C). The method is based on an evaporation-induced self-assembly (EISA) method where the solution gradually became gel and finally dried.

An aliquot of the solution containing 4 mmol of niobium or about 14.6 ml was placed on a Petri dish for the case of normal drying, while an aliquot of about 3.5 ml was applied for the case of thin layered drying (average film thickness of the xerogel of about 550 μm).

For the aged samples, the volume of the aged material synthesized from 4mmol of niobium was placed on a Petri dish and dried in an oven at 110°C (±5°C).

For the drying time, the time for the gel without any aging condition was about 6 days at a relative humidity (RH) >60%, or 1 day at a RH <30% for thin layer drying, and about a few days plus for drying at normal thickness. The hydrothermally aged solution could take about 7-14 days until the sample was dry. For the dialyzed samples having been hydrothermally aged, the remaining wet material after centrifugation could be completely dried within an overnight period on a Petri dish at 100-110°C.

4.1.5 Calcination

The dried material was scratched out of the Petri dish, crushed and calcined in static air using a box furnace at 500°C (or at other temperatures specified) for 5 hours (1°C/min ramp rate).

4.1.6 Sample Codes

The synthetic details of the samples (i.e. concentrations, and aging conditions) with sample codes are shown in Table 4.1.1.

The sample codes are in the form □-cn-ΔDM-◊, where □ indicates the use of F127 (F) or P123 (P), or nopolymer. cn is the concentration indicating ratio of the reagents. ΔDM represents dialysis where DM stands for dialysis membrane and Δ represents the dialysis time. ◊ is the code for aging condition. The ΔDM and/or ◊ would only be present in the code if the sample was dialyzed and/or aged,

respectively. The superscript t, present at the end of the code, indicates that the sample was dried at thin layer thickness.

For example, the sample code F-c1-2dDM-A means the polymer template was F127 with an initial concentration c1. This sample was dialyzed for 2 days and aged with condition A (110°C, 24 hours).

Table 4.1.1 Synthetic details and the sample codes

Sample Code	Template	Niobium-Polymer Solution Concentration[a]	Dialysis Time	Aging Condition[b]
P-c1x [t]	P123	c1x	No	No
F-c1x [t]	F127	c1x	No	No
P-c1 [t]	P123	c1	No	No
F-c1*	F127	c1	No	No
F-c1-d40	F127	c1	No	40°C 24h (dish)
F-c1-H40	F127	c1	No	40°C 24h.
F-c1x-A	F127	c1x	No	110°C 24h.
F-c1-A	F127	c1	No	110°C 24h.
F-c1W(2d)-A	F127	c1W(2d)**	No	110°C 24h.
F-c1W(3d)-A	F127	c1W(3d)	No	110°C 24h.
F-c1-A4	F127	c1	No	40°C 24h, 110°C 24h.
P-c2-A	P123	c2	No	110°C 24h.
P-c2	P123	c2	No	No
F-c1-2dDM-A6	F127	c1	2 days	60°C 24h, 110°C 24h.
F-c1-2dDM-A4	F127	c1	2 days	40°C 24h, 110°C 24h.
F-c1-6hDM-A6	F127	c1	6 hours	60°C 24h, 110°C 24h.
F-c1-2hDM-A6	F127	c1	2 hours	60°C 24h, 110°C 24h.
F-c1-2dDM-A	F127	c1	2 days	110°C 24h.
F-c1-6hDM-A	F127	c1	6 hours	110°C 24h.
F-c1-2hDM-A	F127	c1	2 hours	110°C 24h.
P-c1-2dDM-A	P123	c1	2 days	110°C 24h.
P-c1-6hDM-A	P123	c1	6 hours	110°C 24h.
P-c1-2hDM-A	P123	c1	2 hours	110°C 24h.
P-c2-2dDM-A	P123	c2	2 days	110°C 24h.
P-c2-6hDM-A	P123	c2	6 hours	110°C 24h.
P-c2-2hDM-A	P123	c2	2 hours	110°C 24h.
F-c3-2dDM-A	F127	c3	2 days	110°C 24h.
F-c3-6hDM-A	F127	c3	6 hours	110°C 24h.
F-c3-2hDM-A	F127	c3	2 hours	110°C 24h.
NoPolymer-c1-2dDM-A	-	c1	2 days	110°C 24h.
NoPolymer-c1-A	-	c1	No	110°C 24h.
NoPolymer-c1	-	c1	No	No

[a] where, for (Nb: Water: Ethanol: Template: Y) molar ratio;

c1   = 1: 37: 51: 0.0325: 0
c2   = 1: 37: 51: 0.0543: 0
c3   = 1: 37: 51: 0.0956: 0
c1w   = 1: 14.6: 51: 0.0325: 0
c1x   = 1: 0: 51: 0.0325: 0
c1W(2d) = 1: 37: 51: 0.0325: 472 (Y=Water)
c1W(3d) = 1: 37: 51: 0.0325: 944 (Y=Water)
where Y = Other chemical added to the solution before aging.
*, This sample was dried both at normal thickness and thin layer thickness.
**, The water addition was also done at a slower rate of about 0.23ml/min, added manually by a burette.
[b], aging in a closed vessel, unless indicated as (dish) which means aging on an open Petri dish.

4.1.7 Method for investigation of high temperature condition of an Evaporation-Induced Self-Assembly (EISA) method on the ordered structure of mesoporous niobium oxide

The samples were synthesized by using P123 and F127 as representatives of short and long PEO chain triblock copolymer, respectively. The EISA method was applied at 110°C and the amount of water in the solution was varied. The effect of the thickness of the drying solution was also investigated by comparing thin layer drying with normal drying condition for the condition using F127 and concentration c1. Hence, the samples being investigated are the P-c1x^t, the P-c1^t, the F-c1x^t, the F-c1^t, the F-c1x^t, the F-c1^t, and the F-c1 (see Table 4.1.1).

4.1.8 Method for investigation of aging effect on the properties of mesoporous niobium oxide

The samples were based on the system employing F127 as triblock copolymer and using concentration c1 and simple condition of drying at 110°C in an oven. Hence, the reference sample representing non-aged condition is the F-c1. The aging in an open atmosphere at 40°C was compared to the aging in a closed vessel (hydrothermal aging), and the samples are the F-c1-d40 and the F-c1-H40, respectively. The hydrothermal aging at 110°C was also carried out (the F-c1-A). Hence, the samples being investigated are F-c1, F-c1-d40, F-c1-H40, and F-c1-A (see Table 4.1.1).

4.1.9 Method for investigation of water effect on the properties of niobium oxide synthesized with triblock copolymer F127

The samples were based on the system employing F127 as triblock copolymer with concentration c1 and subjected to hydrothermal aging at 110°C (the F-c1-A). The effect of water was investigated by lowering the amount of water added to prepare polymer solution and by further addition of water to the niobium-polymer solution.

The samples being investigated are F-c1w-A, and F-c1x-A, representing samples of lower amount of water, and the F-c1W(2d)-A, and the F-c1W(3d)-A representing samples of higher amount of water (see Table 4.1.1).

4.1.10 Method for investigation of the influence of dialysis on the formation and structure of mesoporous niobium oxide from niobium(V) chloride

In this work the concentration of HCl was reduced by carrying out the reaction inside a dialysis bag to allow for the release of HCl from the initial sol. The HCl content was varied by varying dialysis time. The concentration and length of block copolymer employed were also varied in the syntheses to investigate their effect on textural properties under the same dialysis processes.

Note that the inorganic condensation is often incomplete after room temperature synthesis and a thermal treatment (aging) step is required to improve inorganic polymerization [10, 51] and preserve the mesoporous framework [48]. Therefore, to study the mesostructure of the dialyzed samples in this work, the properties of samples were compared after aging.

The samples being investigated are the F-c1-serie, F-c3-serie, P-c1-serie, and P-c2-serie (see Table 4.1.1).

4.2 Syntheses of Nanocrystalline Zinc Oxide

4.2.1 Materials and apparatus

4.2.1.1 Materials

Zinc precursors employed are anhydrous zinc acetate ($Zn(CH_3COO)_2$; 99.99%, Aldrich) and zinc acetate dihydrate ($Zn(CH_3COO)_2 \cdot 2H_2O$; 98%, Aldrich).

Four types of organic solvents were used in the experiments, i.e. alcohols, glycols, n-alkanes, and aromatic compounds. The alcohols were 1-butanol (99.4%, Ajax Finechem), 1-hexanol (98%, Aldrich), 1-octanol (99%, Aldrich), and 1-decanol (99%, Aldrich). Glycols used included 1,3 propanediol (98%, Aldrich), 1,4 butanediol (99%, Aldrich), 1,5 pentanediol (99%, Merck) and 1,6 hexanediol (99%, Aldrich). Alkanes were n-hexane (99%, Merck), n-octane (99%, Carlo Erba) and n-decane (98%, Fluka Chemika). Aromatic solvents were benzene (99.7%, Merck), toluene (99.5%, Ajax Finechem), o-xylene (97%, Aldrich), and ethylbenzene (99.5%, Carlo Erba). All chemicals were used as received without further purification.

4.2.1.2 Apparatus

Autoclave reactor is made from stainless steel. An iron jacket was placed inside to reduce the total volume from 1000 cm^3 to 300 cm^3. The test tube was used as chemicals reservoir.

Autoclave reactor used for the experiment is shown in Figure 4.2.1 and the diagram of the autoclave system, connected with nitrogen and temperature controller, is shown in Figure 4.2.2.
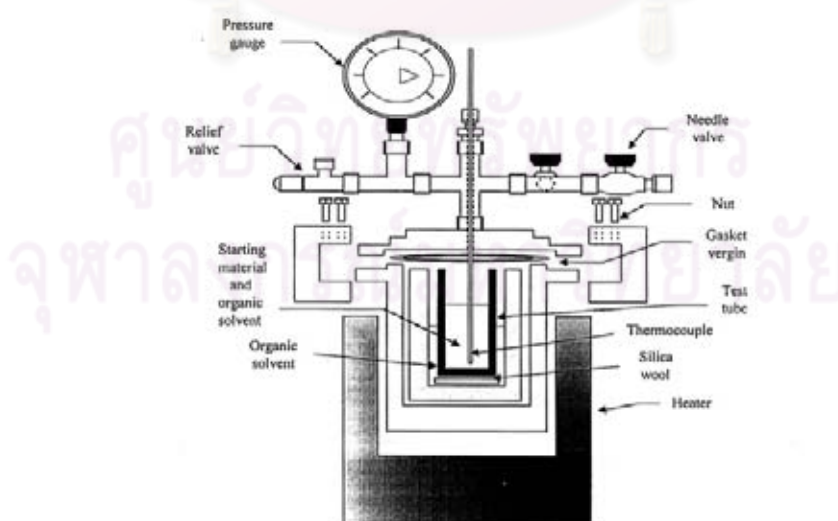
Figure 4.2.1 Autoclave reactor
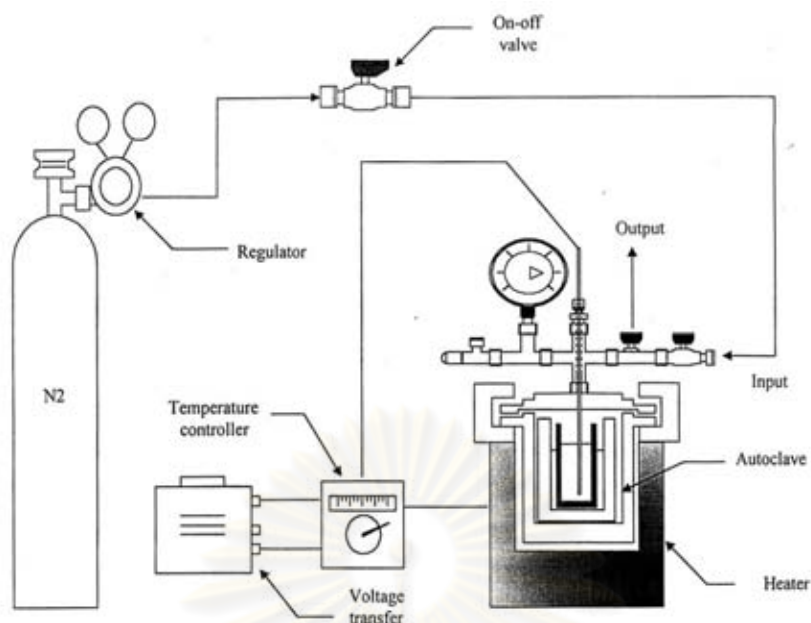
Figure 4.2.2 Diagram of the autoclave system connected with nitrogen and temperature controller

4.2.2 Method in syntheses

First, the precursor was suspended in 100 ml of solvent in a test tube. The test tube was then placed in a 300 ml autoclave. Additional 30 ml of the solvent was added in the gap between the test tube and autoclave wall. After the autoclave was completely purged with nitrogen, the autoclave was heated to desired reaction temperature, in the range of 250-300°C, at the rate of 2.5°C/min. Autogeneous pressure during the reaction gradually increased as the temperature was raised. The system was kept at the reaction temperature for 2 hours, after which the autoclave was cooled to room temperature. The resulting powder in the test tube was collected and repeatedly washed with methanol by centrifugation. The products were then dried in air.

4.3 Sample Characterizations

The pre-calcined products were characterized by thermogravimetric analyzer-differential scanning calorimeter (TGA-DSC), scanning electron microscopy-energy dispersive spectrometer (SEM-EDS), and small-angle X-ray scattering (SAXS). The calcined products were characterized by small-angle X-ray scattering (SAXS), powder X-ray diffractometer (XRD), transmission electron microscope (TEM) and selected area electron diffraction (SAED), nitrogen physisorption measurement and Raman spectrometer. The particle size in polymer solution was analyzed by Zetasizer.

The thermogravimetric analyzer-differential scanning calorimeter (TGA-DSC) analysis was performed with an SDT Q600 instrument. The sample powder of about 5-10 mg. was put in a 90 μl Al_2O_3 cup and heated to 750°C with a heating rate of 5°C/min, under oxygen flowing at 100 ml/min. The derivative thermogravimetric analysis (DTG) data was calculated using the % weight data, derivative to temperature (°C).

The scanning electron microscopy-energy dispersive spectrometer (SEM-EDS) was performed on JEOL (JSM-6400 and JSM-5410LV). The sample powder was dropped on two-sided carbon tape on top of a carbon stud for EDS measurement done at the Scientific and Technological Research Equipment Center, Chulalongkorn University (STREC).

Small-angle X-ray scattering (SAXS) measurements were performed on a Bruker Nanostar U diffractometer with Cu Kα radiation (wavelength, λ=1.54 Å) and 107 cm sample to detector distance. The sample was mounted in between a schotch tape and mounted on the sample holder. The measurements were performed by Mr. Alexander Mastroianni, Alivisatos' Group, Department of Chemistry, University of California, Berkeley, California, USA.

The powder X-ray diffractometer (XRD) was performed by SEIMENS D5000, using Cu-Kα (wavelength, λ=1.54 Å) radiation at 30 kV and 30 mA with a Ni filter. The 2θ range used was of 20-80° with a resolution of 0.04^o.

The transmission electron microscope (TEM) and selected area electron diffraction (SAED) was JEOL JEM-2010 and JEOL JEM-2010. The JEOL JEM-2010, with an accelerating voltage of 120 kV is located at the Scientific and Technological Research Equipment Center, Chulalongkorn University (STREC). The JEOL JEM-2010 operated at 200 kV is located at National Metal and Materials Technology Center (MTEC), Thailand. The sample powder was dispersed in absolute ethanol and sonicated for about 15 minutes before dropping on a copper grid (with Formvar film) or a carbon grid.

The nitrogen physisorption measurements were performed at 77 K using Micromeritics ASAP 2020. The sample was degassed at 180°C for 3 hours under vacuum before the adsorption of nitrogen. The specific surface area was calculated using the BET adsorption-desorption method [162] and pore size distribution was calculated by BJH (Barrett-Joyner-Halenda) desorption branch analysis. Specific pore volume was determined from the single point adsorption total pore volume of pores at relative pressure (p/p$_o$) ~0.99 and the average pore diameter was calculated from BJH desorption branch.

Raman spectrometer was the Perkin Elmer. Raman spectra were obtained with the 1,064 nm line of an Nd-YAG laser source. The exciting laser power was about 200-500 mW. The samples were pressed into the sample holder and measured with resolution of 4 cm^{-1} from 200-3500 cm^{-1}. The measurements were done at the Scientific and Technological Research Equipment Center, Chulalongkorn University (STREC).

The Zetasizer was Malvern, MAN0317. The polymer solution was analyzed without dilution. The refractive index was referred to the value of ethylene oxide. The experiments were done at the National Nanotechnology Center (NANOTECH), THAILAND.

4.4 Method for Investigation of Relative Dielectric Constant

4.4.1 Pelletizing the sample powder

The sample powder was pelletized by single-action mode die compaction under 40kN applied force or the pressure of about 3,073 kg_f/cm^2. The pellet of a disc geometry had diameter of 13 mm and height of about 0.87-0.91 mm.

4.4.2 Obtaining relative dielectric constant from capacitance measurement

The LCR meter was Agilent E4980A. The powder pellet was put in between two electrodes of the LCR meter. The function Cp-D was used to measure capacitance of the pellet. The bias voltage (AC) level was 1 volt, and DC bias was not applied. The frequency range was 50-1000 kHz. The Cp (capacitance) was read at each frequency. The calculation of changing capacitance into relative dielectric constant is shown in Appendix B.

4.5 Method for Investigation of Luminescence Property

The samples powder of 10 mg was dispersed in 10 ml of absolute ethanol and sonicated before measurement.

The spectrofluorophotometer Perkin-Elmer LS-50 at Center of Nanoscience and Nanotechnology, Faculty of Science, Mahidol University was used to examine photoluminescence (PL) performance of the samples. Xenon lamp was used as excitation source at room temperature and the excitation wavelength was 325 nm.

4.6 Method for Investigation of Photocatalytic Ethylene Oxidation Activity

4.6.1 Gases and apparatus

4.6.1.1 Gases

Ethylene gas reactant, supplied by Thai Industrial Gas (TIG) Limited, was 0.01% ethylene in air. Air used for pretreatment process was air zero, supplied by Thai Industrial Gas (TIG) Limited.

4.6.1.2 Apparatus

The reactor used was the Pyrex glass tube having diameter of 5 mm and length of 27 cm. The ultraviolet (UV) light sources were black light blue fluorescent bulbs (8 Watts).

The reaction system was comprised of four light bulbs surrounding the reactor in a square configuration, located at about 1.5 cm away from the reactor tube. The configuration is shown in Figure 4.6.1. Under the UV light, which supplied both light and heat for the system, the photoreactor was covered with two layers of aluminum foil to minimize radiation losses from the system. The system temperature was controlled by temperature controller connected with a fan as cooling system to maintain the temperature at 100°C. The mass controllers were used to control the flow rate of the gases.
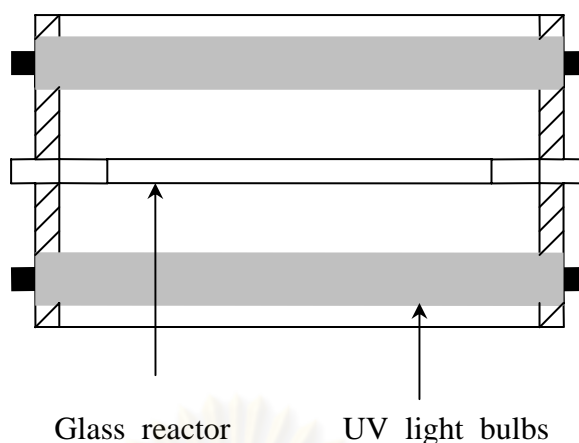
Figure 4.6.1 Photoreactor configuration

4.6.2 Experimental procedure

The sample of about 28 mg was dispersed along the length of the reactor tube plugged by quartz wool at both ends. The sample was pretreated by flowing air at 15 ml/min for 1 hour through the sample in the reactor tube under the UV light from the four bulbs and a temperature maintained at 100°C. After 1 hour, the air was turned off and the ethylene gas reactant was switched on with 17.2 ml/min flow rate. The gas sampling was done using the gas chromatography (GC-14B, SHIMADZU; see operating condition in Appendix C) to analyze the ethylene in the feed and outlet stream.

CHAPTER V

RESULTS AND DISCUSSION

5.1 High Temperature Evaporation-Induced Self-Assembly of Ordered Niobium Oxide

Mesoporous niobium oxide synthesized with P123 (with or without water) is poorly ordered with wormlike mesopores after calcination at 450°C, as indicated by the lack of a discernable SAXS peak (Figure 5.1.1a, b). In contrast, when meso-Nb_2O_5 is synthesized with F127, which has larger PEO blocks than P123, a sharp peak corresponding to a d-spacing of ~9.1 nm is observed, suggestive of a well-ordered mesostructure [10] (Figure 5.1.1c, d).
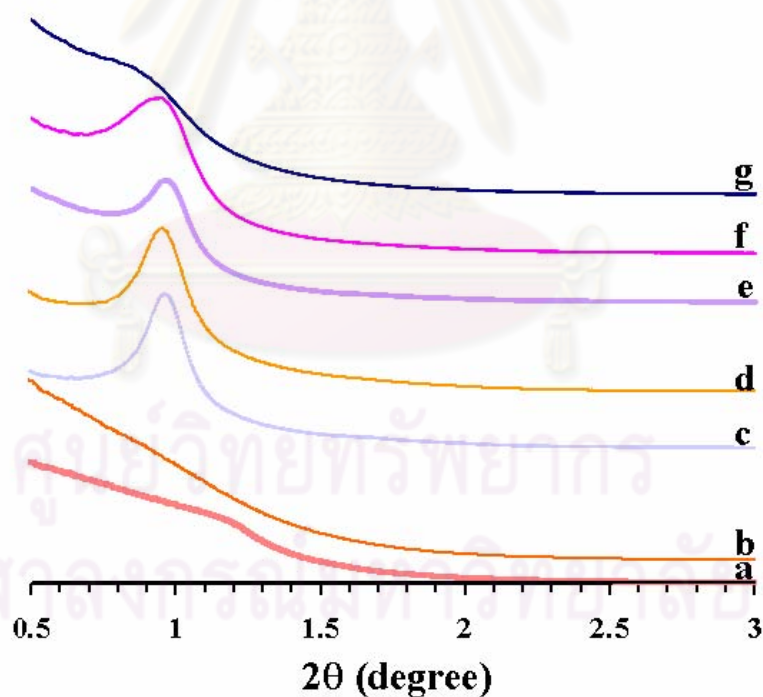
Figure 5.1.1 Small-angle X-ray scattering patterns of the calcined samples: a) P-c1x^t ; b) P-c1^t ; c) F-c1x^t ; d) F-c1^t ; e) F-c1x^t ; f) F-c1^t and g) F-c1. (a)-(d) are samples after calcination at 450°C for 5 hours (1°C/min), (e)-(g) are samples after calcination at 500°C for 5 hours (1°C/min)

Note that the patterns observed were of the calcined samples of which the ordering have been contracted or distorted from the as-synthesized (pre-calcined) state. The SAXS patterns of the as-synthesized samples of the F127 systems as shown in Figure 5.1.2c, d showed the sharp peaks at lower degrees, corresponding to a d-spacing of ~13.2 nm and 13.8 nm for the F-c1x^t and the F-c1^t samples respectively. The SAXS patterns of the as-synthesized samples of the P123 systems as shown in Figure 5.1.2a, b did not show discernible peak as significant as of the samples in F127 systems though the P123 showed some tiny node of scattering peak. Nevertheless, in both P123, and F127 systems, it seems that the anhydrous solution gave better or larger size of ordered structure, yet the differences arisen from the presence of water are so small.
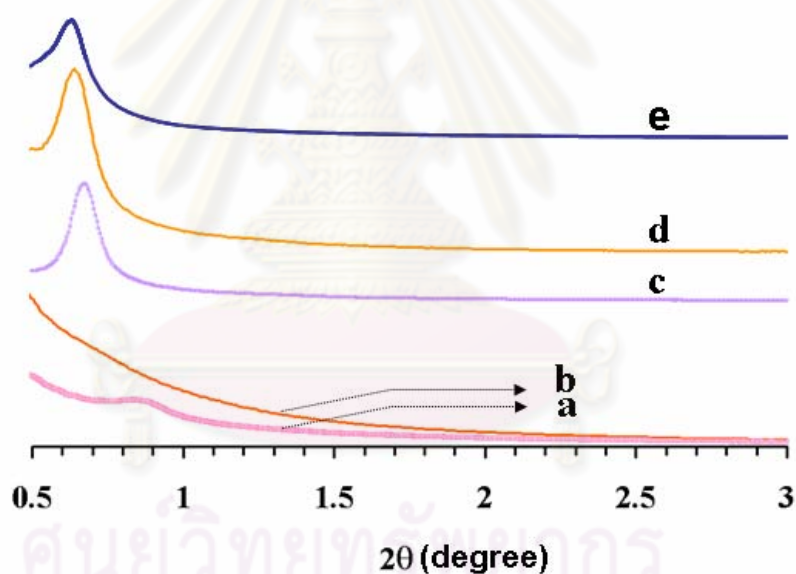
Figure 5.1.2 Small-angle X-ray scattering patterns of the as-synthesized
samples: a) P-c1x^t; b) P-c1^t; c) F-c1x^t; d) F-c1^t and e) F-c1

Well-ordered materials were obtained independent of the presence of water in the starting solution. Only a single diffraction peak is observed, which is difficult to assign to a particular mesophase [163, 164]. TEM indicates a hexagonally ordered assembly (Figure 5.1.3a, c), consistent with observations of mesoporous silica and titania synthesized with F127 as a templating agent [10, 78], though less-ordered, wormlike aggregates were also observed (Figure 5.1.3b, d). After calcination at

500°C, the peaks broadened, indicating degradation of the mesostructural order [10] (Figure 5.1.1e, f) but ordered regions could still easily be found in the TEM images. An example of TEM picture of the F-c1^t is shown in Figure 5.1.4. When the thickness of drying was changed, drastic effect occurred for the ordering of the structure. The results showed that thicker layer drying (drying as normal case) gave lesser predominant SAXS peak, corresponding to minor ordered structure (Figure 5.1.1g). However, the TEM picture of this sample (the F-c1) after calcinations at 500°C still showed well-ordered pore structure region along with the disordered region, as shown in Figure 5.1.5.

The pore size distributions of the samples calcined at 450°C are shown in Figure 5.1.6 and Figure 5.1.7 for the samples employing P123 and F127 respectively. Note that the samples employing P123 possessed the pore sizes below 4 nm while the samples employing F127 showed bimodal pore size distribution comprised of the smaller one centered at below 4 nm and at 5 nm for the bigger one. The pore size distributions of the samples employing F127 with and without water, calcined at 500°C are shown in Figure 5.1.8. Figure 5.1.9 showed the pore size distributions (PSD) of the sample F-c1 in comparison to the F-c1^t showing that drying at thicker layer also showed bimodal PSD. The textural properties of all the samples are shown in Table 5.1.1.

The pore size distributions (PSD) of the samples using F127 with or without water (Figure 5.1.7 and 5.1.8), are bimodal, consistent with the TEM results where the pores in disordered areas of the materials appeared to be smaller than those in well-ordered areas (Figure 5.1.3b, d and 3a, c, respectively). The smaller pore sizes observed were in the same range of what were observed for the non-ordered pore sizes of the samples employing P123 (Figure 5.1.6).
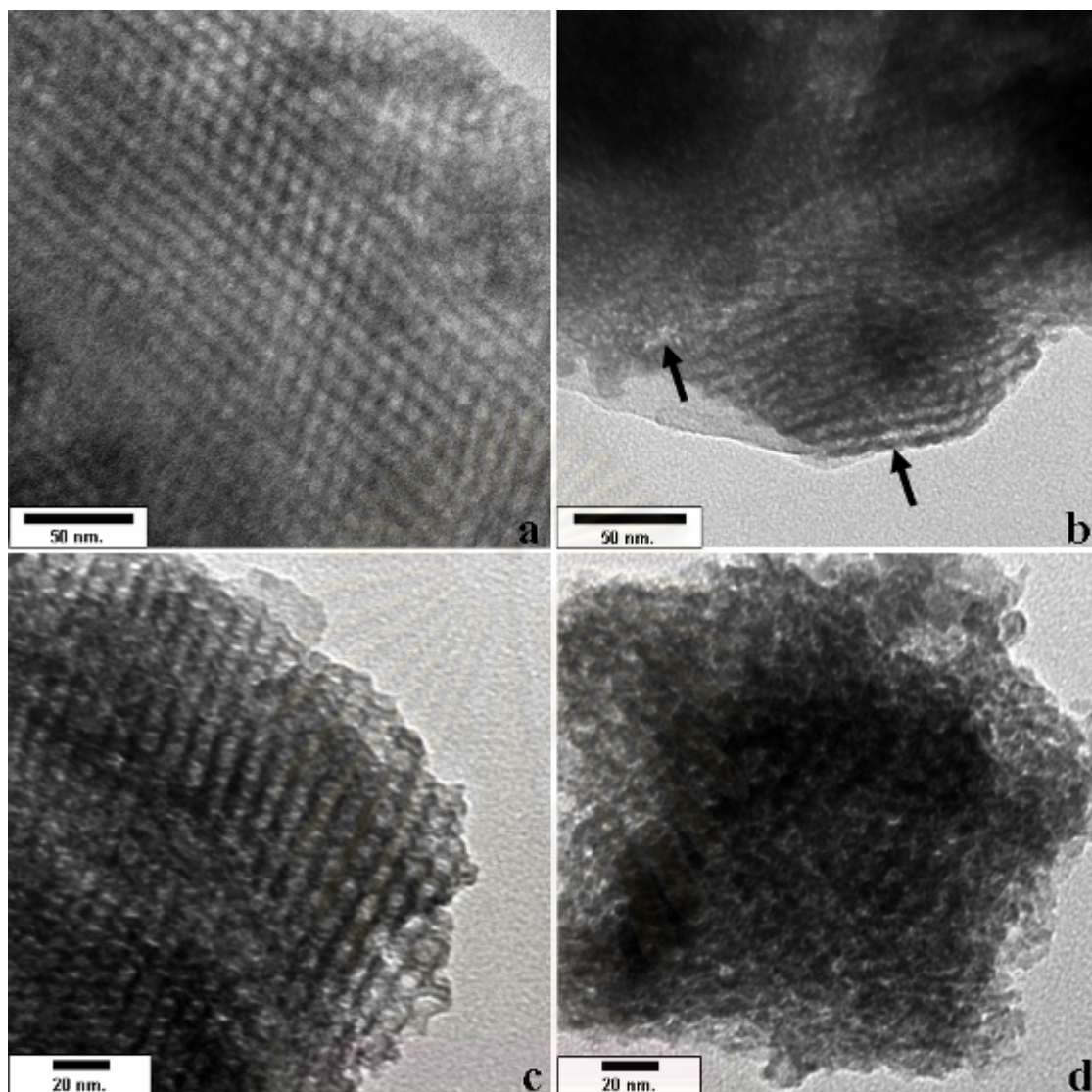
Figure 5.1.3 TEM images of the samples after calcination at 450°C for 5 hours (1°C/min): F-c1^t (a and b) and F-c1x^t (c and d) with (a) and (c) showing good hexagonal ordered assembly, (b) and (d) showing less-ordered wormlike aggregates. The arrows in (b) indicate a less ordered region with smaller pores and a more ordered region with larger pores.
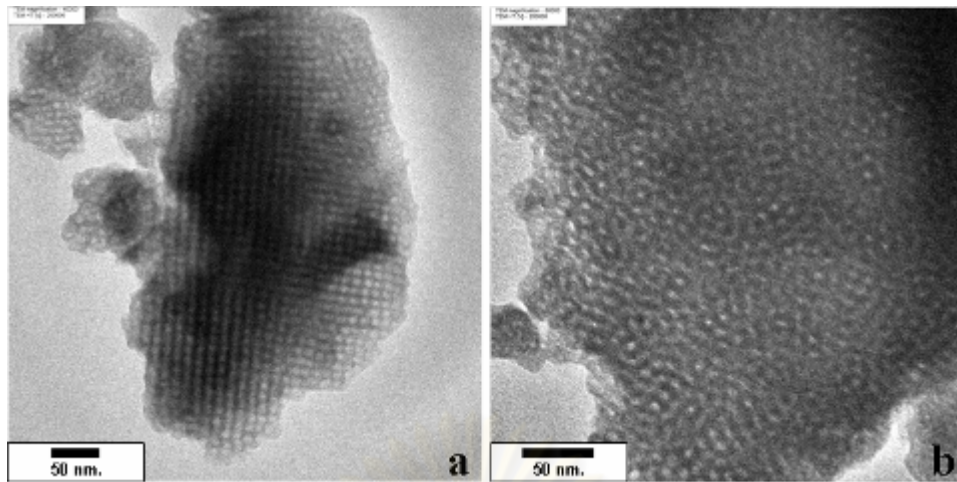
Figure 5.1.4 TEM images of the F-c1^t, after calcination at 500°C for 5 hours
(1°C/min); (a) the well-ordered pore structure region and (b) the less-
ordered region
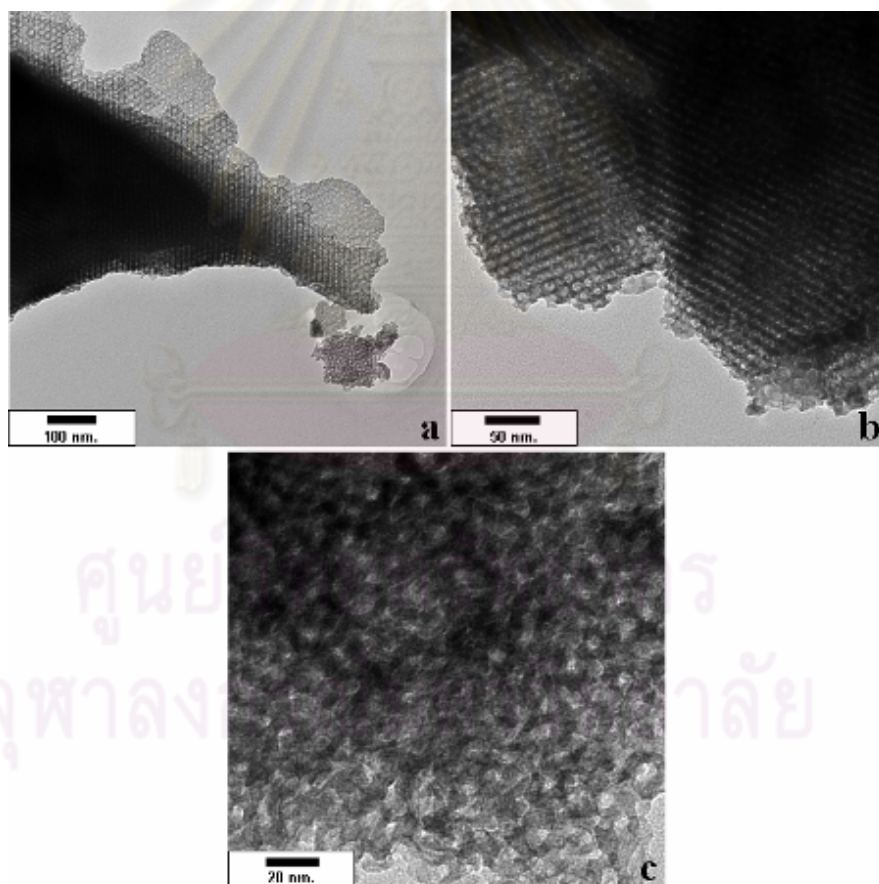
Figure 5.1.5 TEM images of the thicker layer drying (drying as normal case)
of the F-c1after calcinations at 500°C for 5 hours (1°C/min), showing
well-ordered pore structure region (a and b) along with the disordered
region (c)
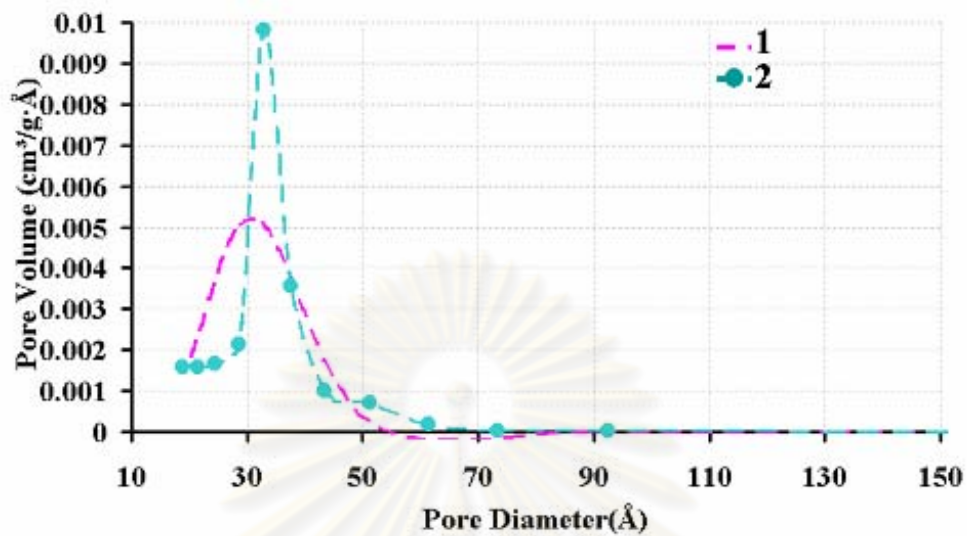
Figure 5.1.6 Pore size distributions (PSD) of the samples after calcinations at 450°C for 5 hours (1°C/min): 1) P-c1^t; 2) P-c1x^t , showing the pore sizes are below 4 nm
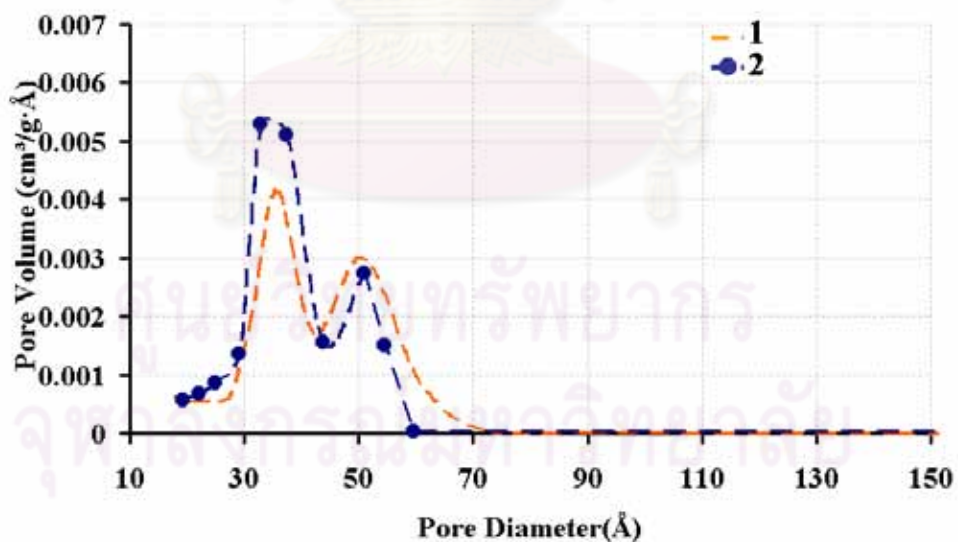
Figure 5.1.7 Pore size distributions (PSD) of the samples after calcinations at 450°C for 5 hours (1°C/min): 1) F-c1^t; 2) F-c1x^t, showing bimodal pore size distribution independent of the presence of water in the initial solution
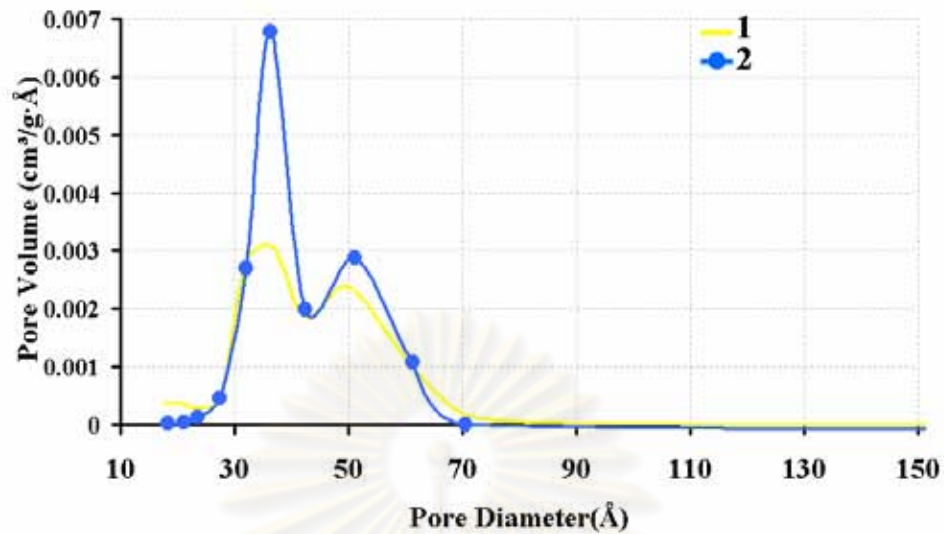
Figure 5.1.8 Pore size distributions (PSD) of the samples after calcinations at 500°C for 5 hours (1°C/min): 1) F-c1^t; 2) F-c1x^t, showing bimodal pore size distribution independent of the amount of water in the starting solution
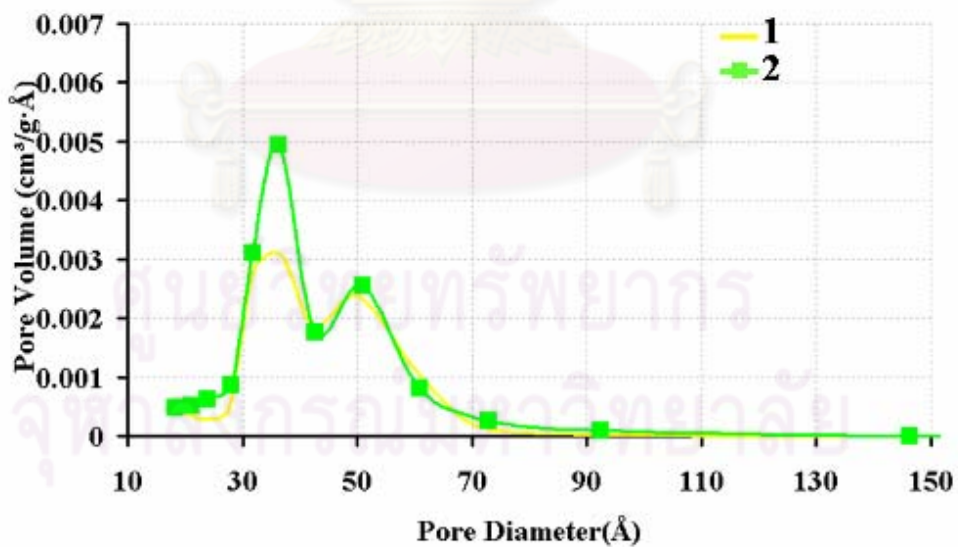
Figure 5.1.9 Pore size distributions (PSD) of the samples after calcinations at 500°C for 5 hours (1°C/min): 1) F-c1^t; 2) F-c1, showing that different drying thickness also showed bimodal PSD

Table 5.1.1 The textural properties of the samples, after calcinations at 450-500°C for 5 hours (1°C/min)

Sample	Calcination Temperature (°C)	BET Surface Area $(m^2/g)^a$	Pore Volume $(cm^3/g)^{a, b}$
P-c1x^t	450	101	0.099
P-c1^t	450	107	0.112
F-c1x^t	450	88	0.096
F-c1^t	450	89	0.104
F-c1x^t	500	78	0.104
F-c1^t	500	61	0.087
F-c1	500	78	0.099

[a], $\pm$ 10-20% error.
[b], determined from the single point adsorption total pore volume of pores at p/p_o~0.99.

At first, the presence of water and ethanol may blur the interaction between metal centers and the block copolymer [56]. However, after solvent evaporation at 110°C, the surfactant-niobium interactions increase, which alters the self-organization of the block copolymer [56, 78]. As the well-ordered structures are presumed to occur when these complexes preferentially chelate the PEO moietie [58], when these interactions strengthen and the metal centers coordinate with both the PEO and PPO blocks [56], the material becomes less ordered. This effect is more pronounced for surfactants with smaller PEO blocks [58, 163]. For F127, the PEO blocks are very long, hence, less interference from chelation effect of the niobium complexes to the block copolymer. Therefore, the polymer is more free to self aggregate into an organized phase giving an ordered structure of the final product more possibly obtained [163].

It has been known that, by the EISA method as used in this work, highly ordered mesostructures are sensitive to many external parameters [52] or the conditions to obtain the highly ordered structure lie in an extremely narrow range [43, 53]. The bimodal distribution of the samples employing F127 might result from the circumstances in which only some fraction of the niobia complexes possessing

appropriate amount of Cl as in the form of metal-oxo-chloride oligomer [44, 57] or as free ion around the molecule could interact with F127 molecules without disrupting their self-organization properties and the rapid condensation of the niobia under such high drying temperature could, at the right time, freeze the structure at the well-ordered state possessing one specific pore size [58, 78, 165]. The other fraction containing too strong interaction between niobia oligomers and the surfactant gave the less-ordered structure of smaller pore size due to improper folding of the polymer. The smaller size pores which might derive from the lack of dependence in molecular mobility of the surfactant could possibly be the pores between the niobia's growing particles after calcination.

For the effect of the water amount, although high polarity of water can promote solubility difference between PEO and PPO blocks and make proper self-organized phases more favored [56, 58], the well-ordered structures along with textural properties of the products obtained by the syntheses using F127 in the presence or absence of water or under drying in different relative humidity condition were not much deviated. These suggest that the longer PEO chain of F127 is more crucial on structural ordering than the presence of water for the present experimental cases. The method employing F127 under high drying temperature in this work ensures reproducible results to be obtained under different laboratory conditions.

Considering the mesophase in the drying period, the hybrid mesophase is highly flexible at a low degree of condensation [54]. Ethanol evaporation can induce or improve phase transformation of block copolymer micelles [78]. Simultaneous cross-linking of an inorganic phase could be enhanced by evaporation of HCl [44, 57]. After the 'rigid' inorganic framework resulted, the mesostructure is 'frozen' at the final structure [58, 78, 165]. For different layer of the drying film, HCl or ethanol evaporation from the mesostructure at the deeper level of the drying film is slower due to longer diffusion distances [10]. The mesostructure might not be 'frozen' and its flexibility could permit further adjustment of hybrid mesophase into a disordered state. The SAXS result of the F-c1 (Figure 5.1.1g) then showed much less discernible peak, compared to the thin drying film. Furthermore, the fraction of smaller pores seems to be larger for the F-c1, compared to that of the F-c1[t]. This may lead to the postulation that the disordered region giving the smaller size pores is a result of the

thick layer gel where evaporation of solvent, HCl is less efficient. However, it should be bared in mind that the discussion is just a presumption and the PSD can deviate and contain errors. The importance of the precise drying conditions to obtain well-ordered mesophase has been well acknowledged [49, 50, 52, 58, 78].

5.1.1 Summary

This work shows that the well-ordered mesoporous niobium oxide could be obtained by EISA method at high drying temperature of 110°C by employing F127, which has longer PEO chain length than the usual employed polymer; P123. At this high temperature drying condition, the importance of long PEO chain length showed more pronounced effect on the obtained reproduced well-ordered phase, than the presence of water in the initial solution. The presence of disordered phase which also observed with the well-ordered structure was believed to contribute to the bimodal pore size distributions. The method should be useful in synthesizing well-ordered mesoporous niobium oxide with reproducibility under different drying humidity of different laboratories.

5.2 Effect of Aging on the Properties of Mesoporous Niobium Oxide Synthesized with Triblock Copolymer F127 [51]

5.2.1 Effect of aging on the textural properties

Table 5.2.1 shows textural properties of the calcined products along with some of the results from the TG-DSC and SEM-EDS. All samples showed IV type isotherm with hysteresis loop (Figure 5.2.1a) which indicates the development of mesoporosity in the samples, and the mesopore volumes were significantly larger than the micropore volumes. Simple drying at 110°C (the F-c1) gave the lowest BET specific surface area and pore volume. The consecutively increases in BET specific surface area and pore volume were observed for the aged samples: F-c1-d40, F-c1-H40 and F-c1-A. The results of the t-plot micropore area and micropore volume also showed little higher microporosity of all the aged samples. The F-c1-A seemed to have highest BET specific surface area, pore volume and microporosity.

Table 5.2.1 Characterization results of the samples after calcinations at 500°C for 5 hours (1°C/min)

Samples	BET Specific Surface Area $(m^2/g)^a$	Pore Volume $(cm^3/g)^{b, c}$	Average Pore Diameter (nm.)	t-plot Micropore Area $(m^2/g)^f$	t-plot Micropore Volume $(cm^3/g)^f$	% Weight Loss at Crystallization[g]	Nb/Cl Ratio[h]
F-c1	78	0.099	4.1[d]	2.928	0.0005	2.1	44
F-c1-d40	91	0.120	4.1[d]	6.307	0.0020	0.6	22
F-c1-H40	105	0.157	4.5[d]	4.400	0.0009	0.6	17
F-c1-A	151	0.252	5.4[d]	9.732	0.0030	0.0	121
NoPolymer-c1-A	85	0.095	3.6[e]	-	-	0.0	n/d[i]
NoPolymer-c1	26	0.069	7.7	-	-	2.7	n/d[i]

[a], $\pm$ 10-20% error.

[b], determined from the single point adsorption total pore volume of pores at p/p_o~0.99.

[c], from BJH desorption.

[d], see pore size distribution in Figure 5.2.1.

[e], see pore size distribution in Figure 5.2.2.

[f], The value of micropore area is obtained from subtraction of t-plot external surface area from the BET surface area.
The t-plot calculations are based on the Harkins and Jura equation.

[g], from TGA in Figure 5.2.4.

[h], from SEM-EDS.

[i], not determined.

The pore size distributions were shown in Figure 5.2.1b. The sample directly dried at 110°C (the F-c1) showed mainly the pore sizes centered at about 3.5 nm with an observable fraction of the larger pore size which centered at 5 nm. Aging in an open air and hydrothermal aging at 40°C both made the larger size pores more widely distributed towards larger sizes. Significant increase of the pore size could be observed for the sample hydrothermally aged at 110°C (the F-c1-A) whose main pore sizes were centered at 6 nm with fraction of the smaller size pores much reduced.
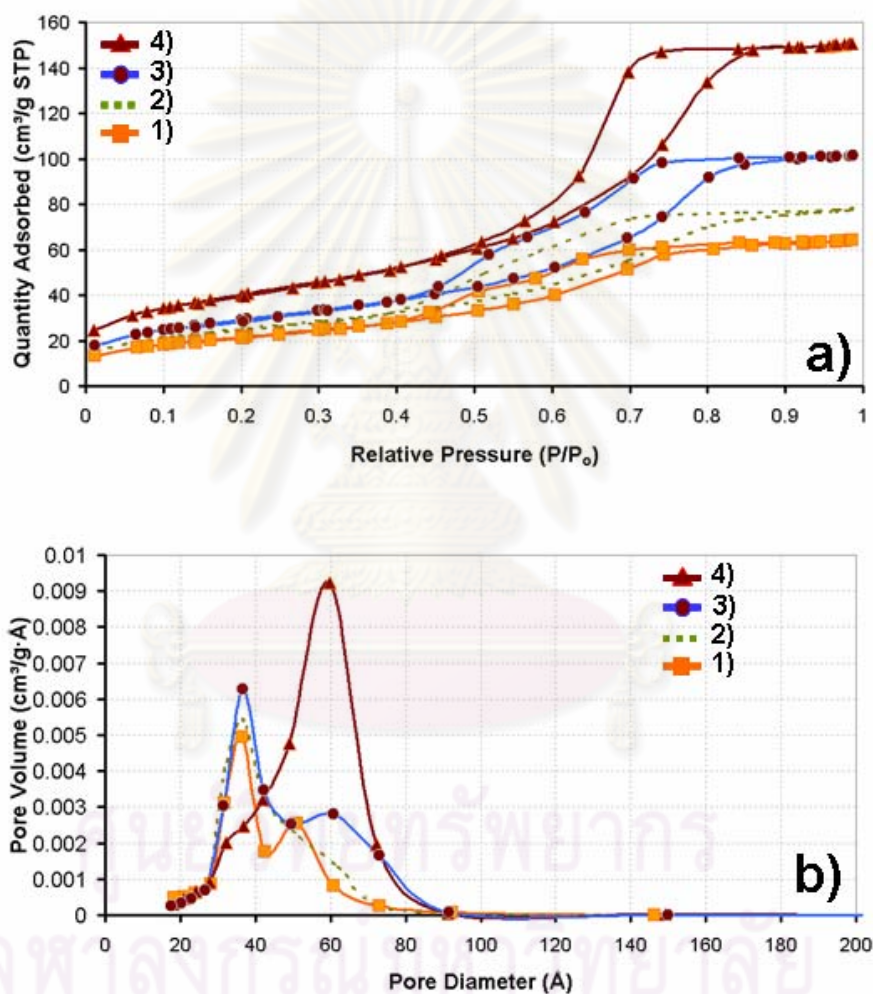
Figure 5.2.1 Isotherms (a) and pore size distributions (b) of the samples after calcinations at 500°C for 5 hours (1°C/min): 1) F-c1; 2) F-c1-d40; 3) F-c1-H40 and 4) F-c1-A

For the shifting of the pore size distributions observed, it seems that the fraction of the larger size pores were more flexible and more easily subjected to

changes. The mesophase having higher chloride anion distribution in the molecular scale might be responsible for the more flexibility of the hybrid mesophase adjustment [10], probably via the favoring chloride-mediated interaction over the direct metal-O-CH-CH$_2$-O [78]. The more flexible hybrid suggests that the inorganic-organic interaction is not too strong and the micellization of the F127 could be easily achieved resulting in the large pore sizes of the final oxide products. The stronger interaction, in contrast, might interfere micellization and gave only the small pore sizes arisen from the space formerly occupied by improper formed micelles. By imitating the synthesis process of the F-c1-A (the sample hydrothermally aged at 110°C) but employing no F127 in the synthesis the pore size distribution gave only one pore size centered at around 3.5 nm, as shown in Figure 5.2.2. It was found that the smaller pore sizes are similar to the pore sizes obtained from the synthesis using the same condition but without block copolymer. This suggests that the small pore size centered at around 3.5 nm in the F-c1-A sample may not be a result of the block copolymer micelles.
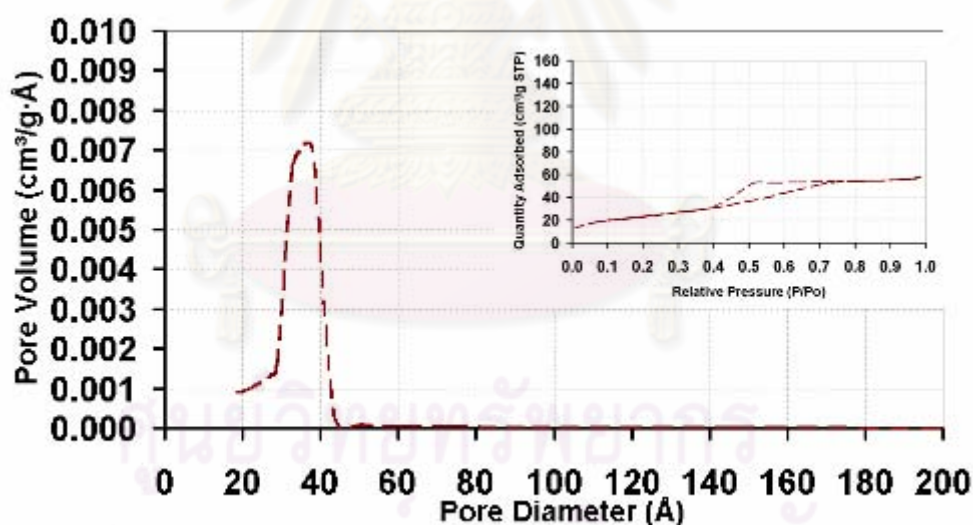
Figure 5.2.2 Pore size distribution and isotherm (inset) of the NoPolymer-c1-A, after calcination at 500°C for 5 hours (1°C/min)

For aging at 40°C, either on an open air or in the closed vessel, the shifting of the larger pore sizes to even larger size could be accounted from micellar expansion induced by ethanol evaporation at 40°C [166] but the consequent drying at 110°C

should have more pronounced effect on the product pore size distributions and only small deviation was observed as shown in Figure 5.2.1b.

The micellar expansion due to ethanol evaporation could also occur for the F-c1-A. However, its significant increase of the pore sizes should arise from the property of EO moieties of the polymer template which expel water and become less hydrophilic when the temperature is higher than 60°C [165]. This tends to provide larger hydrophobic portion of the template aggregates and the inorganic condensation, which takes place ideally in the polar phase (the phase where EO moieties generally occupy), would extend out to occupy the space of the aggregate corona further away from the micelle core, leaving larger pore sizes when the template is burnt out [58] .

The less hydrophilic properties of the EO part also reflects a weaker interaction between the organic and the inorganic (favorably attached to the hydrophilic EO moieties either directly or mediated by chloride anion) and provides more mobility for the proper folding of the block copolymer giving the larger pore sizes of the final mesoporous products. This explains the noticeable reduction of the fraction of smaller size pores with an increase in the fraction of the larger size pores of this sample.

The increase in surface area even with an increase in average pore sizes can be ascribed to the microporosity generated by the aging [59]. Although the t-plot has an error and limitation to access the true microporosity [59, 167], its results (Table 5.2.1) showing larger microporosity for all the aged samples could be used to support the cause of the increase in surface area even with an increase in average pore size. The high temperature aging could dehydrate EO moieties and reduce microporosity generated by entanglement of the EO units in the inorganic wall [58], but microporosity generated from the modification of the inorganic species themselves could contribute to surface area increase. Aging can promote the hydrolysis and condensation of the inorganic framework and the strength and stiffness of the wet gel could be increased [59]. This could yield a tighten structure giving a small pore in the niobium wall [168]. In the silica case [109], the hydrothermal treatment of templated silicate mesostructure at 100°C made silica at the interphase dissolved and

reprecipitated into a more dense phase on the pore wall. The high aging temperature at 110°C gave more remark on these effects than the low aging temperature at 40°C. The F-c1-A showed up to 150 m^2/g BET surface area even with large pore sizes of 6 nm. A less-shrinked gel also provides a greater pore volume of the dried gel due to higher ability to withstand capillary pressure [59] and explains the observations that the pore volume is increased with the surface area.

The TEM picture, along with its SAED pattern, of the F-c1-A is shown in Figure 5.2.3. The mesopores (lighter sections in TEM) and thick Nb$_2$O$_5$ walls (darker sections) can both be seen. The walls of the sample seemed to be comprised of elongated oxide particles and the rings in SAED shown in the inset of the figure indicate a large amorphous character in the sample.
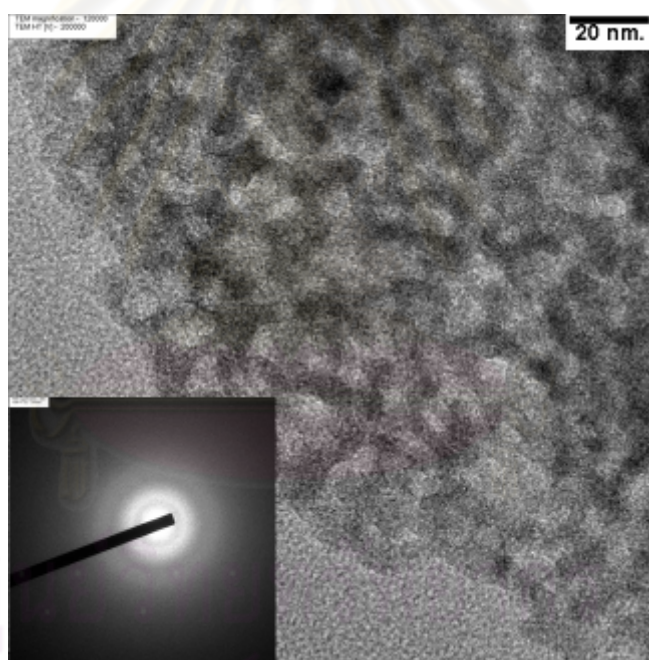
Figure 5.2.3 TEM and SAED pattern (inset) of the sample F-c1-A, after calcination at 500°C for 5 hours (1°C/min)

When the triblock copolymer type and concentration were changed into P-c2 system (see Table 4.1.1) the larger pore size as a result of the aging was also observed, similar to the F127 case. Figure 5.2.4 below shows the results of this system.
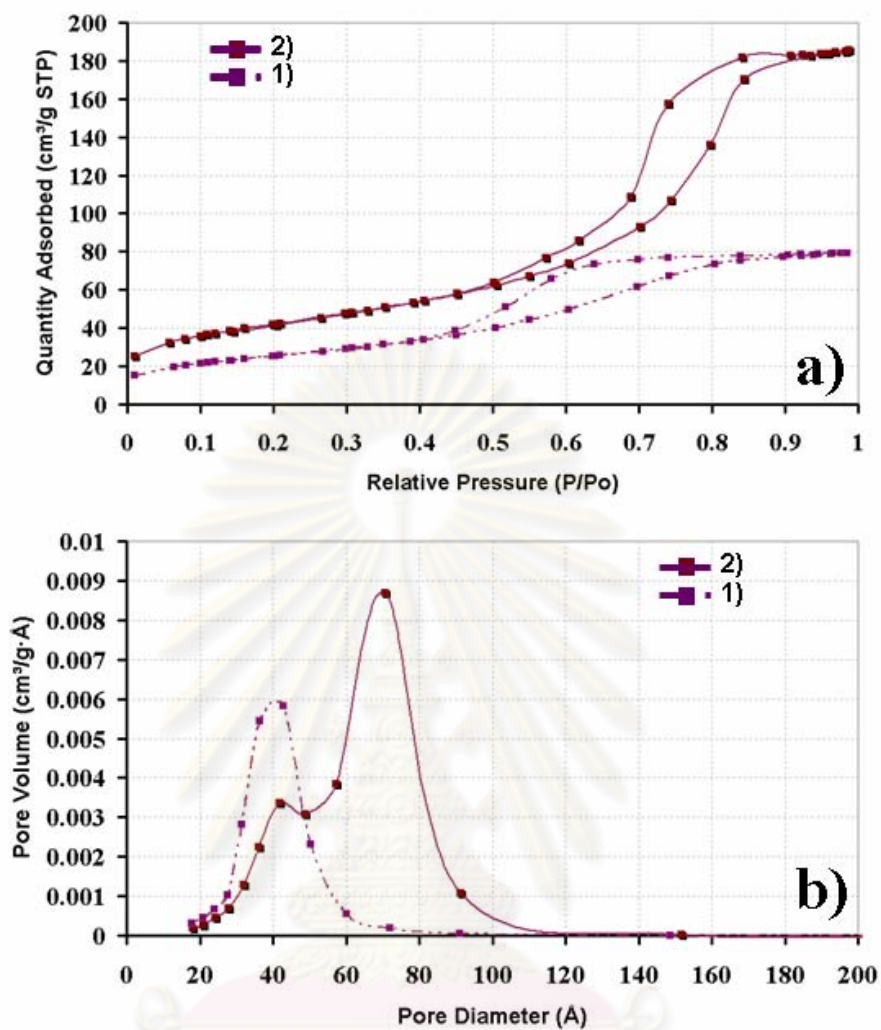
Figure 5.2.4 Isotherms (a) and pore size distributions (b) of the samples after
calcinations at 500°C for 5 hours (1°C/min): 1) P-c2 and 2) P-c2-A

5.2.2 Effect of aging on the thermal and structural properties

The TGA-DSC showing the thermal behavior of the pre-calcined samples are
shown in Figure 5.2.5 and 5.2.6.
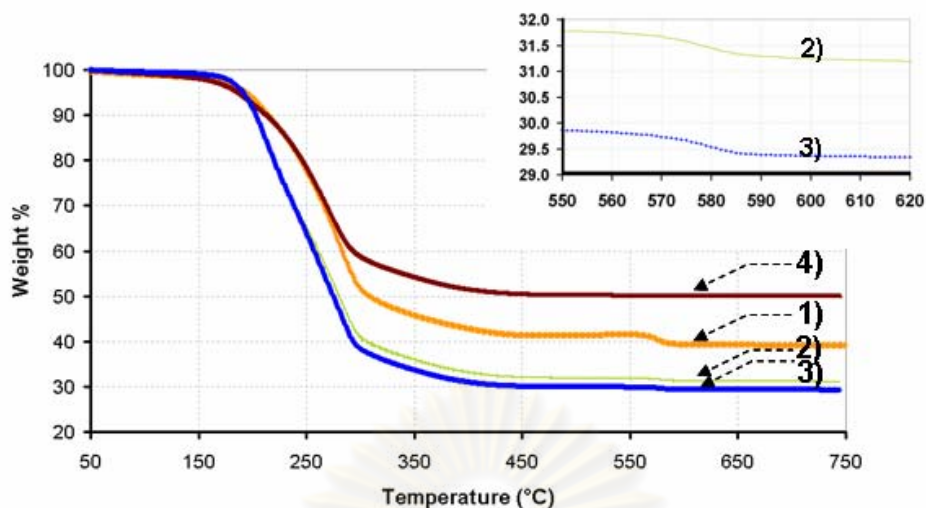
Figure 5.2.5 TGA results of the pre-calcined samples: 1) F-c1; 2) F-c1-d40; 3) F-c1-H40 and 4) F-c1-A. Inset is the enlargement of the 0.6% weight loss of the F-c1-d40 and the F-c1-H40
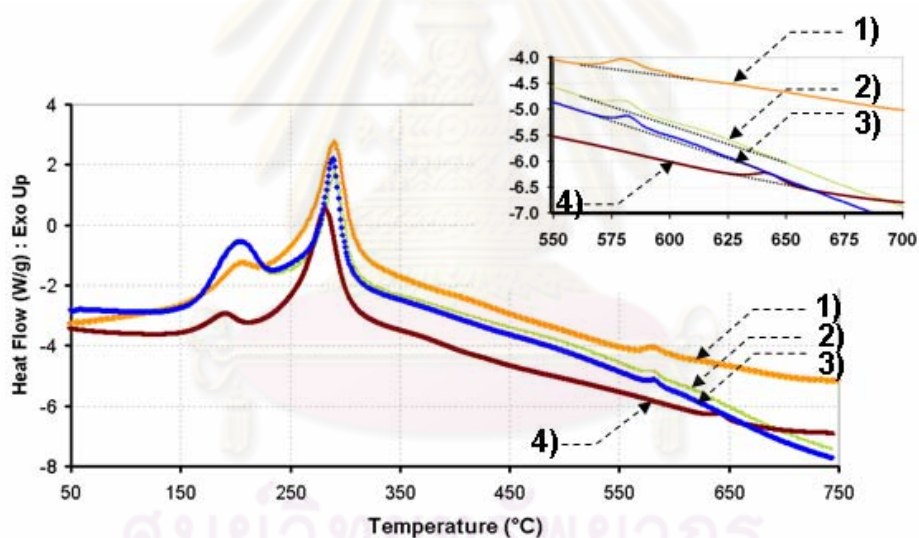
Figure 5.2.6 DSC results of the pre-calcined samples: 1) F-c1; 2) F-c1-d40; 3) F-c1-H40 and 4) F-c1-A. Inset is the enlargement of the crystallization peaks of all samples

In Figure 5.2.5, all TGA curves show an initial slow loss of water below ~200°C. More than 40% weight loss, corresponding to two main exothermic peaks in DSC curve in Figure 5.2.5, was observed from ~180-300°C. The minor exothermic peak occurred at ~180-250°C could be the release of trapped water/ethanol or HCl upon modification of the inorganic network [10, 78, 146]. The presence of this minor

exothermic peak probably depended on the amount of trapped HCl which also contributed to the weight loss observed. Chloride liberation as a result of further condensation, accelerated by thermal energy, was also believed to contribute to the overall weight loss but the event may occur simultaneously along the heating process. The higher the amount of Cl content (roughly inferred from low Nb/Cl ratio detected by SEM-EDS) the higher the weight loss observed in TGA data. The main exothermic peak centered at ~280-290°C, consistent with the large weight loss, is ascribed to main decomposition of the surfactant template [104, 169, 170]. This polymer decomposition shifted to lower temperature for the F-c1-A suggesting a little weaker bonding strength between niobium species and organic triblock copolymer of this sample [104], probably a result of EO dehydration or of a larger amount of Cl anion in the molecular hybrid structure [78]. The slow continuing weight loss after ~300-450°C could be a release of volatile compounds that still trapped inside the very small pores or within the wall structure [64, 78]. At the temperature ~580°C, there is another small exothermic peak in the DSC curve for all the samples except for the F-c1-A of which this peak occurs at ~640°C. These are attributed to crystallization of Nb_2O_5, which normally occurs above 500°C for amorphous Nb_2O_5 [171]. The crystallization of the F-c1, F-c1-d40 and F-c1-H40 all started at ~580°C and seemed to finish by the following small events at below 600°C for the F-c1. The F-c1-d40 and F-c1-H40 showed a continuous crystallization event along the temperature up to ~650°C, as shown by the blown out DSC in the inset of Figure 5.2.6. The crystallizations occurred with weight loss for the F-c1 (non-aged sample; see Figure 5.2.6) and the 40°C aged samples (both the F-c1-d40 and the F-c1-H40; see the inset of Figure 5.2.6) but not for the F-c1-A. The percentages of weight losses observed at the crystallizations of each sample are given in Table 5.2.1.

The weight loss of 2.1% detected at crystallization for the non-aged sample (the F-c1) is in good agreement with the weight loss with HCl removal at more than 500°C in the work of Schmitt et al. [146] and the 3 wt% removal of chloride detected in the work of Ikeya and Senna [38]. The weight loss detected at the crystallization was also observed for the non-aged alumina in the case of nonhydrolytic alumina gel using aluminum chloride as precursor and it was proposed to be from chloride compound liberation [172]. Therefore, chloride should be responsible for the detected

weight loss observed at the crystallization event for each sample in this work. The chloride here is believed to be the one that bonded to the niobium and required crystal structuring before being removed. It is different from the chloride presented as trapped HCl which corresponded to the minor exothermic peak in the DSC data.

The non-aged sample (the F-c1) might contain larger amount of chloride bonded to the niobium, when compared to the F-c1-H40 and the F-c1-d40. The latter two samples showed only 0.6% weight loss at crystallization. It is presumed that the hydrolysis-condensation reaction was enhanced by the aging period resulting in lesser chloride content in the niobium structure but larger fraction of chloride anion dispersed in the system. The lower rate of weight loss in the DTG data of the F-c1-d40 and the F-c1-H40 (see Figure 5.2.7) at 280-290°C should be a result of lower amount of the chloride linked to niobium hence lesser amount evolved with the organic polymer, when compared to the F-c1. The F-c1-A which showed lowest rate of weight loss in the DTG suggests that this sample should have a more complete hydrolysis-condensation reaction giving lesser evolving chloride to contribute to changes in weight loss per temperature.
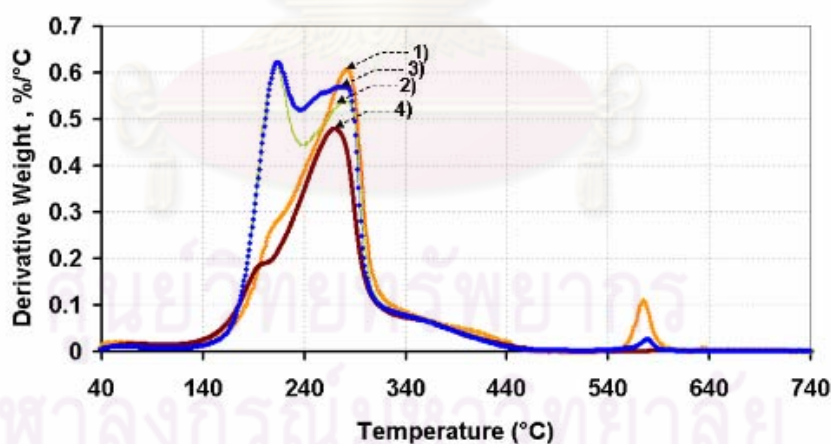
Figure 5.2.7 DTG data of the pre-calcined samples: 1) F-c1; 2) F-c1-d40; 3) F-c1-H40 and 4) F-c1-A

The fact that the F-c1-H40 and the F-c1-d40, when compared to the F-c1, showed longer tail of crystallization continuing along the higher temperatures suggests that the aging at 40°C might provide more fraction of niobia having harder tendency to crystallize. It is presumed that more dispersed chloride could act as an

impurity and prevent the crystallization of the oxide [173]. It is also possible that more entanglement of the block copolymer into the niobium wall could be responsible for this as its presence may prevent continuous structural arrangement of niobium oxide to form its crystallite structure. The F-c1-d40 showed a little longer tail of crystallization event than the F-c1-H40, probably because of more fraction of a less ordered molecular state might be generated while gellation occurred while aging in an open air at 40°C.

For the F-c1-A, its crystallization event occurred at much higher temperature when compared to the others. Besides, there was no detectable weight loss at its crystallization event. These may be related to the role of chloride that linked to the niobium and the high temperature aging condition that provided significant modification of niobia molecular structure.

It was known that chloride anions are able to form bridging in the niobium structure as a chloroalkoxide and still present after hydrolysis [76]. The role of chloride as complexing anion could change the positive charge of the metal atom and affect the metal-ligand bond strength leading to new molecular structure that exhibits new properties such as new chemical reactivity towards hydrolysis, condensation and new phase transition behavior [76]. Similar complexing ability was found in zirconia whose phosphate ligands are strong complexing anions able to act as bridging ligands and the existence of phosphate in the zirconia structure lead to higher crystallization temperature [174]. The hydrothermal aging at high temperature of 110°C possibly enhanced chloride complexing ability making chloride incorporated ('locked') well in the niobium structure and created new organized molecular structure which exhibited much higher crystallization temperature.

The distinct molecular state of the niobium skeleton obtained from the hydrothermal aging at 110°C could be supported by the crystal structure observed from the XRD. The XRD patterns of the samples after calcinations at 500°C for 5 hours (1°C/min) are shown in Figure 5.2.8. The F-c1 (non-aged sample) showed an amorphous characteristic with some evidence of crystallized structure whose pattern matches the pseudohexagonal Nb_2O_5 (TT phase: JCPDS 28-0317). The pattern of the

F-c1-H40 and the F-c1-d40 also indicated a pseudohexagonal structure, similar to the F-c1, with more amorphous nature mainly shown in the F-c1-d40 sample. These are consistent to the DSC results in Figure 5.2.6. For the F-c1-A, its pattern showed mainly amorphous characteristic but with hidden growing structure whose pattern matches the tetragonal structure (JCPDS 18-0911) having maximum intensity at 2theta ~23 degree [175]. These imply different nature of the niobia derived from different aging conditions, especially the distinct developing pathway of the niobia synthesized under hydrothermal aging at 110°C. When the samples were calcined at 600°C (1°C/min) (see Figure 5.2.8b), only the F-c1-A showed an orthorhombic Nb_2O_5 (T phase) with crystalline structure matching JCPDS 30-0873 while all the other three samples clearly showed a fully crystallized pseudohexagonal Nb_2O_5 (TT phase).
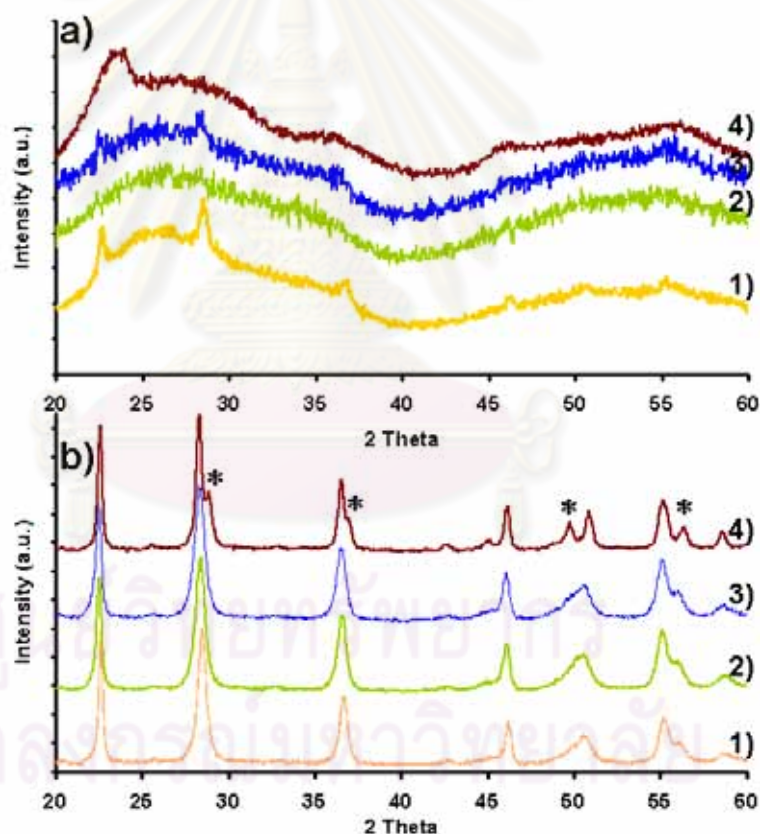
Figure 5.2.8 XRD patterns of the samples: 1) F-c1; 2) F-c1-d40; 3) F-c1-H40 and 4) F-c1-A. (a) after calcinations at 500°C for 5 hours (1°C/min); (b) after calcinations at 600°C for 5 hours (1°C/min). The splits in the pattern of an orthorhombic $T-Nb_2O_5$ which are distinguishable from a pseudohexagonal $TT-Nb_2O_5$ are indicated by the asterisks on the F-c1-A in (b)

The cause of the splits in the XRD pattern of the T phase were thought to be from some vacancies or monovalent species such as Cl^- that replace in some of the oxygen atoms positions of the normal pseudohexagonal TT structure [30]. The T phase was also found in the niobia obtained from high HCl content niobic acid in the work of Shafer et al. [171]. By recalling that an amorphous Nb_2O_5 possesses very similar features with the niobic acid [30], the phase transformation from an amorphous to an orthorhombic T structure of the F-c1-A should be induced by the chloride in the niobium structure even though the remaining Cl-Nb bonds should be very little after the hydrothermal treatment. Note that the T structure did not appear when employing niobium(V) ethoxide as a precursor and no Cl present in the system, comfirming the major role of Cl in inducing the T structure.

By imitating the synthesis process of the F-c1 and the F-c1-A but employing no polymer, or employing P123 ($EO_{20}PO_{70}EO_{20}$) instead of F127 ($EO_{106}PO_{70}EO_{106}$) in the syntheses, the DSC results in Figure 5.2.9 showed consistent results as what were observed for the F127-employed system. These suggest that the obviously higher crystallization temperature observed when the samples were subjected to hydrothermal aging at 110°C is independent of the polymer type and whether the samples were synthesized with or without organic triblock copolymer.
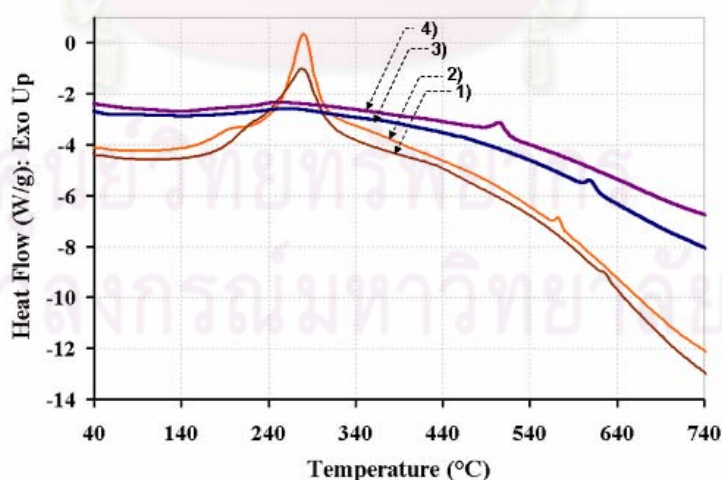
Figure 5.2.9 DSC results of the systems employing no polymer and the systems employing P123, showing an increase of crystallization temperature due to hydrothermal aging at 110°C. The samples are 1) P-c2-A; 2) P-c2; 3) NoPolymer-c1-A and 4) NoPolymer-c1

Apart from the distinct crystallization behavior observed, the hydrothermal aging at 110°C also showed exclusive Raman spectra. The Raman bands of all 500°C-calcined samples were shown in Figure 5.2.10.
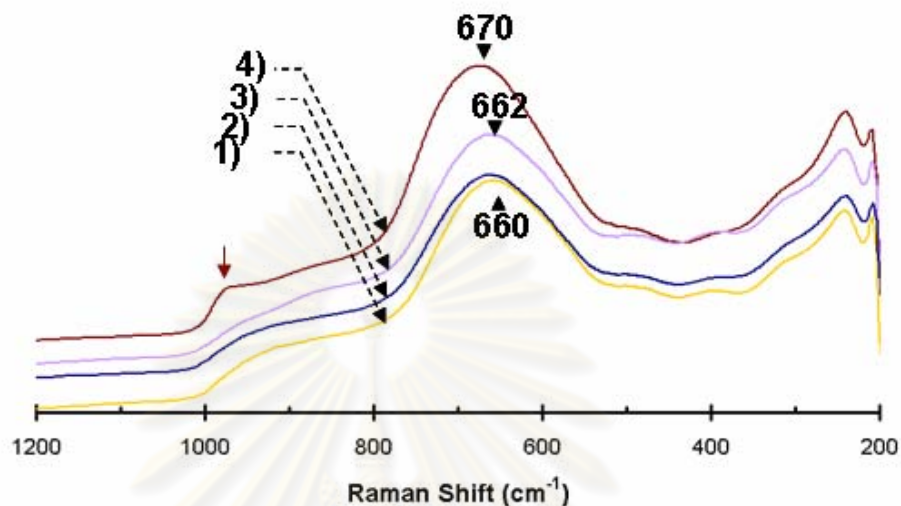
Figure 5.2.10 Raman shifts of the samples after calcinations at 500°C for 5 hours (1°C/min): 1) F-c1; 2) F-c1-d40; 3) F-c1-H40 and 4) F-c1-A. The Raman band between 900 - 1200 cm^{-1} indicating the presence of Nb=O bonds in the highly distorted NbO$_6$ octahedra is pointed by the arrow

All samples have Raman bands in common at ~200-300 cm^{-1} which are angle deformation modes of Nb-O-Nb and bridging Nb-O-Nb bonds [176] and at ~600-700 cm^{-1} which should be slightly distorted NbO$_7$, NbO$_8$ group or slightly distorted NbO$_6$ possessing Nb-O bond with no non-bridging oxygen [30, 176, 177]. The Raman shift between ~800-900 cm^{-1} corresponding to a highly distorted NbO$_6$ [177] was also found in all samples. However, the high frequency Raman bands observed at ~900-1200 cm^{-1} seemed to predominantly occur only for the F-c1-A. These bands and the shifting of the bands from 660 cm^{-1} to 670 cm^{-1} indicates that appreciably distorted octahedra with a higher niobium-oxygen bond order (Nb=O bond) are present in the F-c1-A [178]. This Nb=O bonds in the highly distorted NbO$_6$ octahedra are associated with Lewis acid sites [30, 98] indicating that after calcinations at 500°C, the F-c1-A showed higher Lewis acidity than other samples. However, this strong Lewis acidity was not observed for the same sample after calcination at 600°C when

the structure has been changed into an orthorhombic and the Raman bands at ~900-1200 cm^{-1} disappeared.

It was believed in this work that the high temperature of the hydrothermal aging step that 'locked' the (very small amount) of the chlorides to stay cross-linked with niobium in the structure and withstand the liberation upon thermal treatment might explain no detectable weight loss at the crystallization event of the F-c1-A. These also lead to high crystallization temperature observed in DSC, the distinct phase transformation observed in XRD and to the outstanding Lewis acidity evidenced by the Raman.

5.2.3 Summary

This work shows that the aging could modify the textural, thermal and structural properties of the mesoporous niobium oxide synthesized by using niobium(V) chloride and F127 in a water-ethanol system. The aging at low temperature of 40°C by dish drying and aging in a closed vessel showed small deviation of the pore size distributions, BET specific surface area, and pore volume from those of the non-aged sample. The surfactant micelle adjustment by different condition and the strengthened niobia network in the mesostructure wall due to an accelerated hydrolysis-condensation rate in higher temperature were used to account for the results observed. The hydrothermal aging condition at 110°C showed exclusive properties. This sample showed highest BET surface area, pore volume, pore size, and microporosity. Also, it revealed distinctly high crystallization temperature, with no detectable weight loss. Chloride was proposed to be locked within the niobium structure under the step of hydrothermal aging at 110°C, causing structural modification of the niobium skeleton to have distinct tetragonal phase at which an enhanced Lewis acidity was present and finally an orthorhombic crystalline structure after calcination at 600°C.

5.3 Water Effect on the Properties of Niobium Oxide
Synthesized with Triblock Copolymer F127 under Aging

5.3.1 Effect of water on textural properties

5.3.1.1 Effect of smaller amount of water

The polymer solutions used to prepare the samples were analyzed by the zetasizer to investigate the particle size distributed in the solution. In Figure 5.3.1, the results from the zetasizer showed that the F127 ethanoic solution (F127: EtOH = 0.0325: 18.25), used in the preparation of the sample F-c1x-A, has different particle sizes from the sizes obtained from the F127-ethanol-water solution (F127: EtOH: water = 0.0325: 18.25: 37) used for the sample F-c1-A. The latter solution showed an additional larger size particles of which size are about 10-100 nm. This size range is consistent to the block copolymer micelles size [82, 179], so the micellization was thought to favorably occur when water was present in the F127 solution. The F127 ethanoic solution showed translucent to opaque aspect, rather than the transparent aspect of the solution containing water. Hence, the sizes from 100 nm up which was predominantly observed in the F127 ethanoic solution could possibly be the sizes of the precipitated agglomerates of the polymer. When niobium ethanoic solution was introduced to 45-50°C heating, the opacity aspect of the F127 ethanoic solution disappeared and became translucent liquid.

However, the additional ethanol, niobium complexes, and HCl in the niobium solution might be able to interfere micellization [102, 180] and the block copolymer micellization behavior of the real system after mixing with the niobium solution should be different from the results in Figure 5.3.1. Nevertheless, the micelles sizes observed in pure polymer condition as shown in Figure 5.3.1 should guide for some explanation of the pore size distributions (PSD) of the corresponding samples; the F-c1-A, and F-c1x-A. Figure 5.3.2 shows the pore size distributions (PSD) of the F-c1-A, F-c1w-A, and F-c1x-A. The pore size centered at >4 nm was believed to reflect the pores that arisen from micelle while the pore sizes centered at ~3 nm could be the size of an interparticle void when the polymer was not employed [51], (also see the

previous issue; section 5.2). The PSD of the F-c1x-A comprised of only the small pore size which suggests that the micelle could not properly form in its water absent condition after hydrothermal aging at 110°C.
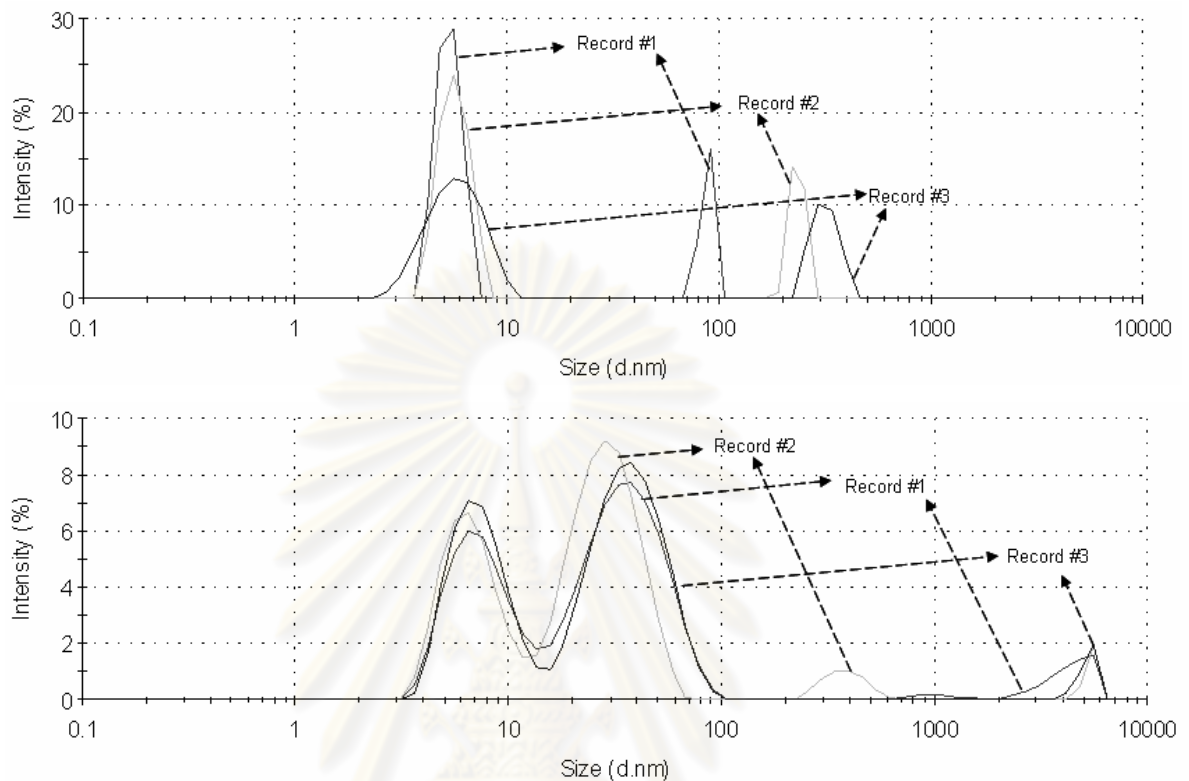
Figure 5.3.1 Particle size distribution: a) F127 ethanoic solution (F127: EtOH = 0.0325: 18.25) and b) F127-ethanol-water solution (F127: EtOH: water = 0.0325: 18.25: 37). Each solution was recorded 3 times
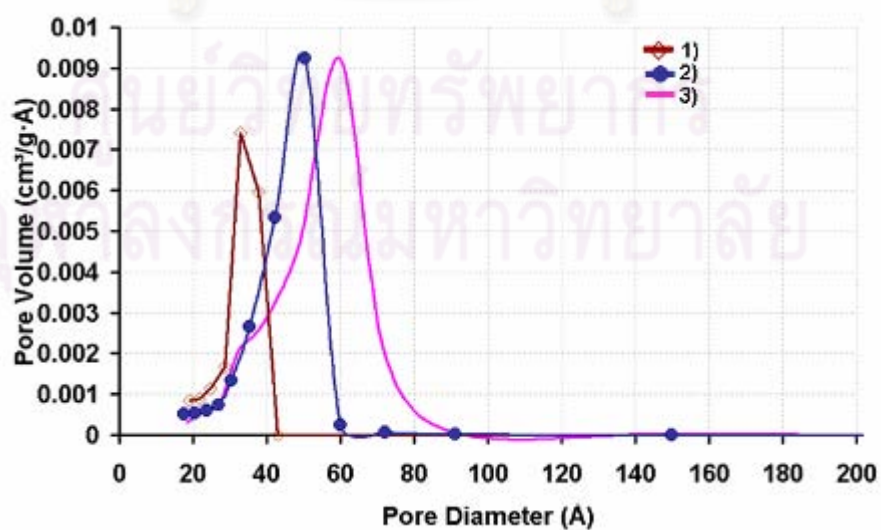
Figure 5.3.2 Pore size distributions of the samples 1) F-c1x-A; 2) F-c1w-A and 3) F-c1-A, after calcination at 500°C, 5 hours (1°C/min)

Table 5.3.1 Characterization results of the samples after calcinations at 500°C for 5 hours (1°C/min)

Samples	BET Specific Surface Area (m²/g)[a]	Pore Volume (cm³/g)[b, c]	Average Pore Diameter (nm.)[d]	t-plot Micropore Area (m²/g)[e]	t-plot Micropore Volume (cm³/g)[e]	Crystallization Temperature (°C)[f]	Crystallite Size (nm.)[g]	Nb/Cl [h]
F-c1x-A	86	0.089	3.2	-	-	590	44	32
F-c1w-A	108	0.152	4.4	-	-	624	49	80
F-c1-A	151	0.252	5.4	9.732	0.0030	642	43	121
F-c1W(2d)-A *(~0.23ml/min of water addition rate)*	108	0.121	3.7	-	-	620	n/d[j]	n/d[j]
F-c1W(2d)-A	134	0.235	5.5	5.720	0.0012	n/d[j]	23	n/d[j]
F-c1W(3d)-A	120	0.174	4.5	2.115	-	610	25	n/d[j]

[a], ± 10-20% error.
[b], determined from the single point adsorption total pore volume of pores at p/p_o~0.99.
[c], from BJH desorption.
[d], see pore size distribution in Figure 5.3.2, and Figure 5.3.3.
[e], The micropore area value was obtained from subtraction of t-plot external surface area from the BET surface area. The t-plot calculations are based on the Harkins and Jura equation.
[f], from DSC results (not shown).
[g],from XRD pattern of the samples calcined at 600°C for 5 hours (1°C/min) in Figure 5.3.4b. The sizes were calculated using Scherrer's formula on the (001) diffraction peak. The T structure corresponds to JCPDS 30-0837, and the TT structure corresponds to JCPDS 28-0317.
[h], from SEM-EDS.
[j], Not determined.

The intermediate amount of water in the sample F-c1w-A showed intermediate pore sizes (see Figure 5.3.2). The polymer concentration of this sample based on the total volume of the solution is still above the critical micelle concentration (cmc) [84] but the micelle size developed in this chemical environment should be smaller than that of the sample F-c1-A, giving smaller pore sizes than those of the F-c1-A [86]. Table 5.3.1 above shows textural properties along with thermal properties and/ or EDS results of the samples.

By comparing among the F-c1-A, F-c1w-A, and F-c1x-A, the lower amount of water added to prepare the F127 solution, the lower the BET surface area and pore volume (see Table 5.3.1). These could be due to the fact that F127 dissolution and micelle formation were unfavored when water was lowered. At the same time, an enhanced microporosity was probably depressed due to inappropriate extent of hydrolysis-condensation [59, 168] of niobium. Hence, the large surface area due to high microporosity and large pore sizes due to developed polymer micelle were reduced, resulting in lower textural properties observed.

5.3.1.2 Effect of larger amount of water

Figure 5.3.3 shows the pore size distribution of the F-c1-A, the F-c1W(2d)-A (of two water addition rates), and the F-c1W(3d)-A.
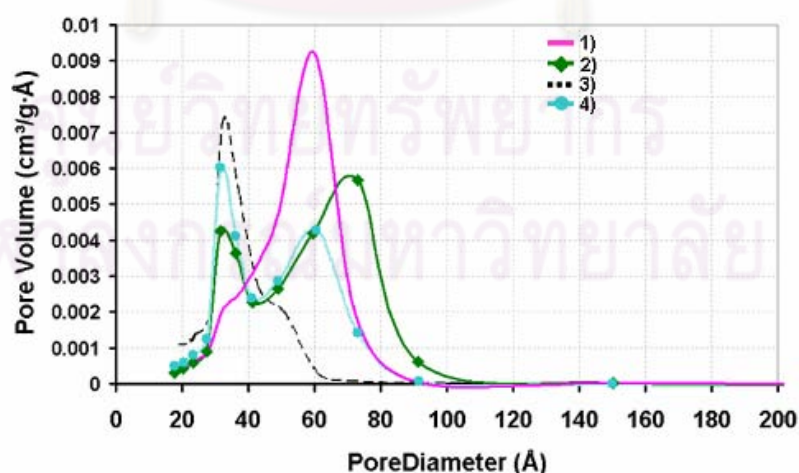
Figure 5.3.3 Pore size distribution of the samples: 1) F-c1-A; 2) F-c1W(2d)-A; 3) F-c1W(2d)-A *0.23ml/min of water addition rate*; and 4) F-c1W(3d)-A, after calcinations at 500°C for 5 hours (1°C/min)

First, the effect of rate of water addition was investigated by comparing among the two samples of F-c1-W(2d)-A obtained from the addition rate of ~0.23ml/min and ~19.4 ml/min. As shown in Figure 5.3.3, and Table 5.3.1, the faster water addition rate made larger pore sizes developed and resulted in significant bimodal pore size distribution. The BET surface area and pore volume of the samples obtained from the condition of water added in a faster rate seemed to be larger from microporosity generated, than those of the condition with slower water addition rate, as shown by t-plot data in Table 5.3.1.

Again, the larger size was believed to reflect the pores that arisen from micelle [51]. Hence, the results suggest that the micelle formation should be effectively enhanced when the water was rapidly added to the system. At the same time, the hydrolysis-condensation reactions were also promoted by the fast addition of water and the strength and stiffness of the wet gel could be increased [59]. This could yield a tighten structure giving a small pore in the niobium wall or the generation of microporosity [168].

Next, at the same water addition rate, the effect of the amount of water was investigated by comparing among the F-c1-A, the F-c1(W2d)-A, and the F-c1(W3d)-A. The final concentration of the solution for the F-c1(W2d)-A, and the F-c1(W3d)-A after water addition were estimated using the total volume to be about 2.6 mM and 1.6 mM, respectively. They are above the cmc of F127 [84]. The results showed that the larger amount of the added water gave lower BET surface area, pore volume, and microporosity. Larger amount of water also seemed to enhance the fraction of the smaller pore sizes in the bimodal distribution (see Figure 5.3.3).

It was presumed that too large amount of water in the samples F-c1(W2d)-A, and the F-c1(W3d)-A could speed the inorganic hydrolysis and condensation. The HCl generated *in situ* from the hydrolysis-condensation reactions could decrease EO solubility in the aqueous phase and decrease the curvature of micelle giving smaller pore size [86]. Also, since the block copolymers might have a broad molecular weight distribution as a result of impurities (originating from the manufacturing process) [84], dilution could partly lead the polymer solution concentration to be

lower than the characteristic concentration of some polymer fraction, giving more part of small pore size originated from non-micelle polymer.

In general, the overall results suggest that there should be a range of an optimum amount of water in the system which would give highest value of the microporosity, BET surface area, pore volume, and pore size. The reprecipitation of more and more dissoluted niobium monomer in the gel skeleton would probably occupy and reduce the micropores contributing to surface area. On the other hand, incomplete hydrolysis might also cause changes in the extent of generated microporosity. The effect of water on these textural properties is quite complex and needs further investigation.

5.3.2 Effect of water on phase transformation behavior

In addition to the textural properties, the various amount of water could play a significant role in phase transformation behavior as a result of the changes in the sol-gel chemistry and the structural characteristics of the niobium skeleton.

Figure 5.3.4 shows the XRD patterns of the samples after calcinations at 500°C (Figure 5.3.4a) and 600°C (Figure 5.3.4b). From Figure 5.3.4a, after calcinations at 500°C, the F-c1-A was amorphous but showed hidden growing tetragonal structure (JCPDS 18-0911), having maximum intensity at 2theta ~23 degree [51, 175]. When water amount was lowered as in the F-c1w-A, the hidden pattern was less noticed. When water was absent as in the F-c1x-A, this pattern disappeared. The addition of water also gave the patterns differing from the pattern of the F-c1-A. The larger amount of water further reduces the tetragonal structure.

The samples presenting hidden tetragonal structure had transformed into an orthorhombic T structure after calcinations at 600°C (Figure 5.3.4b), consistent to the report from Nair et al. [175]. The T phase was most clearly observed in the F-c1-A and in the F-c1w-A while the F-c1W(2d)-A was more likely to display a TT-structure. The absence of water in the F-c1x-A and too large amount of water in the F-c1(W3d)-A only gave TT-structure.
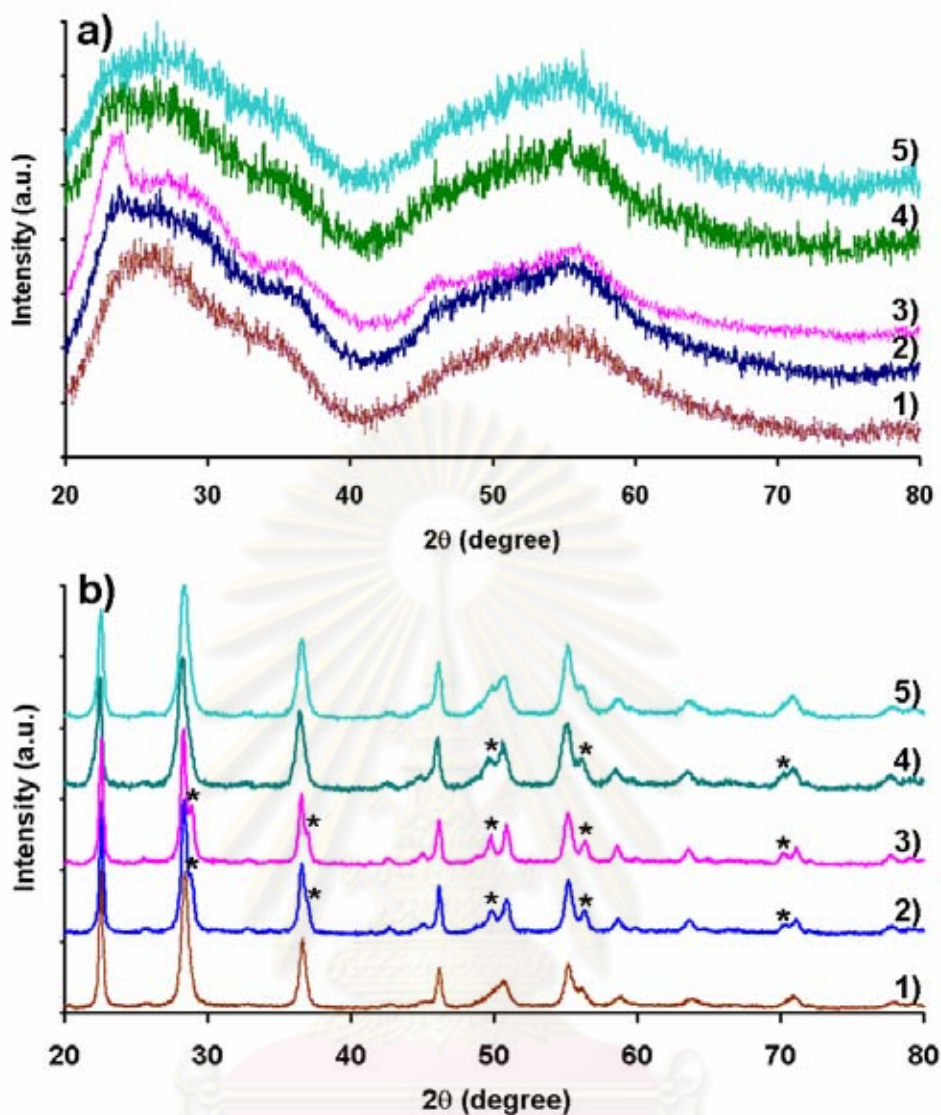
Figure 5.3.4 XRD patterns of the samples 1) F-c1x-A; 2) F-c1w-A; 3) F-c1-A;
4) F-c1W(2d)-A; 5) F-c1W(3d)-A, calcined at 500°C for 5 hours
(1°C/min)(a), and calcined at 600°C for 5 hours (1°C/min)(b). The
splits in the pattern of an orthorhombic T-Nb_2O_5 which are
distinguishable from a pseudohexagonal TT-Nb_2O_5 are indicated by the
asterisks

   All the samples did not show any weight loss at their crystallization events.
This should be due to an announced effect of the hydrothermal aging at 110°C to
enhance hydrolysis but lock the small amount of Cl-Nb bonds in the structure [51].
However, the condition that the chloride is appropriately locked within the structure
to induce the T phase depends on the water amount in the system.

For large amount of water in the solution, HCl is diluted while further enhancement of hydrolysis could occur. These could result in lower amount of the chloride presented as Nb-Cl. For the case of small amount of water, the alcoholysis reaction using ethanol should only provide a small extent of hydrolysis, compared to what could occur when water was present, and the Nb-Cl bonds might remain for a large amount.

The DTG data shown in Figure 5.3.5 showed that the sample synthesized with an absence of water (the F-c1x-A) possessed the highest rate of weight loss at 220-320°C. The more rapid loss of chloride from the hybrid structure the higher rate of weight loss could possibly be observed. The maximum value of DTG of the F-c1x-A was confirmed. Other samples with higher amount of water in the samples showed consecutively lower rate of weight loss as the peaks in the DTG were lowered.
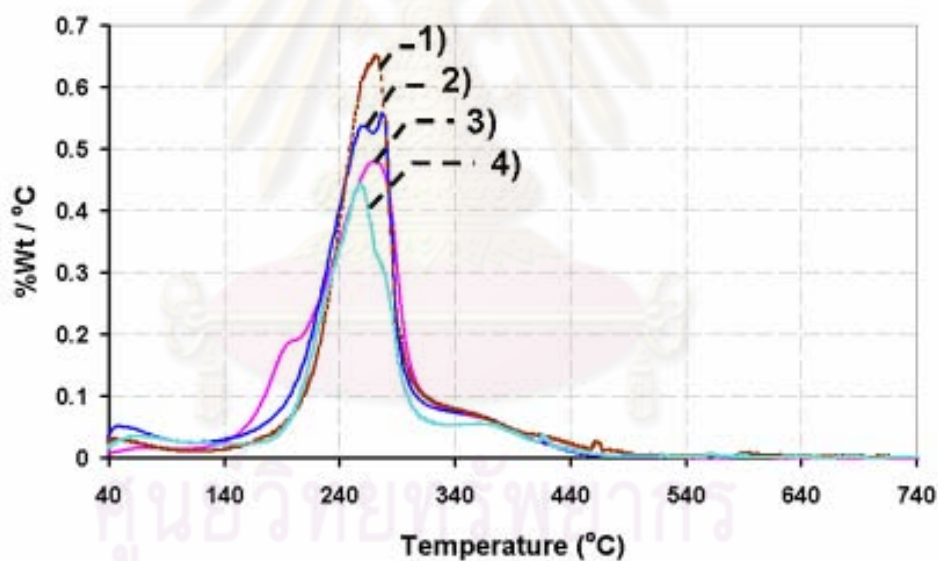
Figure 5.3.5 DTG data of the samples: 1) F-c1x-A; 2) F-c1w-A; 3) F-c1-A
and 4) F-c1W(3d)-A. The data of the F-c1x-A has been confirmed
twice and the highest rate of weight loss (maximum value) was
repeatable

The Nb/Cl ratio obtained from SEM-EDS of the as-synthesized samples (before calcinations) also showed that the amount of chloride in the samples are in the sequence F-c1x-A > F-c1w-A > F-c1-A. Those DTG and SEM-EDS suggest that the

samples synthesized from lesser amount of water resulted in higher amount of chloride as Nb-Cl. However, the possiblility of different amount of trapped species [10, 51, 78, 146] to contribute the Cl detected by SEM-EDS is needed to be awared.

The different amount of bonded chloride should then provide different structural modification of niobia crystal structure. It was believed that there may be some appropriate amount of chloride that remained linked to the niobium and can provide suitable condition to obtain the T-structure under the hydrothermal aging at 110°C. As different preparations or origins can make different behavior upon further heating [171], it was thought that the high amount of chloride as Nb-Cl in the F-c1x-A might be liberated out simultaneously as continuous condensation upon heating and not 'locked' in the niobium structure in the appropriate way that the T structure would result after the crystal restructuring. It is different from the conditions of the F-c1-A or F-c1w-A having initially low Nb-Cl in the network which gave the T structure after crystallization. The phase transformation of an amorphous chloride niobic acid also showed variable behavior depending on the content of HCl; with a high HCl content, the obtained phase could be T structure or TT structure, while with a low HCl content, the TT structure was normally obtained [171]. The system of high water conditions as in the sample F-c1W(2d)-A, and the F-c1W(3d)-A was thought to contain low chloride content and the TT structure was observed.

From Table 5.3.1, the crystallization temperatures of the samples showing TT structure are lower than those showing T structure, agreed with the general observation of the niobia phase transformation behavior [171]. The crystallization temperature of the F-c1w-A was lower than that of the F-c1-A, indicating that the temperature at which the T structure occurred could be lowered by lowering an amount of water introduced to $NbCl_5$, probably due to the fact that different preparations or origins can make different behavior upon further heating [171]. It is, however, in contrast with the observation that lower rate of the hydrolysis/condensation of the metal species in the less water amount condition might hinder subsequent crystallization [28, 79] and the explanation of the T structure behavior is not yet clear. By comparing among the niobia of TT structure; Table 5.3.1 shows that the samples F-c1W(2d)-A, and F-c1W(3d)-A had crystallization temperatures of about 620°C, and 610°C respectively. The results suggest that larger

amount of the added water could lower the crystallization temperature of the TT-structure, probably due to a more complete hydrolysis-condensation of the niobium precursor [28, 79]. The dilution of HCl, occur due to larger amount of water, could lower its effect to act as an impurity preventing the crystallization of the oxide [173].

5.3.3 Effect of water on crystallite size

The crystallite size of the F-c1W(2d)-A, and F-c1W(3d)-A, whose structure are TT structure, are about 23-25 nm. These suggest that the amount of added water of these samples did not show much difference on the crystallite sizes of the TT structure. This is probably a result of excessively high water to niobium ratio in the reaction medium which ensures a more complete hydrolysis of niobium precursor, favoring nucleation versus particle growth [60].

Smaller amount of water induced larger crystallite size as seen from the nonhydrolytic system, the F-c1x-A; its TT structure crystallite size turned out to be ~44 nm. The size of the T-structure obtained from either F-c1-A or F-c1w-A were also ~44 nm though their crystallization temperatures were higher than those of the samples possessing TT structure. This and the finding from the literatures that the T structure usually forms after the TT structure is further heated [171] suggest that there might be the critical nuclei size of the crystal before the T structure could form, similar to the case of anatase and rutile phases of titania [60].

5.3.4 Effect of water on acidity

In this work, the Lewis acidity of the sample might also be expected depending on the amount of water and the resulting crystal structure. For the sample after calcinations at 500°C, the F-c1w-A showed slight evidence of hidden tetragonal structure and gave Raman bands at 669 cm^{-1} and at ~900-1200 cm^{-1}, similar to the observations from the F-c1-A (see Figure 5.3.6). These indicate that appreciably distorted octahedra with a higher niobium-oxygen bond order (Nb=O bond) should be present and Lewis acidity could also be expected in the samples of tetragonal structure, including the F-c1w-A, calcined at 500°C.
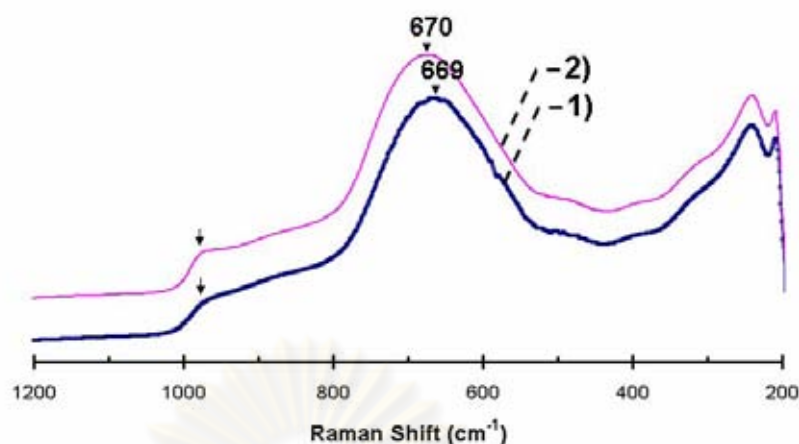
Figure 5.3.6 Raman shifts of the samples: 1) F-c1w-A and 2) F-c1-A, after
calcinations at 500°C for 5 hours (1°C/min)

5.3.5 Summary

This work investigated the effect of an amount of water added in the syntheses
of mesoporous niobium oxide. The results can be summarized as follows:-

1) In low water condition, lower surface area, pore volume, and pore size
resulted. When water amount was added, the faster addition rate gave larger BET
surface area, pore volume, and pore size. Larger amount of added water gave lower
BET surface area, pore volume, and microporosity and build more fraction of the
smaller pore sizes. All these results should relate to the dissolution ability of F127,
micelle formation behavior, and the hydrolysis-condensation reaction which are
affected by the amount of water. Too low water gave unfolding behavior of micelle
and too large water could dilute polymer concentration and destroy micelle. Only
appropriate amount of water would give highest textural properties.

2) For the effect of water on the product crystalline structure, the tetragonal
structure, along with the expected Lewis acidity was found for the 500°C-calcined
samples synthesized from intermediate amount of water. After calcinations at 600°C,
the T structure was also observed for the samples earlier displayed tetragonal phase.

An absence of water or too large amount of water only gave the TT structure followed the aging conditions.

3) The temperature at which the T structure occurred could be lowered by lowering an amount of water introduced to $NbCl_5$ while larger amount of the added water could lower the crystallization temperature of the TT structure.

4) The amount of added water did not show much difference on the TT crystallite sizes probably due to favoring nucleation versus particle growth in the large water amount conditions. The crystallite sizes of the T structure were larger than those of the TT structure, probably a result of the existence of a critical nuclei size of the T structure.

5.4 Influence of Dialysis on the Formation and Structure of Mesoporous Niobium Oxide from Niobium(V) Chloride

The dialysis process was introduced in this work to let the molecules which were smaller than the pore sizes of the membrane to permeate through the membrane pores, thus HCl and ethanol leached out from the solution while water permeated into the system, leading to a larger volume and a significant increase of pH of the sol inside the dialysis membrane bag. For example, for the sample made using F127 and the c1 concentration, the initial pH was 0, which is consistent with the $[H^+]$ calculated assuming 5 eq. HCl per $NbCl_5$, ~1.33 M (or pH = -0.124). When the sample was dialyzed for 2 hours, the resulting pH was 1.28 ($[H^+]$ = 0.052 M), and when it was further dialyzed for 6 hours, the resulting pH was 1.64 ($[H^+]$ = 0.023 M). After 2 days (replacing the dialysate at 24 hours), the pH was 3.24 ($[H^+]$ = 0.575 mM). Concurrently, the outside dialysate dropped in pH but remained a clear solution with no evidence that niobium compounds dialyzed out (ICP-AES). The resulting material in the dialysis membrane was a translucent-to-opaque soft chunky precipitate with a clear supernatant.

5.4.1 Effect of dialysis on textural properties

The isotherms of all samples in this study are type IV, indicative of mesopores [53]. Table 5.4.1 lists the textural properties of each sample. All samples synthesized in this work have BET specific surface areas in the range of 120-170 m^2/g, a pore volume of 0.20-0.30 cm^3/g and an average pore size >4 nm after calcinations at 500°C.

Table 5.4.1 Textural properties of the samples after calcination at 500°C for 5 hours (1°C/min)

Samples	BET Surface Area $(m^2/g)^a$	Pore Volume $(cm^3/g)^{a, b}$	Average Pore Diameter $(nm.)^{c, d}$
F-c1-2dDM-A6	169	0.278	5.0
F-c1-2dDM-A4	154	0.243	4.9
F-c1-6hDM-A6	164	0.300	5.5
F-c1-2hDM-A6	178	0.308	5.3
F-c1-A4	124	0.246	6.6
NoPolymer-c1-2dDM-A	72	0.166	7.6
F-c1-2dDM	113	0.141	3.9
F-c1-2dDM-A	144	0.281	6.1
F-c1-6hDM-A	143	0.227	4.8
F-c1-2hDM-A	152	0.238	4.8
F-c1-A	150	0.252	5.4
F-c1W(2d)-A	108	0.121	3.7
P-c1-2dDM-A	125	0.241	5.8
P-c1-6hDM-A	136	0.205	4.7
P-c1-2hDM-A	125	0.180	4.4
P-c2-2dDM-A	98	0.204	6.9
P-c2-6hDM-A	126	0.230	5.8
P-c2-2hDM-A	133	0.225	5.2
P-c2-A	152	0.287	6.1
F-c3-2dDM-A	163	0.319	5.9
F-c3-6hDM-A	143	0.232	4.7
F-c3-2hDM-A	134	0.196	4.3

[a], $\pm$ 10% error.
[b], determined from the single point adsorption total pore volume of pores at $p/p_o \sim 0.99$.
[c], from BJH desorption.
[d], see pore size distribution in Figure 5.4.1 and Figure 5.4.2 and Figure 5.4.8.

In Figure 5.4.1, most samples have bimodal or broad pore size distribution which may be the result of different pore sizes merged together. It was not sure of the origin of the bimodal characteristics observed in this work since only rare examples of bimodal systems with two consecutive mesoporous sizes have been reported [181, 182].
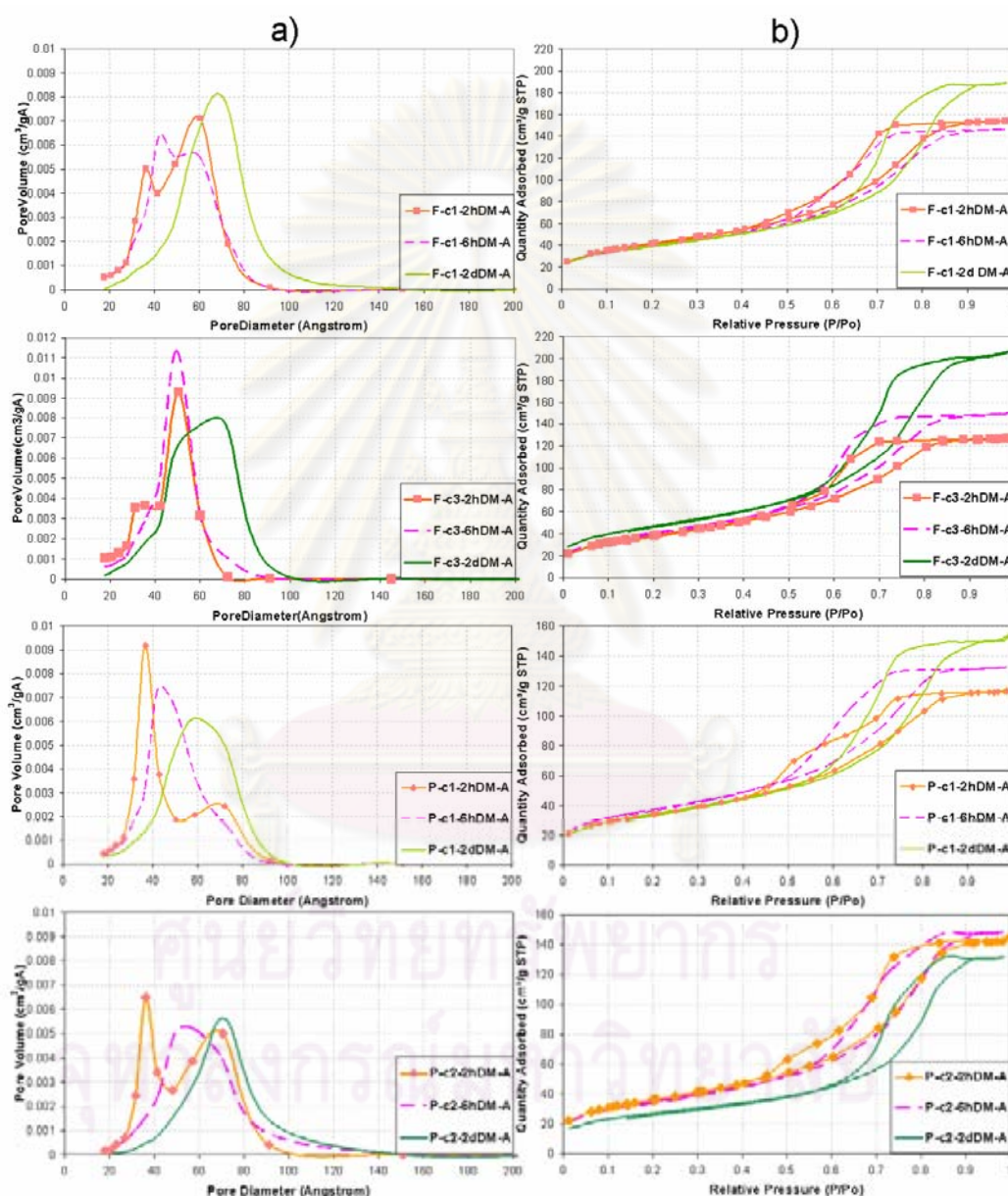
Figure 5.4.1 Pore size distributions (a) and the isotherms (b) of the samples
synthesized with different concentrations and polymer templates,
showing the pores shifting to larger sizes with the longer dialysis time.
All samples were calcined at 500°C for 5 hours (1°C/min)

Howver, the bimodal porosity observed from many conditions used in this work offers a combination of fast mass transport of a large pore size with the high specific surface of a small pore size and could be expected to show interesting properties for adsorptive and catalytic applications [183]. These pores sizes developed to larger sizes with longer dialysis time, independent of the initial triblock copolymer type and concentration. A 2-day dialysis (the samples of -2dDM- serie) resulted in the largest pore size.

The formation of larger mesopores with longer dialysis times could be the result of the decrease in HCl and ethanol concentration, and/or the diffusion of water into the reaction mixture. The obvious enlargement of the pore size observed for samples dialyzed for 2 days could not be obtained only by dilution alone, as seen by the pore size distribution of the sample F-c1W(2d)-A shown in Figure 5.4.2. This sample was not dialyzed, but diluted before the aging process such that the total water content of the sample was roughly equal to the sample dialyzed for two days. The water addition rate was done manually by a burette at a rate of about 0.23ml/min with slow stirrer speed to imitate the water diffusion through the dialysis. The F-c1W(2d)-A sample had a comparable amount of water, but higher HCl and ethanol concentration compared to the 2-day dialyzed sample (F-c1-2dDM-A). Both samples have different textural properties (Table 5.4.1) and pore size distributions (Figure 5.4.2). F-c1W(2d)-A has a bimodal pore size distribution dominated by smaller pores. This corresponds with the trend that longer dialysis times (and thus lower HCl and ethanol concentration) leads to larger pores. Thus, the smaller pores in F-c1W(2d)-A compared to F-c1-2dDM-A was attributed to higher HCl and ethanol concentration. Dialysis lowers HCl concentration with respect to niobium and polymer while also diluting the entire sol with water, and yields larger pores.
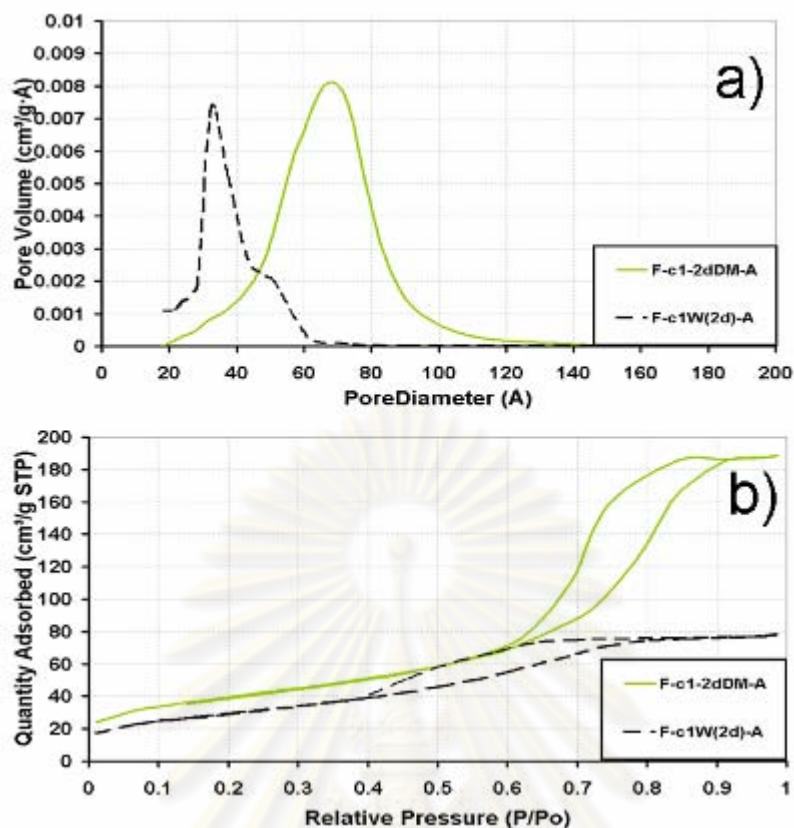
Figure 5.4.2 Pore size distributions (a) and the isotherms (b) of the samples F-c1-2dDM-A and F-c1W(2d)-A. All samples were calcined at 500°C for 5 hours (1°C/min)

The observed mesopores of the dialyzed samples were believed to be attributed partly to the space generated after the polymer micelle was removed. The initial surfactant: water molar ratio for all samples in this study is similar to that for the monolithic mesoporous silica system [163] and its concentration is well above the critical micelle concentration (cmc). Although the polymer concentration is significantly lower after dialysis, its concentration is still above the cmc (see Table 5.4.2a and b). The dialysis has also been used to form micelle in drug delivery system [82]. Thus, the polymer was believed to remain aggregated as micelles throughout the dialysis and act as a spacer among inorganic network.

Table 5.4.2a The polymer template molar concentration in the solution

Polymer Template	Concentration[a]	Estimated Molar Concentration [mM] of Template in the Starting Solution[b]	Estimated Molar Concentration [mM] of Template in the Final Solution (*After 2days Dialysis*)[b]
F127	c1	8.7	2.8
P123	c1	9.0	3.1
P123	c2	14.5	4.9
F127	c3	24.3	6.7

[a] see Table 4.1.1.
[b] estimated using the total volume of the solution.

Table 5.4.2b The polymer template critical micelle concentration (cmc) [84]

T (°C)	Polymer Template	cmc [mM]
25	P123	0.052
	F127	0.555
30	P123	0.009
	F127	0.079
35	P123	0.002
	F127	0.019

The pore size distributions of the 2days-dialyzed samples with (the F-c1-2dDM-A) and without F127 (the NoPolymer-c1-2dDM-A), after calcination at 450°C for 5 hours (1°C/min) are shown in Figure 5.4.3 and suggest a significant larger pore sizes of the product employing F127, compared to the one without it. The presence of the triblock copolymer that contributed to significantly larger pore sizes should evidence the importance of presence of the triblock copolymer as aggregates separating niobium species and forming the porous structure of the final calcined materials. Note that here the samples were calcined at 450°C to evade the effect of crystallization which may result in growth of the niobia wall.
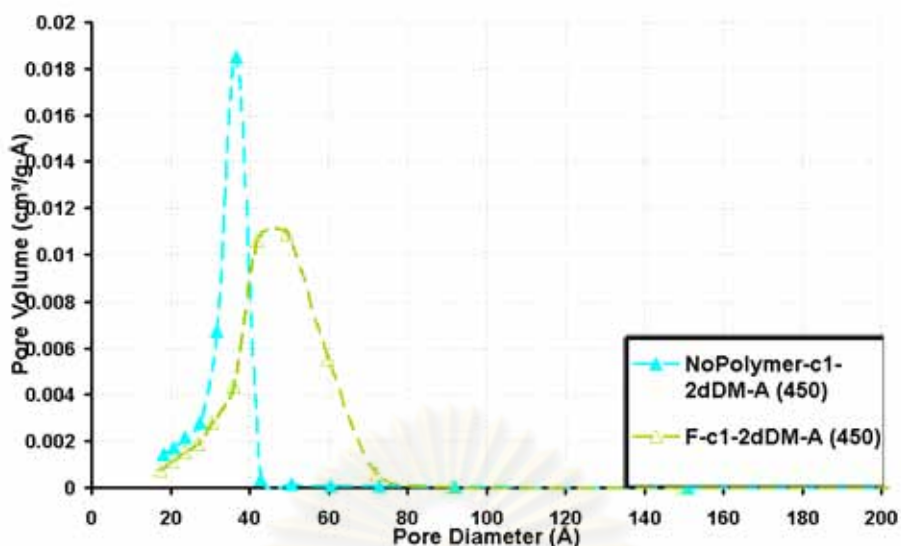
Figure 5.4.3 Pore size distributions of the 2days dialyzed samples with (the
F-c1-2dDM-A) and without F127 (the NoPolymer-c1-2dDM-A), after
calcinations at 450°C for 5 hours (1°C/min)

The high magnification of transmission electron microscopy (TEM) of the
dialyzed samples is shown in Figure 5.4.4. It revealed continuous domains that
involved mesopores, supporting the role of the polymer to provide an intraparticle
porosity.
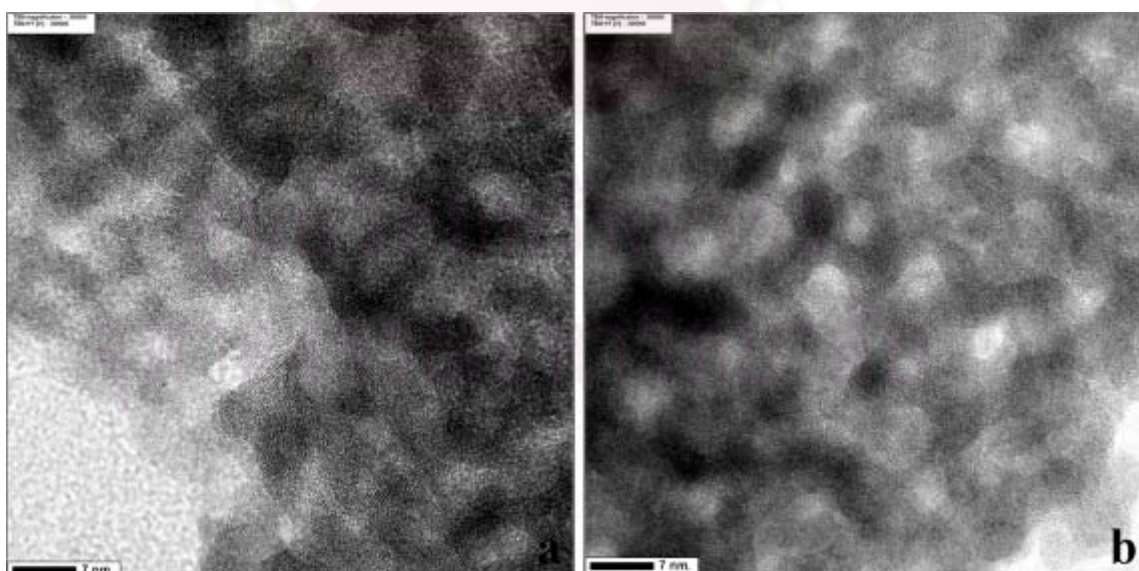
Figure 5.4.4 TEM pictures of the samples after calcinations at 500°C for
5 hours (1°C/min); a) F-c1-2hDM-A, b) F-c1-2dDM-A

In the work of Lettow et al. [86], addition of HCl decreased EO solubility in the aqueous phase and ethanol generated *in situ* from the silica precursor increased the solubility of the PO core. This led to a reduction in micelle curvature, transforming spherical micelles to cylindrical micelles and resulting in a smaller median pore size. In the present work, the dialysis process lowers HCl concentration and increases the aqueous nature of the solvent (higher water: ethanol ratio). According to the work by Lettow et al. [86], this should lead to increased EO solubility and decreased PO solubility, discouraging formation of cylindrical micelles. At the same time, as the amount of water increases, the increased solvent polarity should promote PEO-PPO domain separation [58, 64]. As dialysis takes place, water becomes the dominant component of the sol, resulting in enhanced PEO solubility relative to PPO and thus greater micelle curvature. Hence, longer dialysis time encourages greater curvature of micelles and thus larger pores. Micellar expansion by reducing ethanol concentration was also observed in the bulk ethanol/water/CTABr system [166]. These suggest that the larger mesopores with longer dialysis times is a result of the components exchange occurred throughout the dialysis.

Apart from the impact of the dialysis on the polymer micelle, the lower HCl content which favors condensation of niobium species could also account for the larger pore sizes observed for longer dialysis time. By lowering the acid content the larger pore sizes of niobia whose pore sizes were larger than 10 nm, has been early reported by the method employing sol-gel synthesis and supercritical carbon dioxide (aerogel) without an organic polymer [37]. In low acidic conditions, the highly branched inorganic network leading to a large interconnected particle was promoted. The larger an interconnected particle, the larger the resulting pore sizes [37]. These pores were believed to be a result of growing niobia wall. As the samples were calcined at 500°C which could partially crystallize [44, 50] and make niobia grow beyond the disordered mesoporous wall, the pores observed could partly be voids among these growing particles.

The XRD patterns of the dialyzed samples of the F-c1 serie, along with the corresponding non-dialyzed sample were shown in Figure 5.4.5 for comparison. The samples calcined at 500°C in this work showed mainly amorphous character.

Partially crystallized phase of the pseudohexagonal Nb_2O_5 (TT phase: JCPDS 28-0317) was observed for the 2-day dialyzed sample, as evidenced by the small peaks appeared. The other dialyzed samples were also believed to involve the start of crystallization though no clear peak of the crystallized phase was observed for the other dialyzed samples. The non-dialyzed samples showed distinct phase formation as early reported in the previous two issues.
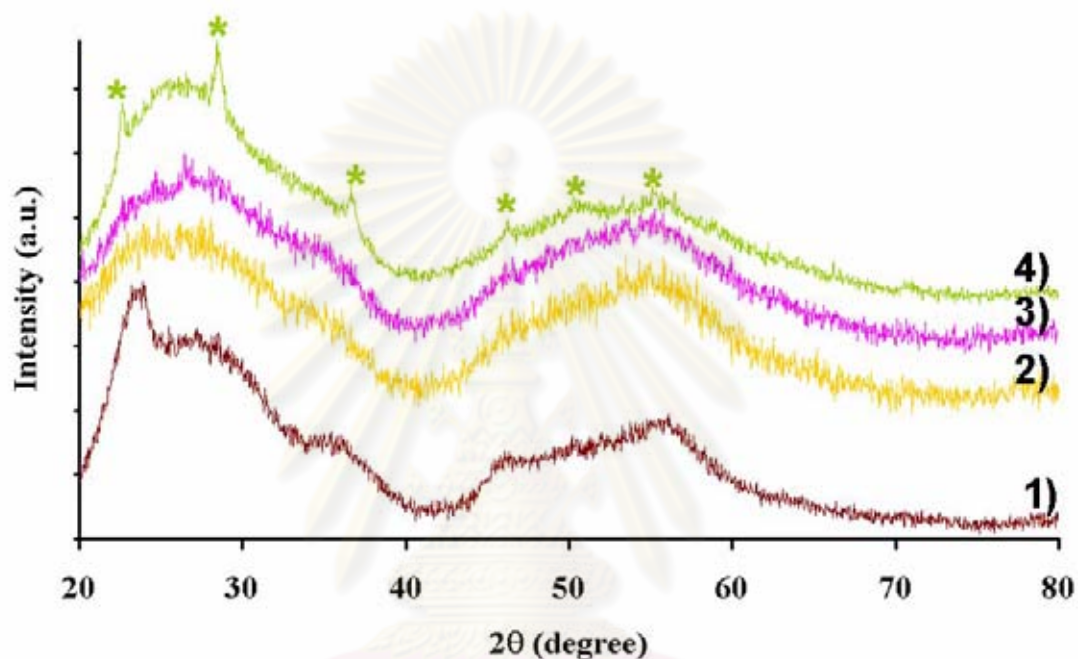
Figure 5.4.5 XRD patterns of the samples in the F-c1-series, after calcinations at 500°C for 5 hours (1°C/min ramp rate): 1) F-c1-A; 2) F-c1-2hDM-A; 3) F-c1-6hDM-A and 4) F-c1-2dDM-A. An asterisk (*) corresponds to pseudohexagonal TT structure (JCPDS 28-0317)

These particles growth could result in the larger niobia wall and destroy the porous structure originally formed by intraparticle porosity. The TEM pictures of the 500°C-calcined dialyzed samples showing parts of the pores that should be arisen from an interparticle void are shown in Figure 5.4.6. The insets in Figure 5.4.6 are the SAED patterns of the corresponding images. The F-c1-2hDMA showed only amorphous ring while the F-c1-2dDM-A showed some spots indicative of partly crystallized nature, consistent with the XRD results in Figure 5.4.5.
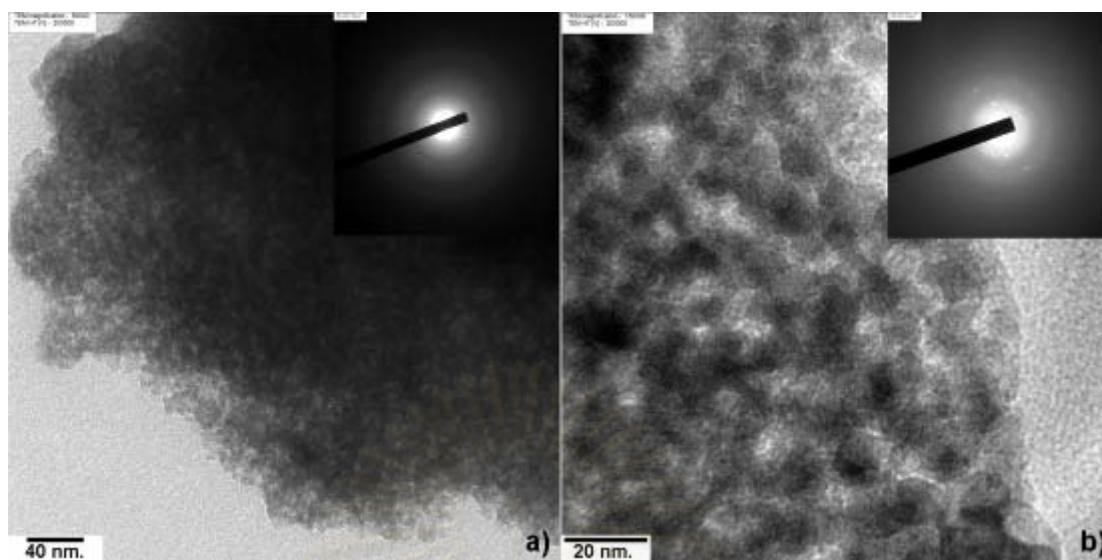
Figure 5.4.6 TEM images and SAED patterns (insets) of the samples after calcinations at 500°C for 5 hours (1°C/min); (a) F-c1-2hDM-A, (b) F-c1-2dDM-A

The DSC data, along with the corresponding TG data shown in Figure 5.4.7 also showed that the samples subjected to longer dialysis time had lower crystallization temperature. All these data showed correspondence to each other and could be contribute to the possibility that the pore sizes probably are of an interparticle porosity, and the larger the dialysis time, the larger these sizes could be.

The bimodal pore size distribution of which the sizes of the pores were very close to each other, similar to our work, was observed in decane-trimethylbenzene swelling CTAB micellar system when both decane and trimethylbenzene were added simultaneously, not consequently [181]. Therefore, it was presumed in our work that the competitive effect of HCl, ethanol, and water on the shape and size of micelle and/or on the size of niobia wall particles may occur more profoundly in the shorter dialysis time where all these components were present in competitive quantities. When the samples were dialyzed for long time, the water became a dominant component in the system and the pore sizes were mainly ruled by the effect of water alone.
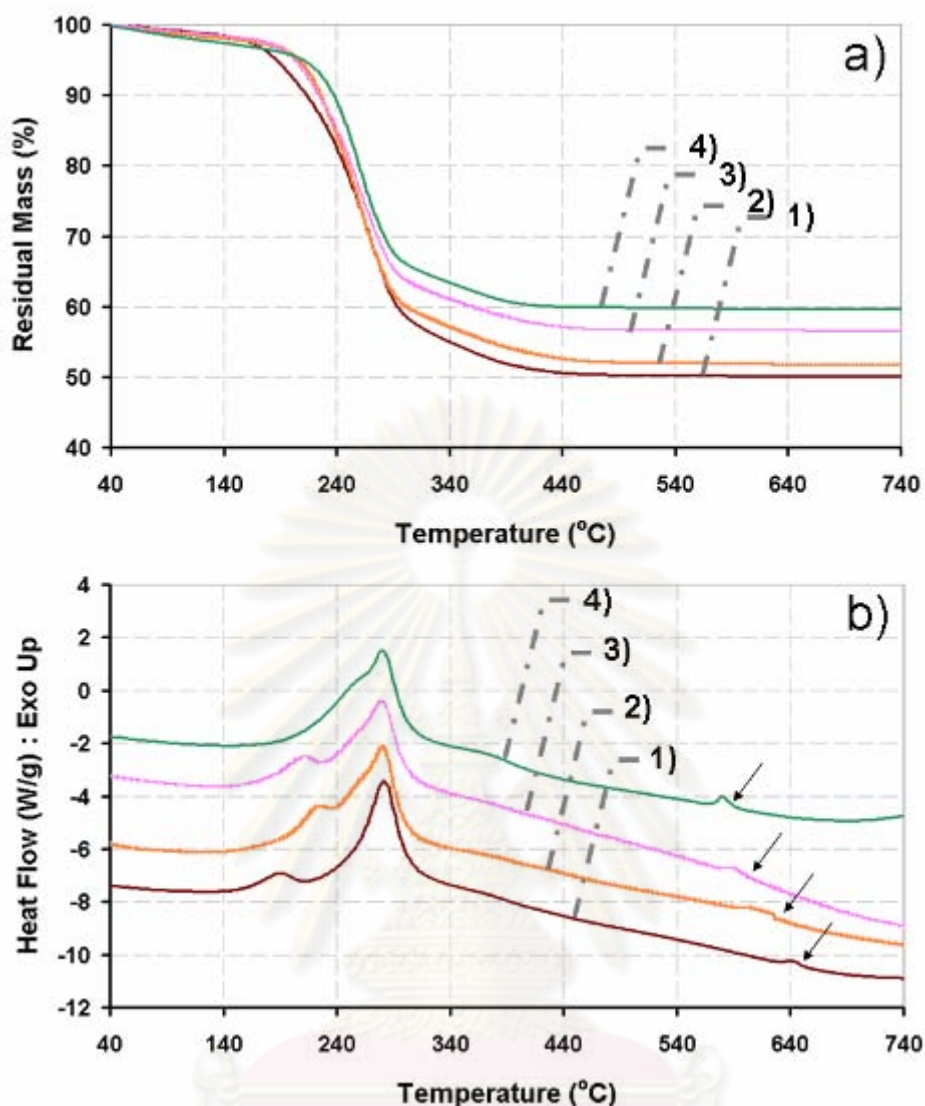
Figure 5.4.7 TG (a) and DSC (b) results of the samples in the F-c1 series: 1)
F-c1-A; 2) F-c1-2hDM-A; 3) F-c1-6hDM-A and 4) F-c1-2dDM-A.
The arrows in DSC indicate the crystallization events. (Samples offset
in DSC for clarity)

5.4.2 Dialysis method vs. Non-dialysis method

A key difference between the dialysis and non-dialysis syntheses is the way in
which the condensation reaction proceeds. The dialysis method resulted in a
precipitate form which is much more rapid to dry, compared to the non-dialyzed
samples which were viscous and required unspecific long drying time up to two
weeks.

In the synthesis of meso-Nb_2O_5 from niobium(V) ethoxide [37], turbid gels of precipitated material formed under weakly acidic conditions, while the addition of nitric acid to prevent condensation led to transparent polymeric gels. In the synthesis of meso-SiO_2 from a silicon alkoxide precursor, slow condensation led to weakly branched polymeric gel networks, whereas highly branched SiO_2 and colloidal gels formed when condensation was more rapid [37]. Therefore, the synthesis via dialysis should promote highly branched niobium species and resulted in a precipitate form by lowering the concentration of HCl, a condensation inhibitor [10].

The structures formed in the non-dialysis procedure prior to aging are more sensitive to framework disruption than those formed during the procedure involving dialysis.

An additional aging step at 40°C or 60°C before aging at 110°C was performed to investigate the robustness of the synthetic strategies (dialysis versus non-dialysis). Experiments were carried out for (F-c1-) samples for the 2-day, 6-hour, and 2-hour dialyzed samples, as well as the non-dialyzed sample; the pore size distributions are shown in Figure 5.4.8.

Comparing Figure 5.4.8a and c, the pore structure of the non-dialyzed meso-Nb_2O_5 is more susceptible to large changes than the 2-day dialyzed meso-Nb_2O_5 when an additional aging step at 40°C was included. The 6-hour and the 2-hour dialyzed samples also showed little change in pore structure with the additional aging (Figure 5.4.8b), similar to the 2-day dialyzed sample. These observations suggest that the wall structure of the dialyzed sample should be more rigid and its pore size could be adjustable to a smaller extent than what was observed for the non-dialyzed sample. The non-dialyzed method didn not provide controllable tuning of the pore sizes. It only gave wider distribution of the pore.
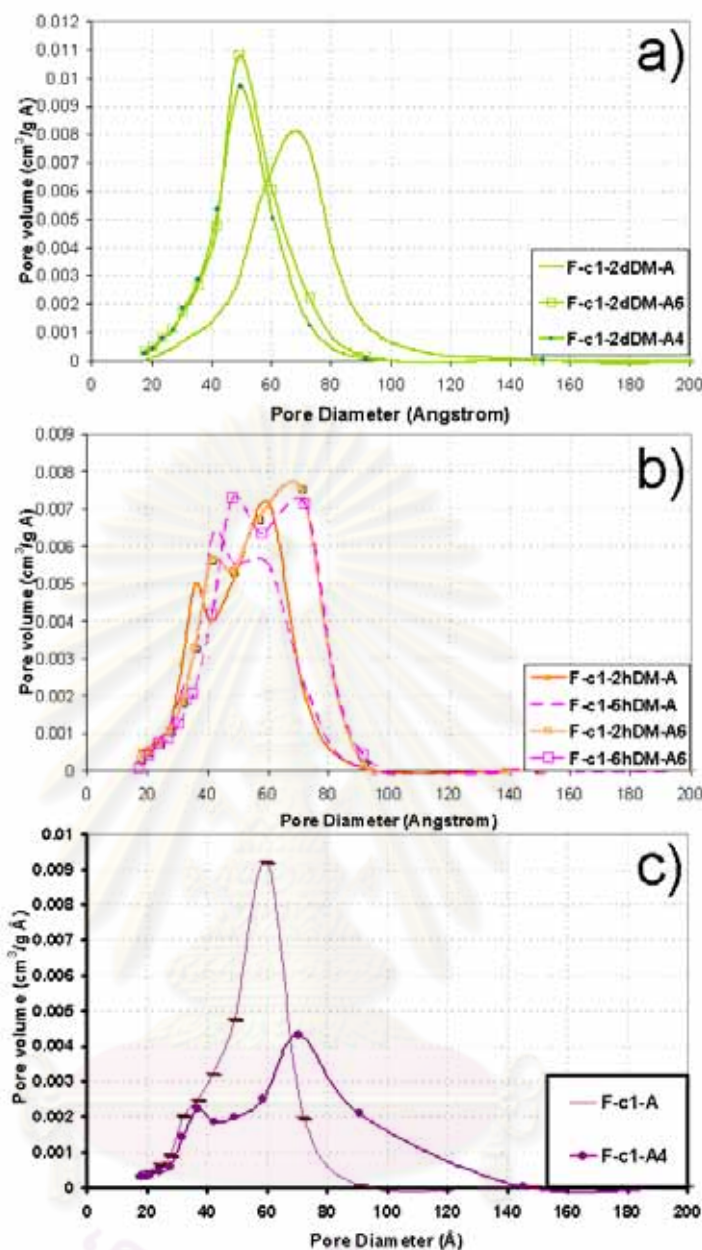
Figure 5.4.8 Pore size distributions of the samples subjected to different aging
conditions; a) F-c1-2dDM-serie, b) F-c1-2hDM-serie and F-c1-6hDM-
serie, and c) F-c1- serie. All samples were calcined at 500°C for 5
hours (1°C/min)

The large amount of chloride but lesser amount of water in the non-dialyzed
system could favor the stronger interaction between organic and inorganic, compared
to the dialyzed system. While the inorganic network is weakly branched, the
mesostructure in this case is then susceptible to changes in parameters that affect the
organic polymer micelle [10]. The dialysis synthesis, on the other hand, has

proceeded through condensation giving a highly branched network of the inorganic which is rigid enough to maintain its structure.

The dialysis method employed in this work not only provided mesoporous oxide having high surface area and pore volume, but also showed potential for fine tuning of the pore size with similar surface area and pore volume. The method is believed to be useful for applications that need high surface area such as catalysts and that needs pore size matching such as biosensor, where the conformation of biomolecules (whose sizes of <10nm) should be controlled [26].

5.4.3 Summary

Niobium(V) chloride and F127 or P123 were employed with dialysis process to obtain mesoporous niobium oxide. The dialysis step removed the HCl and ethanol out while allowing water to permeate into the system. When employing longer dialysis time, the pore sizes were larger, independent of the type or concentration of the polymer in the starting solution. In one way, it was believed that the polymer self-aggregation was affected by the components exchange throughout the dialysis process and that the micelle curvature was changed. The longer dialysis time, the more curvature of the micelle and the larger the mesopore sizes of the final product.

In another way, the reduction of HCl as a result of the dialysis process lead to a large interconnected particle and a decreasing crystallization temperature which also possibly reflected the larger size of the pores observed.

The dialysis process helps forming a highly branched inorganic network which resulted in a precipitate form that much shortened drying time could be noticed. The inorganic wall is more rigid but the pore size could be adjusted with the same pore distribution. This is useful for fine tuning of the pore and expected to be useful for applications that require pore size matching. The dialysis conditions used in this work led to mesoporous niobia with high specific surface areas of 120-170 m^2/g, pore volumes of 0.20-0.30 cm^3/g, and the pore sizes >4 nm after a high thermal treatment of 500°C. The dialysis method shown here should be able to contribute to development of future material for applications such as sensors and catalysts.

5.5 Solvothermal Synthesis of ZnO with Various Aspect Ratios using Organic Solvents

5.5.1 Results

In this work, the solvothermal synthesis of ZnO in alcohols or glycols was conducted at 250°C, where the decomposition of the precursor to form ZnO was completed [130]. On the other hand, our preliminary studies have suggested that the reaction in either n-alkanes or aromatic compounds at 250°C was not complete to result in ZnO formation. Therefore, the reaction temperature was raised to 300°C for these two types of solvent. Figure 5.5.1 shows the XRD patterns of products synthesized in various groups of organic solvents. All samples were ZnO in hexagonal phase (wurtzite structure) [130, 184, 185] without contamination from other crystalline phases. Similar intensity ratio of diffraction peaks indicates that ZnO crystals grow along the same lattice direction, regardless of the solvent used [186].
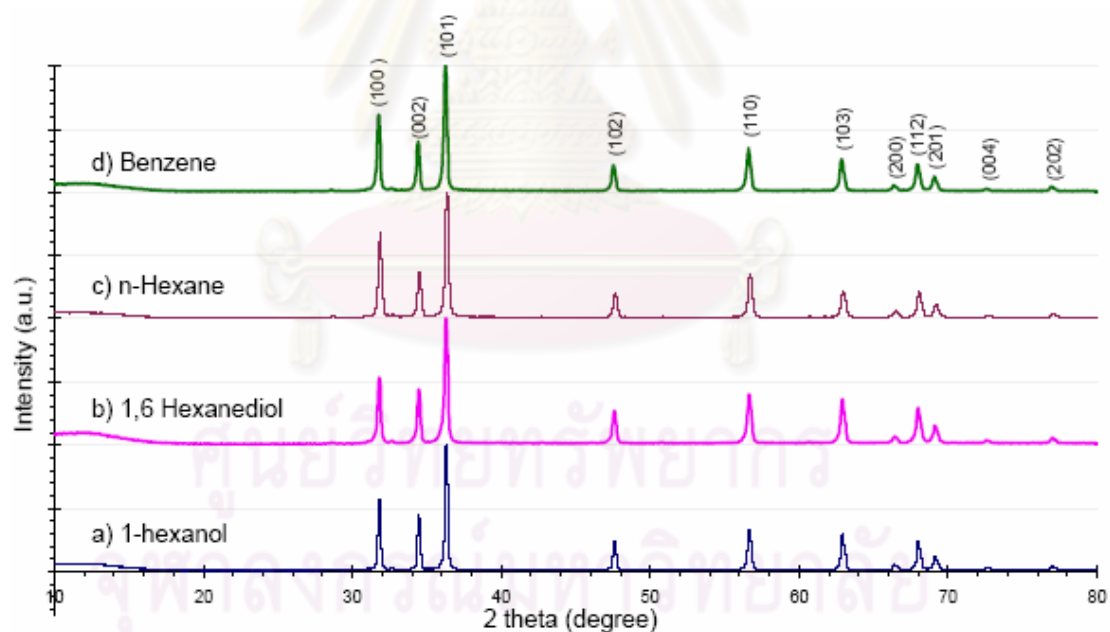
Figure 5.5.1 XRD patterns of ZnO powders synthesized in: a) 1-hexanol; b) 1,6 hexanediol; c) n-hexane and d) benzene

Morphologies of the products synthesized in various organic solvents are shown in Figure 5.5.2-5.5.4. It can be clearly observed that size and shape of ZnO nanoparticles generally depend upon type of the solvent employed. The products synthesized in glycols (Figure 5.5.2) consisted of polyhedral crystals with the lowest

aspect ratio (length-to-diameter ratio), while those synthesized in alcohols (Figure 5.5.3) had moderate aspect ratio. Finally, the products obtained by using n-alkanes or aromatic compounds as solvent (Figure 5.5.4) were ZnO nanorods with extremely high aspect ratio. The results from the selected area electron diffraction (SAED) analysis revealed that all products were the collection of ZnO single crystals.
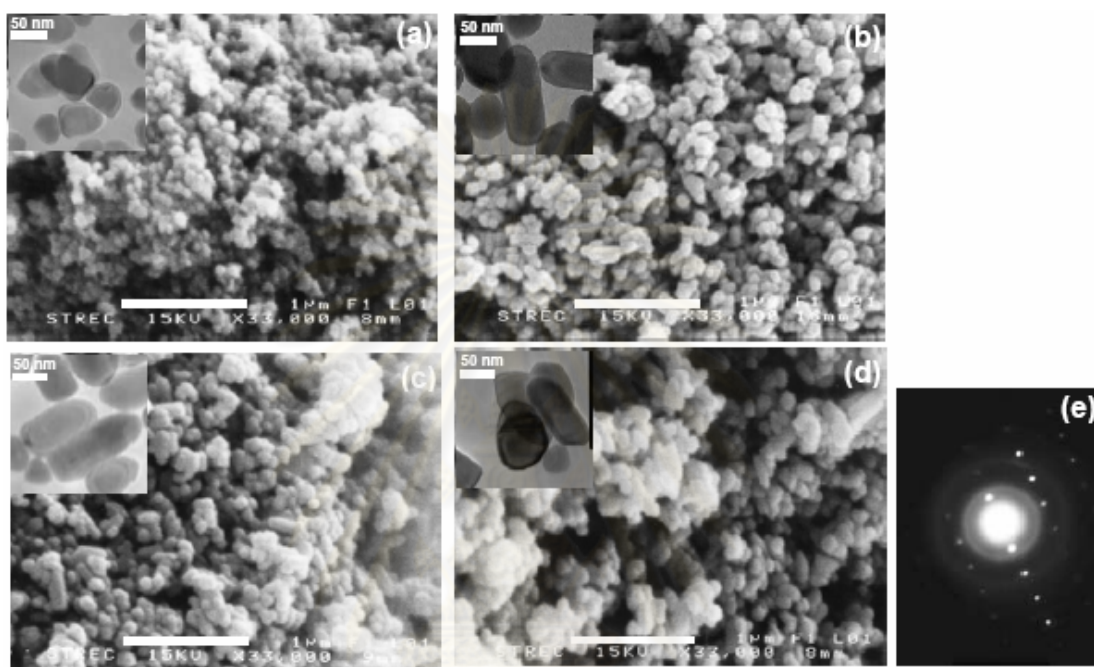
Figure 5.5.2 SEM micrographs of ZnO particles synthesized via the
solvothermal process in: (a) 1,3 propanediol; (b) 1,4 butanediol;
(c) 1,5 pentanediol and (d) 1,6 hexanediol. Insets in the images are
corresponding TEM micrographs. Sample of the SAED pattern of the
synthesized ZnO is shown in (e)
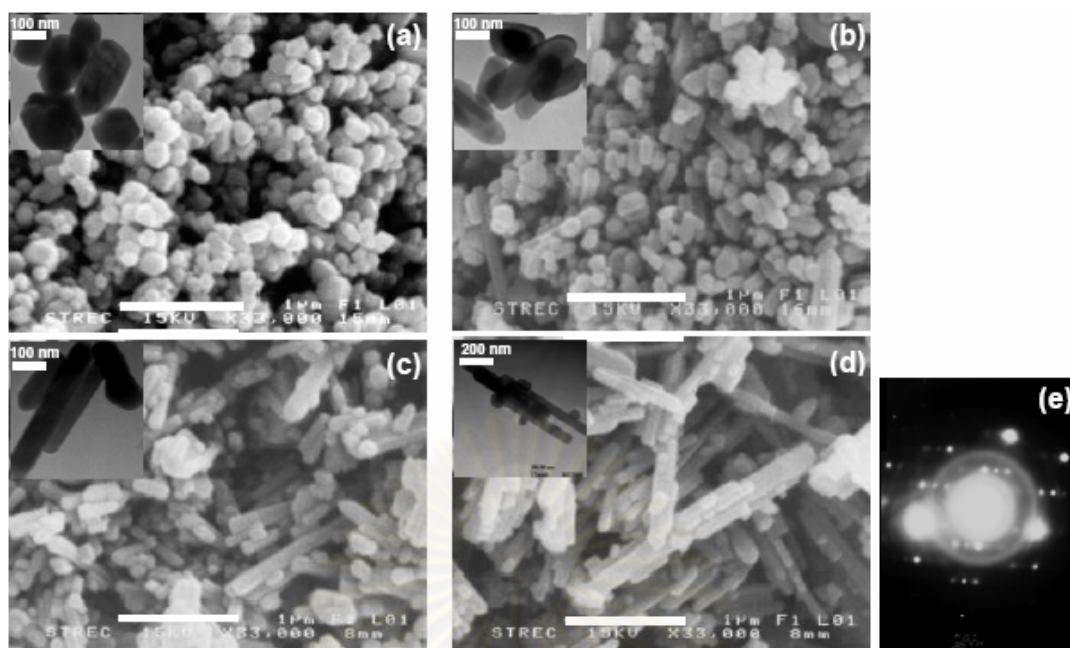
Figure 5.5.3 SEM micrographs of ZnO particles synthesized via the solvothermal process in: (a) 1-butanol; (b) 1-hexanol; (c) 1-octanol; and (d) 1-decanol. Insets in the images are corresponding TEM micrographs. Sample of the SAED pattern of the synthesized ZnO is shown in (e)
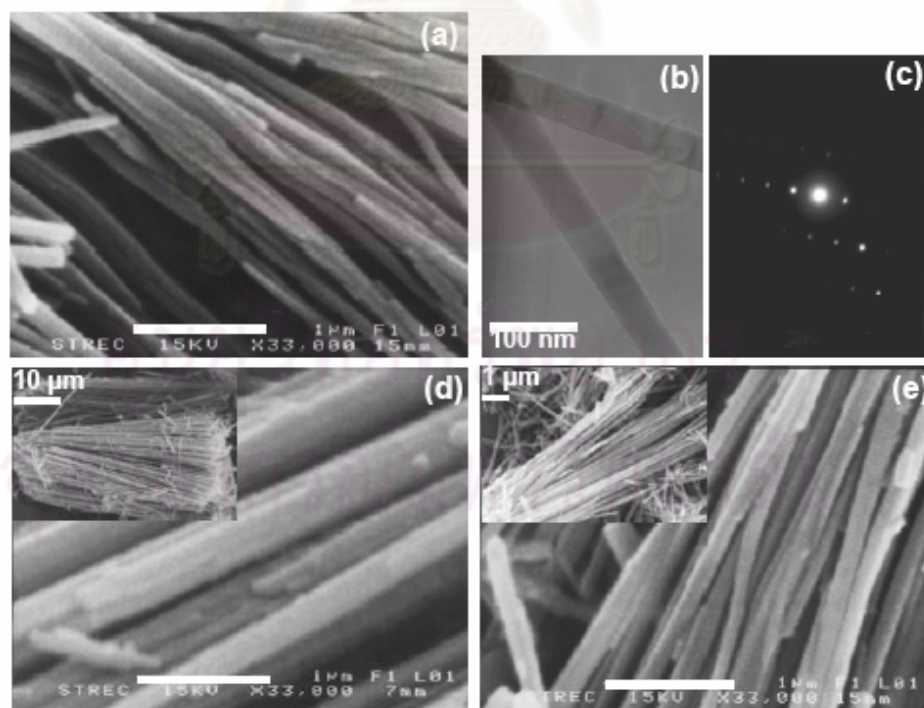
Figure 5.5.4 Micrographs of ZnO particles synthesized via the solvothermal process in: (a) n-hexane; (b)-(c) n-decane; (d) benzene and (e)

ethylbenzene. Insets in the images are SEM images in lower magnification

It is interesting to note that morphology of ZnO nanoparticles synthesized in alcohols strongly depended on the chain length of alcohol molecule (see Figure 5.5.3). The aspect ratio of the products increased when the long-chain alcohol, such as 1-decanol, was used. Lesser effect from solvent chain length was observed on products obtained in glycols. For n-alkanes and aromatic compounds, this effect was unnoticeable.

Sizes of products synthesized in alcohols and glycols, as well as the physical properties of the solvent, are summarized in Table 5.5.1. The particle size was determined from TEM micrographs of particles, using image analysis software. Similar data for the rod-like products synthesized in n-alkanes or aromatic compounds are shown in Table 5.5.2.

Table 5.5.1 Physical features of the anisotropic ZnO synthesized via solvothermal process using alcohols and glycols as solvent

Solvents	B.P. (°C) [187]	Dielectric constant [187]	Diameter (nm)		Length (nm)		Aspect ratio	
			average	deviation[*]	average	deviation[*]	average	deviation[*]
1-Butanol	117	17.24	107	22.4	184	31.1	1.72	0.27
1-Hexanol	156	13.03	91	14.8	264	64.0	2.90	0.66
1-Octanol	196	10.30	84	14.6	343	109.9	4.08	1.58
1-Decanol	231	8.10	81	20.8	455	223.0	5.62	1.89
1,3 Propanediol	214	35.10	42	8.3	55	13.6	1.32	0.26
1,4 Butanediol	230	31.90	69	13.1	139	35.2	2.05	0.41
1,5 Pentanediol	242	26.20	56	8.6	96	24.7	1.89	0.45
1,6 Hexanediol	252	25.86	62	11.0	94	28.7	1.72	0.51

* population standard deviation.

Table 5.5.2 Physical features of the rod-like ZnO synthesized via solvothermal process using n-alkanes and aromatic compounds as solvents

Solvents	B.P. (°C) [187]	Dielectric constant [187]	Diameter (nm)	
			average	deviation[*]
n-Hexane	69	1.89	59	15.1
n-Octane	126	1.95	67	13.0
n-Decane	174	1.99	48	13.7
Benzene	80	2.28	73	14.9
Toluene	111	2.38	78	25.9
o-Xylene	144	2.56	63	23.7
Ethylbenzene	136	2.45	43	12.2

* population standard deviation.

It should be noted that the length of the synthesized ZnO nanorods was in a very wide range from submicrometered size to that longer than 10 μm, which was too large to be captured via TEM technique. Therefore, the size determination was done on SEM micrographs instead. The samples were sonicated to separate the agglomerated rods, in the same fashion as the preparation for TEM analysis. The sample of SEM image of the sonicated sample is shown in Figure 5.5.5. However, it has been reported that sonication can break ZnO nanorods [21]. Thus, it is not certain whether the shorter rods observed in Figure 5.5.5 were as-synthesized particles or being parts of long rods that was broken off by sonication. On the other hand, visual observation from the SEM micrographs of samples without sonication (see inset in Figure 5.5.4) could not clearly determine the length of individual rod, since several rods were bundled together. Nevertheless, it was indicated that the rods generally had very high aspect ratio, as high as 100. Due to this inconclusive observation, data for length and aspect ratio in Table 5.5.2 was omitted, but it was reasonable to claim that the products synthesized in either n-alkanes or aromatic compounds had much higher

aspect ratio, at least one order of magnitude higher than those obtained in alcohols or glycols.
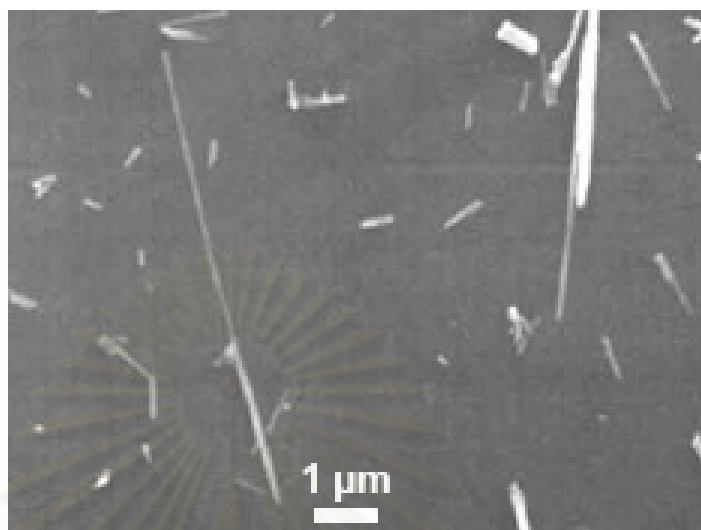
Figure 5.5.5 SEM micrograph of ZnO synthesized in ethylbenzene after

sonication in ethanol for 15 minutes

By changing the precursor from anhydrous zinc acetate to zinc acetate dihydrate, using n-hexane conditions, the resulting morphology as shown by the SEM and TEM pictures in Figure 5.5.6, showed the rod particles having lower aspect ratio than that obtained from anhydrous precursor. The particle morphology was also mixed with unidentified shape.
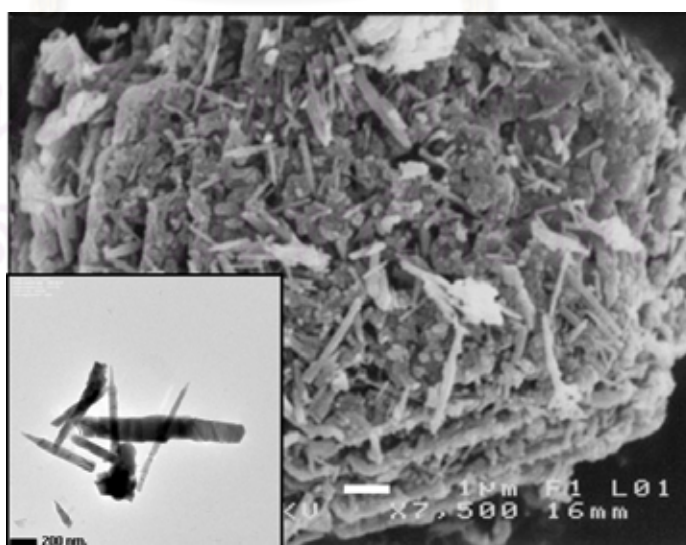
Figure 5.5.6 SEM micrographs of ZnO particles synthesized via the solvothermal process using zinc acetate dihydrate in the n-hexane conditions. Inset is TEM images in low magnification

5.5.2 Discussion

For the solvothermal synthesis in alcohols or glycols, the nucleation as well as the continuing growth of ZnO crystals are similar to those occur in the hydrothermal process since the solvent also consists of hydroxyl group, which is a key factor for ZnO nucleus formation in the hydrothermal method [91, 123, 136, 138]. However, the solvothermal reaction in the medium that lacks of hydroxyl group such as n-alkanes and aromatic compounds has been rarely reported. The plausible mechanism for the results in this work is discussed as follows.

It has been reported that anhydrous zinc acetate, which was use as a precursor in this work, can undergo decomposition and form ZnO nuclei within zinc acetate particles without forming any intermediates [130-132]. Nevertheless, thermal stability of zinc acetate has been reported to depend upon its interaction with the surrounding solvent [105, 130] . It was confirmed by the results in this work that higher temperature was required to synthesize ZnO in n-alkanes or aromatic compounds than in alcohols or glycols. This observation was contributed to different physico-chemical properties of solvents. One of the dominant factors was dielectric constant of the solvent. The dissociation of ionic bonding as well as the weakening of electrostatic interactions within crystals has been generally acknowledged to be favored in the medium with high dielectric constant. The decomposition of zinc acetate has also been reported to be enhanced by increasing the content of water, which has very high dielectric constant, in the system [131]. Therefore, within low-dielectric constant solvents such as n-alkanes or aromatic compounds, high temperature was required to overcome relatively strong attractions within zinc acetate crystal to trigger the decomposition of zinc acetate to form ZnO nuclei.

Effects of solvents on the growth of ZnO crystals have also been reported in literatures [20, 136]. Nevertheless, unlike the discussion in the previous researches,

varieties of solvent were employed in this work. It was obvious to find that type of solvent (e.g. alcohols, glycols, n-alkanes and aromatic compounds) greatly influenced the growth of ZnO crystals. The chain length of the solvent molecule also affected the crystal growth. However, the effect of chain length was apparent only in alcohols (see Figure 5.5.3). For glycols, n-alkanes and aromatic compounds, the chain length had small or unnoticeable effect on morphology of the ZnO products.

For ZnO nano-crystals, the growth of crystal is preferential in *c*-axis. However, it has been reported that the (0001) facet of the crystal, which is the slight positively charged Zn surface, can be adsorbed by negatively charged chemical species [20, 91, 138, 186, 188]. The adsorbed molecules, therefore, retard the growth of crystal in that direction. The interface-solvent interaction can be applied to justify the results in this work as well. Glycols, which are consisted of two hydroxyl groups at both ends, could effectively attach to the (0001) surface of ZnO crystals and resulted in non-preferential growth of the crystals, as shown in Figure 5.5.2. On the contrary, for non-polar species such as n-alkanes and aromatic compounds, which were not compatible to such electrostatic interaction with (0001) surface, ZnO crystals grew preferentially in *c*-direction to form nanorods (Figure 5.5.4). For alcohols, in which the polarity decreases with the chain length of the molecule, ZnO particles with high aspect ratio were obtained only when long-chained alcohol, e.g. octanol or decanol, was employed. Similar observation for ZnO synthesized in alcohols was also reported by Cheng and Samulski [20].

Zhang et al. [136] have reported that polarity of the solvent affects not only the nucleus formation and preferential direction of crystal growth, but also the amalgamation of crystals. Polarity compatibility between the reactant and the solvent led to homogeneous dispersion of the reactant in the mixture. Consequently, the growth of the crystal was less confined to the boiling droplet of solvent in the reaction system, and resulted in crystal with flowerlike morphology. The results from this work contrasted the observation by Zhang et al. It was found in this work that type of solvent affected the *shape* of ZnO primary particle. No such shaped amalgamation was observed, regardless of the solvents employed.

The effects of solvents on ZnO nanoparticles synthesis, i.e. both nuclei formation and crystal growth, were indeed complex. Other properties of the solvent, such as viscosity [135], saturated vapor pressure [136] and molecular structure leading to the steric hindrance effect [135], have been proposed to be key parameter controlling nanoparticles formation. Nevertheless, according to systematic investigation in this work, no general conclusion could be drawn on these properties of solvents.

However, as shown in Table 5.5.1 and 5.5.2, it is noticeable that the dielectric property of the solvents is significantly correlated with shape of ZnO nanocrystals. The higher the dielectric constant of the solvent, the lower the aspect ratio of the product resulted. Note that this is to be explained from the system employing anhydrous zinc acetate wherein the zinc precursor has directly converted into ZnO and the system environment is the simplest condition. When zinc acetate dihydrate was used, not only the different behavior of zinc oxide nuclei formation, but the interference effect of water in the dihydrate precursor would also deviate the solvent affect on the growth of the crystal. The effect of different zinc precursor on different morphology has been observed and different preferential adsorption was claimed for the explanation [189].

Although parts of the mechanism have been discussed above, detailed characterizations are still needed to investigate the actual mechanism of ZnO nanoparticles formation by the solvothermal synthesis.

5.5.3 Summary

Single crystalline ZnO nanoparticles in different aspect ratios were successfully prepared by the solvothermal method. The hydroxyl group from the alcohol or glycol solvents is polar and could effectively attach to the (0001) plane of zinc oxide, which believed to be positively charged by Zn^{2+}. This retards the fast growth rate of this plane and reduces anisotropic growth nature of zinc oxide. These circumstances did not occur in the absence of hydroxyl group such as the systems using solvents alkanes and aromatic groups. These gave zinc oxide nanorods having very high aspect ratio of up to 100. The nucleation of zinc oxide nuclei could also be

affected by the solvents surrounding the zinc precursor. The temperature needed for zinc oxide nuclei formation was higher for the non-polar solvents. Dielectric constant of the solvent was proposed to be an index that was well correlated with morphology of the synthesized products. The thermal decomposition of the precursor, i.e. anhydrous zinc acetate, to form ZnO nuclei is more spontaneous in the solvent with high dielectric constant. Changing the precursor from anhydrous to zinc acetate dihydrate also changed the resulting morphology, possibly due to the interference of water of the dihydrate precursor.

5.6 Preliminary Investigations of Materials Properties Related to Applications

5.6.1 Mesoporous Niobium Oxides

Among all the niobia samples synthesized in this whole work, two samples in the F127 system of a concentration c1 that subjected to hydrothermal aging at 110°C; with 2-day dialysis and non-dialysis conditions (the F-c1-2dDM-A, and the F-c1-A), showed large surface areas, pore volumes and pore sizes after calcinations at 500°C for 5 hours (1°C/min), and were selected as core representatives for preliminary experiments.

As stated in the literature reviews (chapter III) that the crystallinity can affect the dielectric constant and photocatalytic activity of the materials, the samples subjected to calcinations at 600°C for 5 hours (1°C/min) were also investigated for comparisons in both textural properties and the dielectric and photocatalytic properties. Other samples such as niobium pentoxide (Aldrich) and the F-c1^t, showing well-organized mesopores, were also included for comparisons.

The textural properties and crystallite sizes of the samples mentioned above are summarized in Table 5.6.1. The pore size distributions of the samples are shown for comparison in Figure 5.6.1; the pore size distribution of the niobium pentoxide purchased from Aldrich is shown in separation, in Figure 5.6.2. The XRD patterns of the samples are shown in Figure 5.6.3.

Table 5.6.1 Textural properties and crystallite sizes of the samples

Sample	Calcination Temperature (°C)	BET Surface Area (m²/g)	Pore Volume (cm³/g)	Crystallite Size (nm.)[a]	Crystal Structure[b]
F-c1-2dDM-A	500	144	0.252	-	(partially pseudohexagonal)
F-c1-A	500	150	0.281	-	(partially tetragonal)
F-c1[t]	500	78	0.099	-	(partially pseudohexagonal)
F-c1-2dDM-A	600	59	0.241	27	pseudohexagonal or TT-structure
F-c1-A	600	48	0.236	43	orthorhombic or T-structure
F-c1[t]	600	26	0.117	48	pseudohexagonal or TT-structure
Niobium pentoxide Aldrich[c]	-	3	0.002	n/d	mixed phase

[a], from Scherrer's formula, using the (001) plane.
[b], see also Figure 5.6.3.
[c], Niobium(V) Oxide, 99.99%; Product Number 20392-0, Lot Number 00806PB, Formula: Nb_2O_5, Formular Weight: 265.81.
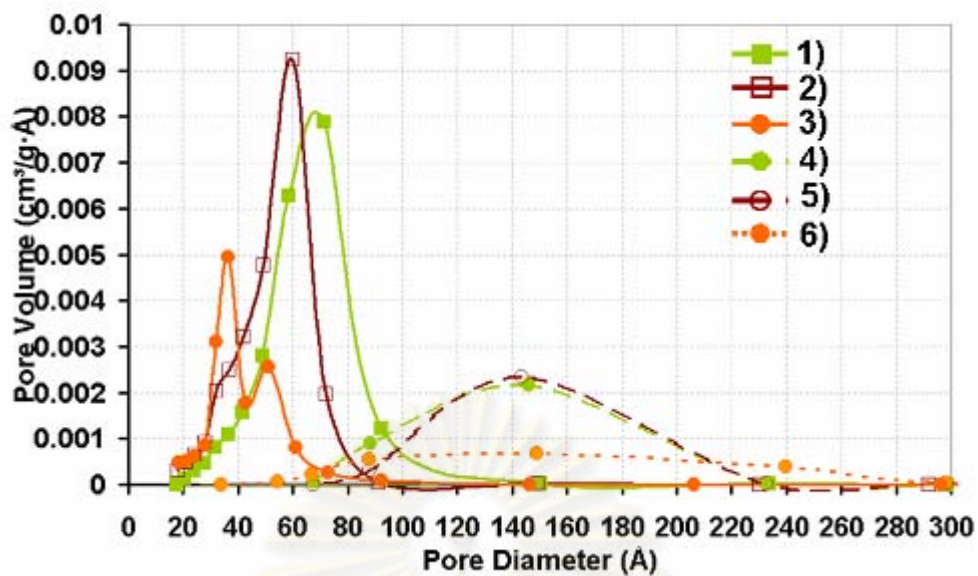
Figure 5.6.1 Pore size distributions of the samples: 1) F-c1-2dDM-A, calcined at 500°C; 2) F-c1-A, calcined at 500°C; 3) F-c1^t, calcined at 500°C; 4) F-c1-2dDM-A, calcined at 600°C; 5) F-c1-A, calcined at 600°C and 6) F-c1^t, calcined at 600°C
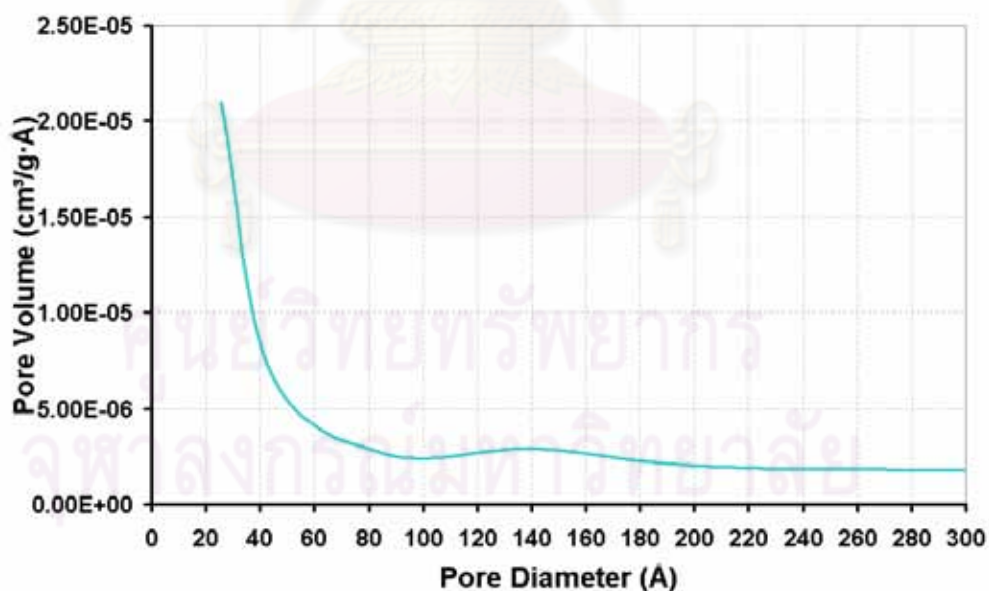
Figure 5.6.2 Pore size distribution of niobium(V) oxide, Aldrich
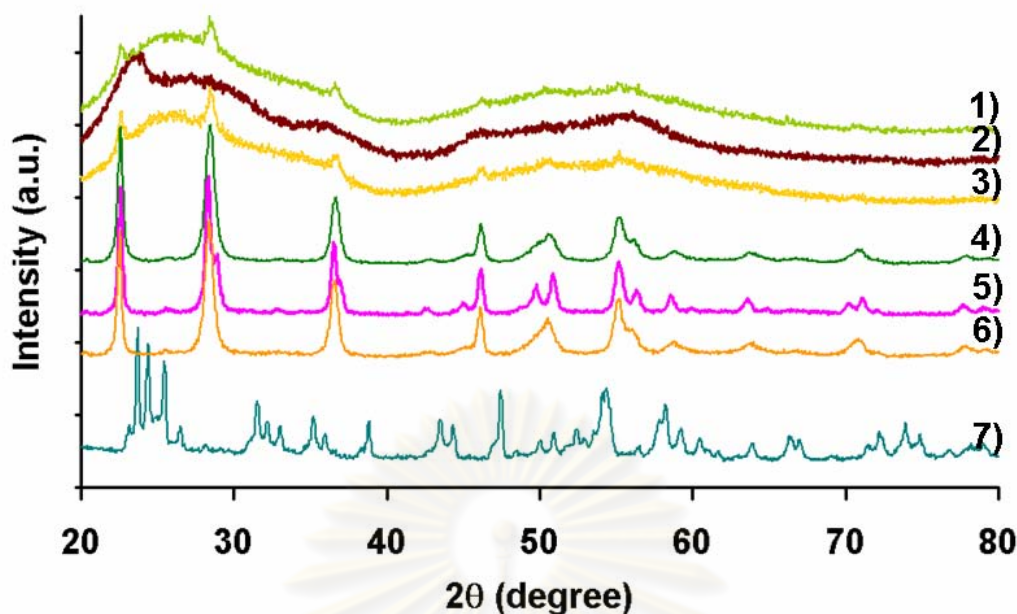
Figure 5.6.3 XRD patterns of the samples: 1) F-c1-2dDM-A, calcined at 500°C; 2) F-c1-A, calcined at 500°C; 3) F-c1^t, calcined at 500°C; 4) F-c1-2dDM-A, calcined at 600°C; 5) F-c1-A, calcined at 600°C; 6) F-c1^t, calcined at 600°C and 7) Niobium(V) Oxide, Aldrich

5.6.1.1 Dielectric constant measurement

The samples being compared are Niobium(V) oxide, Aldrich; the F-c1-2dDM-A (calcined at 500°C and 600°C); and the F-c1-A (calcined at 500°C and 600°C).

Figure 5.6.4 shows the results of the relative dielectric constant of the samples at frequency in the range of 50-1000 kHz. The measurement of the capacitance was repeatedly done on the same pellet and/or on the re-pelletized sample to obtain the error of the measurement, which was shown by the error bar in the figure. The variable frequency did show effect on the value of the dielectric constant of the sample pellets, except the one made of niobium pentoxide, Aldrich. It could be possible that the obtained capacitance read might be affected by the variable packing density or grain boundaries of the pellet under the pelletization process. The magnified pictures of the representative pellets are shown in Appendix D. However, it is assumed here that the value of the capacitance measured at frequency of >500 kHz should be reliable since the properties are determined by the grain boundary effects on the lower frequency while at higher frequency, the effect from bulk grains

dominate [190]. The measured capacitance did not vary with the applied bias (AC) voltage level varied from -10V to 20V. The current leakage given from the LCR meter was also recorded (not shown) where all samples displayed same trend of increasing current leakage with higher measurement frequency.
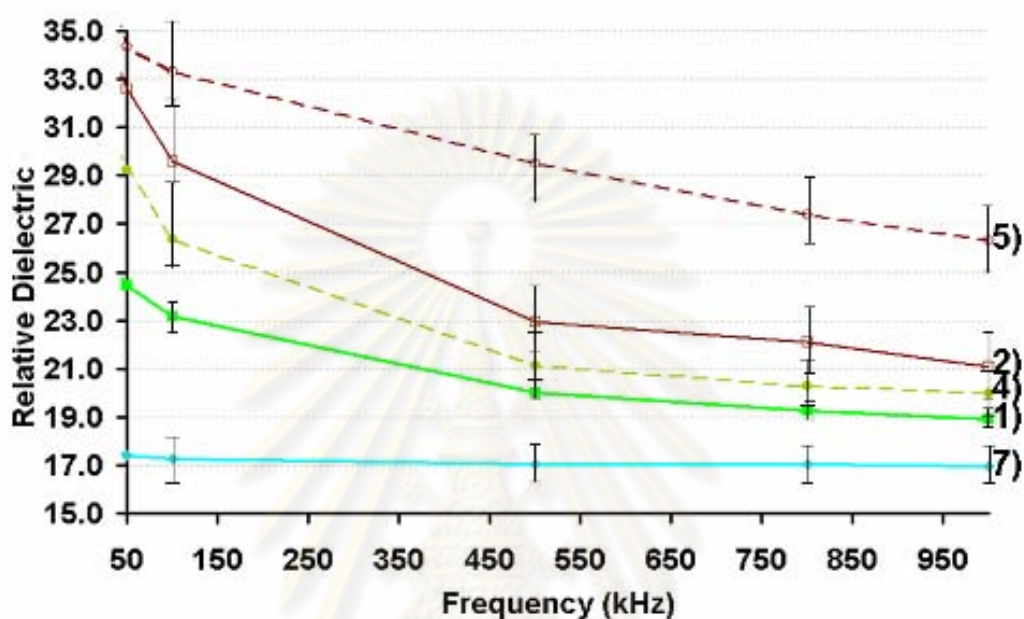
Figure 5.6.4 Relative dielectric constant of the samples: 1) F-c1-2dDM-A, calcined at 500°C; 2) F-c1-A, calcined at 500°C; 4) F-c1-2dDM-A, calcined at 600°C; 5) F-c1-A, calcined at 600°C; 7) Niobium(V) oxide, Aldrich

The results could be summarized as follows:-

1) The niobium(V) oxide purchased from Aldrich showed lowest relative dielectric constant, probably because of the mixed phase in this sample as shown in its XRD pattern. The XRD pattern should be mainly comprised of Nb_2O_5 whose structure is correspondent to JCPDS 05-0379. The unit cell of this structure was reported as: a=21.50, b=3.825, c= 20.60 and angle β=121.75°. These are different from the pseudohexagonal structure of the JCPDS 28-0317 (a=3.607 and c=3.925) or the orthorhombic structure of the JCPDS 30-0873 (a=6.175, b=29.27 and c=3.93) which are the structures of the F-c1-2dDM-A, calcined at 600°C and the F-c1-A, calcined at 600°C, respectively. The Nb_2O_5 referred to JCPDS 19-0862, 37-1468, and $NbO_{2.432}$ of JCPDS 30-0870 could also be possible phases present as a mixed phase in the niobium(V) oxide purchased from Aldrich. The results suggest that the niobium

oxide synthesized under sol-gel in this work, having different crystalline unit cells or structures showed superior dielectric property than the niobium oxide purchased. The synthesis method is then a crucial factor on determining the dielectric properties.

2) For the mesoporous samples, the F-c1-A, calcined at 500°C showed higher relative dielectric constant than the F-c1-2dDM-A, calcined at 500°C but the difference was not much.

3) When the samples were crystallized, the relative dielectric constant increased. Significant increase could be seen from transition of an amorphous with hidden tetragonal phase in the F-c1-A, calcined at 500°C to an orthorhombic (T) phase of the same sample after calcination at 600°C.

4) The increase of the relative dielectric constant from the samples calcined at 500°C to the samples calcined at 600°C is not as significant as the change in the BET surface areas, pore volumes, and pore sizes.

The pore size distributions of the 600°C-calcined samples become much widen which might not be suitable for effective adsorption of chemicals. The large decrease in the BET surface areas, and pore volumes could also result in negative effect the sensing performance [26]. The small increase in the dielectric value of the crystallized products should not be worthy to compensate for the lower textural properties. Hence, it is believed that the samples synthesized by employing triblock copolymer and subjected to 500°C calcinations are the most attractive samples for further investigations of the real capacitive thick film sensor in the future.

5.6.1.2 Photocatalytic ethylene oxidation

In this case, well-ordered mesoporous niobium oxide (the F-c1) was compared with the two main samples having no ordering but higher in surface area and pore size (the F-c1-2dDM-A, and the F-c1-A). The samples after crystallizations (calcined at 600°C) were also tested to see the effect of crystallinity on photocatalytic activity. Hence, the samples being compared are the F-c1-2dDM-A (calcined at 500°C); the F-c1-A (calcined at 500°C and 600°C); the F-c1 (calcined at 500°C and 600°C). Table 5.6.2 shows the ethylene conversion of each sample.

Table 5.6.2 Ethylene photocatalytic conversion of the niobia samples (reactions carried out under UV light and reaction temperature of 100°C using 0.01% ethylene in air; see section 4.6)

Sample	Calcination Temperature (°C)	Ethylene Conversion (%)[a]
F-c1-2dDM-A	500	43
F-c1-A	500	34
F-c1^t	500	30
F-c1-A	600	13
F-c1^t	600	6

[a], after steady state (within 2-3 hours) and equal to the 23 hours of reaction time.

It could be concluded from the results that

1) The F-c1^t, calcined at 500°C sample which has better pore organization but lower surface area showed similar photocatalytic activity with the F-c1-A, calcined at 500°C.

2) The F-c1-2dDM-A, calcined at 500°C, possessing developing TT structure showed little higher ethylene conversion than the F-c1-A, calcined at 500°C having hidden tetragonal phase.

3) The fully crystallized samples (the samples calcined at 600°C) showed poorer photocatalytic activity than the partly crystallized samples (the samples calcined at 500°C)

The overall results suggested that surface area and crystal structure might be important for photocatalytic activity. The mesoporosity could reduce the possibility for electron-hole recombination due to its shorter distance of the excited electrons and holes to migrate to the surface, compared to bulk material [34]. The samples calcined at 600°C were already crystallized and the growth of crystals beyond the wall of the porous structure could result in lower photocatalytic activity. The presence of major amorphous nature of the mesoporous wall of the samples calcined at 500°C reflects higher surface area than that of the crystallized samples; hence, surface area could be regarded as one factor influencing photoactivity. The importance of surface area to the photocatalytic decomposition of probe molecules was also suggested in titania (TiO$_2$) system [191]. The defects at the pore surface after surfactant removal of the mesoporous sample might also exist [25]. The surface defects could provide holes or

electron trapping sites which give lower electron-hole recombination rate and better photocatalytic activities [192].

Different crystal developing pathway and the partially crystallized structure are still not clear for their participation in photocatalytic properties but the partial crystallization into the TT structure of the F-c1-2dDM-A, after calcination at 500°C which showed higher conversion than that of the amorphous with hidden tetragonal phase of the F-c1-A, calcined at 500°C is possibly responsible for the high conversion observed in the F-c1^t, calcined at 500°C, despite its much lower surface area, compared to surface area of the F-c1-A, calcined at 500°C. The conclusion of the advantage from continuity of the inorganic phase [23] in the well-organized wall structure of the F-c1^t, calcined at 500°C is still uncertain to be drawn out.

5.6.2 Nanocrystalline Zinc Oxides

5.6.2.1 Luminescence property and photocatalytic ethylene oxidation

The PL spectra and the photocatalytic activity in ethylene photooxidation were carried out for ZnO samples. The samples being investigated are the sample synthesized from 1-hexanol and n-hexane solvents, as representatives for low and high aspect ratio ZnO. The zinc oxide synthesized by zinc acetate dihydrate as precursor in n-hexane conditions was also tested.

The PL spectra of the samples are shown in Figure 5.6.5 and the ethylene conversions are summarized in Table 5.6.3.
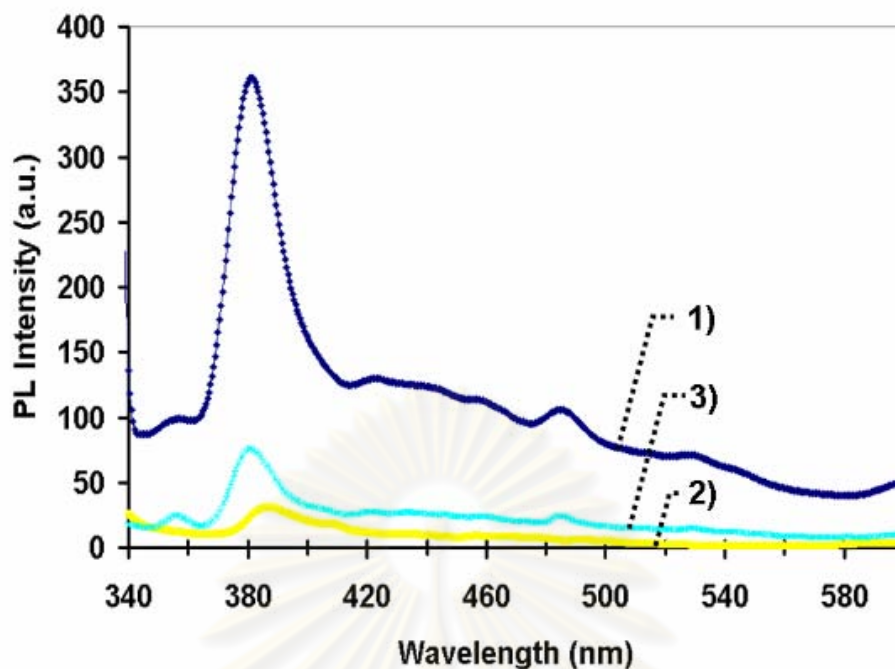
Figure 5.6.5 Photoluminescence (PL) Spectra of ZnO samples synthesized via conditions: 1) Anhydrous zinc acetate, 1-Hexanol, 250°C; 2) Anhydrous zinc acetate, n-Hexane, 300°C and 3) Zinc acetate dihydrate, n-Hexane, 300°C

Table 5.6.3 Ethylene photocatalytic conversion of the ZnO samples synthesized via different conditions (reactions carried out under UV light and reaction temperature of 100°C using 0.01% ethylene in air; see section 4.6)

ZnO Synthesis Condition	Ethylene Conversion (%)[a]
1) Anhydrous zinc acetate, 1-Hexanol, 250°C	16.6
2) Anhydrous zinc acetate, n-Hexane, 300°C	1.6
3) Zinc acetate dihydrate, n-Hexane, 300°C	1.5

[a], after steady state (within 2-3 hours).

The obtained ZnO from the condition (1) and (3), see Table 5.6.3, which have hydroxyl group from alcohol and water, showed small UV emission at ~356 nm. This emission is absence in the non-hydroxyl condition in the condition (2). These suggest that hydroxyl group either from the solvent or from the precursor may passivate the surface of ZnO product [124]. The UV emission at ~382 nm arisen from recombination of excitonic centers [186] was observed for every sample but the

intense emission occurred for the condition (1). This large UV emission intensity suggests that the photo-excited holes have a better chance of finding an oxygen defect [186]. The stong UV emission properties shows that the samples synthesized via conditions containing hydroxyl group may be more promising to be applied to nanoscale optoelectronic devices [193].

The green band emission (~486 nm) was observed for all samples suggesting the presence of the surface oxygen vacancies in ZnO [159, 193]. The higher intensity in the condition using zinc acetate dihydrate; condition (3), compared to the anhydrous; condition (2), indicates that zinc acetate dihydrate induces oxygen vacancies to the ZnO product. These suggest that the passivation of hydroxyl group on the surface should increase surface oxygen defects.

From the overall of the PL intensity, the ZnO synthesized in the absence of hydroxyl group showed lowest defect while those samples synthesized in the presence of hydroxyl group showed higher defect with high UV emission. The high PL intensity in the ZnO obtained from 1-hexanol (condition 1) reflecting high content of surface oxygen vacancies can also contribute to the higher the photocatalytic activity observed [159].

The PL intensity could also be affected by the nanoparticles size as the increasing ZnO particle size decreases the PL intensity [159]. In this case, the larger aspect ratio ZnO could be considered as larger size and provide more possibility for electron-hole recombination, giving low photocatalytic activity as observed for the ZnO obtained from n-Hexane (conditions 2 and 3). Rod-like particles, in the work of Li and Haneda, also showed lower photoactivity than the spherical or ellipsoidal particles [161].

It is, therefore, concluded from the preliminary tests in this work that the high aspect ratio ZnO obtained in the absence of hydroxyl group e.g. using anhydrous zinc acetate and n-hexane as solvent might not be suitable for photocatalytic application or for nanoscale optoelectronic devices due to its low photoactivity and less UV emission [193]. However, it showed least defects as its PL intensity was lowest.

CHAPTER VI

CONCLUSIONS AND RECOMMENDATIONS

6.1 Conclusions

In the mesoporous niobium oxide sol-gel syntheses using niobium(V) chloride and triblock copolymers, the conclusions could be drawn as follows:-

1) Well-ordered mesoporous structure of niobium oxide could be obtained under high drying temperature, to evade the irreproducible problem arisen from different relative humidity of drying condition at low temperature, by employing F127, the triblock copolymer with high ethylene oxide (EO) chain length.

2) Hydrothermal aging at 110°C in F127-ethanol-water system exerts significant effect on textural and structural characteristics of niobium skeleton; larger pore size, pore volume, surface area, tetragonal phase transformation pathway, and enhanced Lewis acidity were obtained.

3) Under the hydrothermal aging at 110°C in F127 system, the amount of water in the system is an important factor influential pore size distribution and structural characteristics of the niobium wall. Lower or higher amount of water resulted in more fraction of the smaller pore size in the bimodal pore size distribution. The tetragonal phase transformation pathway with an enhanced Lewis acid property was not observed for the system with too much amount of water and for the anhydrous system.

4) Dialysis process was believed to be an interesting method to synthesize mesoporous niobium oxide with high surface area and pore volume, with tunable pore sizes. It provides the products in a precipitate form, which is more rapid to dry and with more rigid niobium wall. The latter property makes fine tuning of the pores more possibly achievable than the non-dialyzed method.

In nanocrystalline (non-porous) zinc oxide synthesis, the shape control was successfully attained by solvothermal method using the key strategy as follows:-

1) The crystal structure of zinc oxide is hexagonal structure which has unit cell dimension in long axis, c, longer than those of the x-y axis and the growth rate of (0001) plane of crystal is reported to be significantly faster than other faces. These make anisotropic shape easily possible and the high aspect ratio nanorod could be achieved by allowing the fastest growth plane to grow freely.

2) Physico-chemical properties of the solvent, which was employed as the reaction medium for ZnO synthesis, showed significant impact on both the formation of ZnO nuclei and the growth of the crystals. The solvent with high dielectric constant tended to favor zinc oxide nuclei formation while inhibited the preferential growth of ZnO crystals in c-direction, resulting in the product with relatively low aspect ratio. The high dielectric constant of the solvent is related to high amount of hydroxyl group in the solvent molecule. The hydroxyl group from the zinc precursor also diviated the solvent affect on the growth of the crystal and the non-hydroxyl solvent gave lower aspect ratio when zinc acetate dihydrate was used instead of zinc acetate anhydrous.

From the preliminary properties investigation, the mesoporous niobium oxide having high surface area and pore size showed little lower dielectric constant than those of their crystallized forms whose crystallized natures were literaturally believed to favor the dielectric property. These suggest that the synthesized mesoporous samples are potential candidates as good capacitive materials for thick film sensors. The high surface area of mesoporous samples also exhibited higher photocatalytic activity than their crystallized forms.

The zinc oxide samples obtained under the presence of hydroxyl group showed higher defect, higher light emission intensity, and higher photoactivity than those of the samples with higher aspect ratio synthesized under non-hydroxyl condition. The latters showed much lower surface defect and also lower photoactivity.

6.2 Recommendations

There are still some unclear explanation needed to be explored or the properties of the synthesized materials needed to be improved as are specifically detailed below:-

1) For mesoporous niobium oxide syntheses, an investigation of niobium-polymer interaction via characterizations, such as nuclear magnetic resonance (NMR) or X-ray photoelectron spectroscopy (XPS), should provide a clearer explanation of the properties of the samples. It should help shaping the conditions to obtain desired mesostructural properties both prior to and after the calcinations. Also, the effect of water on these textural properties is quite complex and needs further investigation.

2) For zinc oxide syntheses, although shape control was accomplished via solvothermal method, the particle size obtained still showed large standard deviation. Further improvement of the synthesis procedures such as applying sonication to zinc precursor prior to solvothermal reaction should be tried.

3) More detailed applications of the synthesized materials should be carried out. The dielectric related properties such as current leakage and voltage dependent behavior of the material are also needed to be explored, with the notes to be bared in mind that those properties may also depend on the configuration and the preparation method of the finished capacitor derived from the materials. The examples of the fabrication of the niobium capacitors can be found in References [13, 194]. Other expecting properties should also be investigated. For example, mesoporous niobium oxide suspected to have an enhanced Lewis acidity should be tested as solid acid catalysts in reaction such as total oxidation reaction [35]. Efficiency in electrical conductivity or performance of light-emitting diode is also an interesting investigation of zinc oxide with various aspect ratios [19]. It is also challenging to find the way to align the nanorod to extract its real benefits from an anisotropic property. Otherwise, the high aspect ratio nanorods might be tried in applications of zinc oxide fiber.

REFERENCES

[1] Kresge, C. T.; Leonowicz, M. E.; Roth, W. J.; Vartuli, J. C.; Beck, J. S. Ordered Mesoporous Molecular Sieves Synthesized by a Liquid-Crystal Template Mechanism. <u>Nature</u> 359 (1992): 710-712.

[2] Tanev, P. T.; Pinnavaia, T. J. A Neutral Templating Route to Mesoporous Molecular Sieves. <u>Science</u> 267 (1995): 865-867.

[3] Mercier, L.; Pinnavaia, T. J. Direct Synthesis of Hybrid Organic-Inorganic Nanoporous Silica by a Neutral Amine Assembly Route: Structure-Function Control by Stoichiometric Incorporation of Organosiloxane Molecules. <u>Chem. Mater.</u> 12 (2000): 188-196.

[4] Huo, Q.; Margolese, D. I.; Stucky, G. D. Surfactant Control of Phases. in the Synthesis of Mesoporous Silica-based Materials. <u>Chem. Mater.</u> 8 (1996): 1147-1160.

[5] Goltner, C. G.; Antonietti, M. Mesoporous Materials by Templating of Liquid Crystalline Phases. <u>Adv. Mater.</u> 9, 5 (1997): 431-436.

[6] Patarin, J.; Lebeau, B.; Zana, R. Recent Advances in the Formation Mechanisms of Organized Mesoporous Materials. <u>Curr. Opin. Colloid Interface Sci.</u> 7, 1-2 (2002): 107-115.

[7] Moller, K.; Bein, T. Inclusion Chemistry in Periodic Mesoporous Hosts. <u>Chem. Mater.</u> 10 (1998): 2950-2963.

[8] Wu, C.-G.; Bein, T. Polyaniline Wires in Oxidant-Containing Mesoporous Channel Hosts. <u>Chem. Mater.</u> 6 (1994): 1109.

[9] Vettraino, M.; Trudeau, M. L.; Antonelli, D. M. Synthesis and Electronic Properties of Reduced Mesoporous Sodium Niobium Oxides. <u>Adv. Mater.</u> 12 (2000): 337-340.

[10] Grosso, D.; Soler-Illia, G. J. d. A. A.; Babonneau, F.; Sanchez, C.; Albouy, P. A.; Brunet-Bruneau, A.; Balkenenende, A. R. Highly Organized Mesoporous Titania Thin Films Showing Mono-Oriented 2D Hexagonal Channels. <u>Adv. Mater.</u> 13, 14 (2001): 1085-1090.

[11] Schuth, F. Non-siliceous Mesostructured and Mesoporous Materials. <u>Chem. Mater.</u> 13 (2001): 3184-3195.

[12] Monnier, A. S.; Huo, Q.; Kumar, D.; Margolese, D.; Maxwell, R. S.; Stucky, G. D.; Drishnamurty, M.; Petroff, P.; Firouzi, A.; Janicke, M.; Chmelka, B. Cooperative Formation of Inorganic-Organic Interfaces in the Synthesis of Silicate Mesostructures. <u>Science</u> 261 (1993): 1299.

[13] Pignolet, A.; Mohan Rao, G.; Krupanidhi, S. B. Rapid Thermal Processed Thin Films of Niobium Pentoxide (Nb_2O_5) Deposited by Reactive Magnetron Sputtering. <u>Thin Solid Films</u> 261, 1-2 (1995): 18-24.

[14] Wang, J.; Gudiksen, M. S.; Duan, X.; Cui, Y.; Lieber, C. M. Highly Polarized Photoluminescence and Photodetection from Single Indium Phosphide Nanowires. <u>Science</u> 293, 5534 (2001): 1455-1457.

[15] Tans, S. J.; Devoret, M. H.; Dai, H.; Thess, A.; Smalley, R. E.; Geerligs, L. J.; Dekker, C. Individual Single-Wall Carbon Nanotubes as Quantum Wires. <u>Nature</u> 386 (1997): 474-477.

[16] Chung, S.-W.; Yu, J.-Y.; Heath, J. R. Silicon Nanowire Devices. <u>Appl. Phys. Lett.</u> 76 (2000): 2068-2071.

[17] Davydov, D. N.; Sattari, P. A.; AlMawlawi, D.; Osika, A.; Haslett, T. L.; Moskovits, M. Field Emitters Based on Porous Aluminum Oxide Templates. <u>J. Appl. Phys.</u> 86, 7 (1999): 3983-3987.

[18] Wu, Y.; Yan, H.; Huang, M.; Messer, B.; Song, J. H.; Yang, P. Inorganic Semiconductor Nanowires: Rational Growth, Assembly, and Novel Properties. <u>Chem. Eur. J.</u> 8, 6 (2002): 1260-1268.

[19] Brinker, C. J.; Scherer, G. W., <u>Sol-Gel Science The Physics and Chemistry of Sol-Gel Processing</u>. Acedemic Press: San Diego, p 358-373, 1989.

[20] Cheng, B.; Samulski, E. T. Hydrothermal Synthesis of One-Dimensional ZnO Nanostructures with Different Aspect Ratios. <u>Chem. Commun.</u> (2004): 986-987.

[21] Vik, A. F.; Dracopoulos, V.; Papatheodorou, G. N.; Østvold, T. Solubility and Raman Spectra of Nb(V) in LiF–NaF–KF–Na_2O Melts. <u>J. Alloy. Comp.</u> 321 (2001): 284-299.

[22] Jun, Y.-W.; Seo, J.-W.; Oh, S. J.; Cheon, J. Recent Advances in the Shape Control of Inorganic Nano-Building Blocks. <u>Coord. Chem. Rev.</u> 249, 17 (2005): 1766-1775.

[23] Kondo, J. N.; Domen, K. Crystallization of Mesoporous Metal Oxides. <u>Chem. Mater.</u> 20 (2008): 835-847.

[24] Zillgen, H.; Stenzel, M.; Lohwasser, W. New Niobium Capacitors with Stable Electrical Parameters. Active and Passive Elec. Comp. 25 (2002): 147-153.

[25] Stone, V. F., Jr. ; Davis, R. J. Synthesis, Characterization, and Photocatalytic Activity of Titania and Niobia Mesoporous Molecular Sieves. Chem. Mater. 10, 5 (1998): 1468-1474.

[26] Xu, X.; Tian, B.; Zhang, S.; Kong, J.; Zhao, D.; Liu, B. Electrochemistry and Biosensing Reactivity of Heme Proteins Adsorbed on the Structure-Tailored Mesoporous Nb_2O_5 Matrix. Anal. Chim. Acta 519 (2004): 31-38.

[27] Murray, S.; Trudeau, M.; Antonelli, D. M. Synthesis and Magnetic Tuning in Superparamagnetic Cobaltocene-Mesoporous Niobium Oxide Composites. Adv. Mater. 12, 18 (2000): 1339-1342.

[28] Yang, P.; Zhao, D.; Margolese, D. I.; Chmelka, B. F.; Stucky, G. D. Generalized Syntheses of Large-Pore Mesoporous Metal Oxides with Semicrystalline Frameworks. Nature 396 (1998): 152-155.

[29] Bizeto, M. A.; Constantino, V. R. L. Niobium Oxide Mesophases Obtained by Self-Assembly of an Aqueous Soluble Niobium Complex Precursor and Organic Templates. Eur. J. Inorg. Chem. (2007): 579-584.

[30] Nowak, I.; Ziolek, M. Niobium Compounds: Preparation, Characterization, and Application in Heterogeneous Catalysis. Chem. Rev. 99, 12 (1999): 3603-3624.

[31] Prado, A. G. S.; Faria, E. A.; SouzaDe, J. R.; Torres, J. D. Ammonium Complex of Niobium as a Precursor for the Hydrothermal Preparation of Cellulose Acetate/Nb_2O_5 Photocatalyst. J. Mol. Catal. A: Chem. 237 (2005): 115-119.

[32] Dragone, L.; Moggi, P.; Predieri, G.; Zanoni, R. Niobia and Silica-Niobia Catalysts from Sol-Gel Synthesis: an X-Ray Photoelectron Spectroscopic Characterization. Appl. Surf. Sci. 187 (2002): 82-88.

[33] Ciesla, U.; Schuth, F. Ordered Mesoporous Materials. Micropor. Mesopor. Mater. 27 (1999): 131-149.

[34] Chen, X.; Yu, T.; Fan, X.; Zhang, H.; Li, Z.; Ye, J.; Zou, Z. Enhanced Activity of Mesoporous Nb_2O_5 for Photocatalytic Hydrogen Production. Appl. Surf. Sci. 253, 20 (2007): 8500-8506.

[35] Ohuchi, T.; Miyatake, T.; Hitomi, Y.; Tanaka, T. Liquid Phase Photooxidation of Alcohol Over Niobium Oxide Without Solvents. Catal. Today 120 (2007): 233-239.

[36] Vettraino, M.; He, X.; Trudeau, M.; Drake, J. E.; Antonelli, D. M. Synthesis of a Stable Metallic Niobium Oxide Molecular Sieve and Subsequent Room Temperature Activation of Dinitrogen. Adv. Funct. Mater. 12 (2002): 174-178.

[37] Suh, D. J.; Park, T.-J. Sol-Gel Strategies for Pore Size Control of High-Surface-Area Transition Metal Oxide Aerogels. Chem. Mater. 8 (1996): 509-513.

[38] Ikeya, T.; Senna, M. Amorphization and Phase Transformation of Niobium Pentoxide by Fine Grinding. J. Mater. Sci. 22 (1987): 2497-2502.

[39] Silva, C. L. T. d.; Camorim, V. L. L.; Zotin, J. L.; Pereira, M. L. R. D.; A.da.C. Faro, J. Surface Acidic Properties of Alumina-Supported Niobia Prepared by Chemical Vapour Deposition and Hydrolysis of Niobium Pentachloride. Catal. Today 57 (2000): 209-217.

[40] Ko, E. I.; Hupp, J. M.; Rogan, F. H.; Wagner, N. J. Preparation, Reduction, and Chemisorption Behavior of Niobia-Supported Nickel Catalysts. J. Catal. 84 (1983): 85-94.

[41] Passos, F. B.; Aranda, D. A. G.; Soares, R. R.; Schmal, M. Effect of Preparation Method on the Properties of Nb_2O_5 Promoted Platinum Catalysts. Catal. Today 43 (1998): 3-9.

[42] Passos, F. B.; Lopes, I. S.; Silva, P. R. J.; Saitovitch, H. Hyperfine Interactions Studies on Pt-In/Nb_2O_5 Catalysts. Catal. Today 78 (2003): 411-417.

[43] Lee, B.; Lu, D.; Kondo, J. N.; Domen, K. Three-Dimensionally Ordered Mesoporous Niobium Oxide. J. Am. Chem. Soc. 124 (2002): 11256-11257.

[44] Yang, P.; Zhao, D.; Margolese, D. I.; Chmelka, B. F.; Stucky, G. D. Block Copolymer Templating Syntheses of Mesoporous Metal Oxides with Large Ordering Lengths and Semicrystalline Framework. Chem. Mater. 11 (1999): 2813-2826.

[45] Hiyoshi, M.; Lee, B.; Lu, D.; Hara, M.; Kondo, J. N.; Domen, K. Supermicroporous Niobium Oxide as an Acid Catalyst. Catal. Lett. 98, 4 (2004): 181-186.

[46] Tian, B.; Liu, X.; Tu, B.; Yu, C.; Fan, J.; Wang, L.; Xie, S.; Stucky, G. D.; Zhao, D. Self-Adjusted Synthesis of Ordered Stable Mesoporous Minerals by Acid-Base Pairs. Nature Mater. 2 (2003): 159-163.

[47] Xu, X.; Tian, B. Z.; Kong, J. L.; Zhang, S.; Liu, B. H.; Zhao, D. Y. Ordered Mesoporous Niobium Oxide Film: A Novel Matrix for Assembling Functional

Proteins for Bioelectrochemical Applications. <u>Adv. Mater.</u> 15, 22 (2003): 1932-1936.

[48] Lee, B.; Lu, D.; Kondo, J. N.; Domen, K. Preparation of Ordered Supermicroporous Niobium Oxide. <u>Chem. Lett.</u> (2002): 1058-1059.

[49] Wan, Y.; Shi, Y.; Zhao, D. Designed Synthesis of Mesoporous Solids via Nonionic-Surfactant-Templating Approach. <u>Chem. Comm.</u> (2007): 897-926.

[50] Choi, S. Y.; Mamak, M.; Coombs, N.; Chopra, N.; Ozin, G. A. Thermally Stable Two-Dimensional Hexagonal Mesoporous Nanocrystalline Anatase, Meso-nc-TiO$_2$: Bulk and Crack-Free Thin Film Morphologies. <u>Adv. Funct. Mater.</u> 14, 4 (2004): 335-344.

[51] Kunjara Na Ayudhya, S.; Soottitantawat, A.; Praserthdam, P.; Satayaprasert, C. Effect of Aging on the Properties of Mesoporous Niobium Oxide. <u>Mater. Chem. Phys.</u> (2008): In Press.

[52] Soler-Illia, G. J. d. A. A.; Sanchez, C.; Lebeau, B.; Patarin, J. Chemical Strategies To Design Textured Materials: from Microporous and Mesoporous Oxides to Nanonetworks and Hierarchical Structures. <u>Chem. Rev.</u> 102 (2002): 4093-4138.

[53] Nakajima, K.; Hara, M.; Domen, K.; Kondo, J. N. Synthesis of Highly Ordered Mesoporous Tantalum Oxide. <u>Chem. Lett.</u> 34, 3 (2005): 394-395.

[54] Lindén, M.; Blanchard, J.; Schacht, S.; Schunk, S.; Schüth, F. Phase Behavior and Wall Formation in Zr(SO$_4$)$_2$/CTABr and TiOSO$_4$/CTABr Mesophases. <u>Chem. Mater.</u> 11, 10 (1999): 3002-3008.

[55] Antonelli, D. M.; Ying, J. Y. Synthesis of a Stable Hexagonally Packed Mesoporous Niobium Oxide Molecular Sieve Through a Novel Ligand-Assisted Templating Mechanism. <u>Angew. Chem. Int. Ed. Engl.</u> 35, 4 (1996): 426-430.

[56] Soler-Illia, G. J. d. A. A.; Sanchez, C. Interactions between Poly(ethylene oxide)-Based Surfactants and Transition Metal Alkoxides: their Role in the Templated Construction of Mesostructured Hybrid Organic–Inorganic Composites. <u>New J. Chem.</u> 24 (2000): 493-499.

[57] Alquier, C.; Vandenborre, M. T.; Henry, M. Synthesis of Niobium Pentoxide Gels. <u>J. Non-Cryst. Solids</u> 79, 3 (1986): 383-395.

[58] Soler-Illia, G. J. d. A. A.; Crepaldi, E. L.; Grosso, D.; Sanchez, C. Block Copolymer-Templated Mesoporous Oxides. <u>Curr. Opin. Colloid Interface Sci.</u> 8 (2003): 109-126.

[59] Smitha, S.; Shajesh, P.; Aravind, P. R.; Kumar, S. R.; Pillai, P. K.; Warrier, K. G. K. Effect of Aging Time and Concentration of Aging Solution on the Porosity Characteristics of Subcritically Dried Silica Aerogels. Micropor. Mesopor. Mater. 91 (2006): 286-292.

[60] Wang, C.-C.; Ying, J. Y. Sol-Gel Synthesis and Hydrothermal Processing of Anatase and Rutile Titania Nanocrystals. Chem. Mater. 11, 11 (1999): 3113-3120.

[61] Khunshalani, D.; Ozin, G. A.; Kuperman, A. Glycometallate Surfactants Part 2: Non-Aqueous Synthesis of Mesoporous Titanium, Zirconium and Niobium Oxides. J. Mater. Chem. 9 (1999): 1491-1500.

[62] Antonelli, D. M. Synthesis of Macro-Mesoporous Niobium Oxide Molecular Sieves by a Ligand-Assisted Vesicle Templating Strategy. Micropor. Mesopor. Mater. 33 (1999): 209-214.

[63] Antonelli, D. M.; Nakahira, A.; Ying, J. Y. Ligand-Assisted Liquid Crystal Templating in Mesoporous Niobium Oxide Molecular Sieves. Inorg. Chem. 35 (1996): 3126-3136.

[64] Soler–Illia, G.; Sanchez, C. Interactions between poly(ethylene oxide)-based surfactants and transition metal alkoxides: their role in the templated construction of mesostructured hybrid organic–inorganic composites. New Journal of Chemistry 24 (2000): 493-499

[65] Lopes, J. R.; Loh, W. Investigation of Self-Assembly and Micelle Polarity for a Wide Range of Ethylene Oxide-Propylene Oxide-ethylene Oxide Block Copolymers in Water. Langmuir 14 (1998): 750-756.

[66] Kriesel, J. W.; Sander, M. S.; Tilley, T. D. General Route to Homogeneous, Mesoporous, Multicomponent Oxides Based on the Thermolytic Transformation of Molecular Precursors in Non-polar Media. Adv. Mater. 13 (2001): 331-335.

[67] Liu, B.; Zeng, H. C. Hydrothermal Synthesis of ZnO Nanorods in the Diameter Regime of 50 nm. J. Am. Chem. Soc. 125 (2003): 4430-4431.

[68] Zhang, Y.; Yu, K.; Jiang, D.; Zhu, Z.; Geng, H.; Luo, L. Zinc Oxide Nanorod and Nanowire for Humidity Sensor. Appl. Surf. Sci. 242 (2005): 212-217.

[69] Minami, T. Transparent and Conductive Multicomponent Oxide Films Prepared by Magnetron Sputtering. J. Vac. Sci. Technol. A 17 (1999): 1765-1772.

[70] Weibenrieder, K.-S.; Muller, J. Conductivity Model for Sputtered ZnO-Thin Film Gas Sensors. Thin Solid Films 300, 1-2 (1997): 30-41.

[71] Fan, H. J.; Bertram, F.; Dadgar, A.; Christen, J.; Krost, A.; Zacharias, M. Self-Assembly of ZnO Nanowires and the Spatial Resolved Characterization of their Luminescence. Nanotechnology 15 (2004): 1401-1404.

[72] Alivisatos, A. P. Semiconductor Clusters, Nanocrystals, and Quantum Dots. Science 271 (1996): 933-937.

[73] Lieber, C. M. One-Dimensional Nanostructures: Chemistry, Physics & Applications. Solid State Comm. 107, 11 (1998): 607-616.

[74] Albe, V.; Jouanin, C.; Bertho, D. Influence of II-VI Nanocrystal Shapes on Optical Properties. J. Cryst. Growth 184-185 (1998): 388-392.

[75] Williamson, A. J.; Zunger, A. InAs Quantum Dots: Predicted Electronic Structure of Free-Standing Versus GaAs-Embedded Structures. Phys. Rev. B 59, 24 (1999): 15819-15824.

[76] Aegerter, M. A.; Jafelicci, M., Jr.; Souza, D. F.; Zanotto, E. D., Sol-Gel Science and Technology: Proceedings of the Winter School on Glasses and Ceramics from Gels. World Scientific: Singapore, p 63-156, 1989.

[77] Rahaman, M. N., Ceramic Processing and Sintering. 2nd ed.; Marcel Dekker, Inc.: New York, p 18, 248-254, 2003.

[78] Soler-Illia, G. J. d. A. A.; Scolan, E.; Louis, A.; Albouy, P. A.; Sanchez, C. Design of Meso-Structured Titanium Oxo Based Hybrid Organic–Inorganic Networks. New J. Chem. 25 (2001): 156-165.

[79] Vioux, A. Nonhydrolytic Sol-Gel Routes to Oxides. Chem. Mater. 9 (1997): 2292-2299.

[80] Forster, S.; Plantenberg, T. From Self-Organizing Polymers to Nanohybrid and Biomaterials. Angew. Chem. Int. Ed. 41 (2002): 688-714.

[81] Nakashima, K.; Bahadur, P. Aggregation of Water-Soluble Block Copolymers in Aqueous Solutions: Recent Trends. Adv. Colloid Interface Sci. 123-126 (2006): 75-96.

[82] Letchford, K.; Burt, H. A Review of the Formation and Classification of Amphiphilic Block Copolymer Nanoparticulate Structures: Micelles, Nanospheres, Nanocapsules and Polymersomes. Eur. J. Pharm. Biopharm. 65 (2007): 259-269.

[83] www.basf.com

[84] Alexandridis, P.; Holzwarthf, J. F.; Hatton, T. A. Micellization of Poly(ethylene oxide)-Poly(propylene oxide)-Poly(ethylene oxide) Triblock Copolymers in

Aqueous Solutions: Thermodynamics of Copolymer Association. Macromolecules 27 (1994): 2414-2425.

[85] Goyal, P. S.; Aswal, V. K. Micellar Structure and Inter-Micelle Interactions in Micellar Solutions: Results of Small Angle Neutron Scattering Studies. Curr. Sci. 80, 8 (2001): 972-979.

[86] Lettow, J. S.; Han, Y. J.; Schmidt-Winkel, P.; Yang, P.; Zhao, D.; Stucky, G. D.; Ying, J. Y. Hexagonal to Mesocellular Foam Phase Transition in Polymer-Templated Mesoporous Silicas. Langmuir 16, 22 (2000): 8291-8295.

[87] Zhao, D.; Huo, Q.; Feng, J.; Chmelka, B. F.; Stucky, G. D. Nonionic Triblock and Star Diblock Copolymer and Oligomeric Surfactant Syntheses of Highly Ordered, Hydrothermally Stable, Mesoporous Silica Structures. J. Am. Chem. Soc. 120 (1998): 6024-6036

[88] Brinker, C. J.; Lu, Y.; Sellinger, A.; Fan, H. Evaporation-Induced Self-Assembly: Nanostructures Made Easy. Adv. Mater. 11, 7 (1999): 579-585.

[89] Li, W.-J.; Shi, E.-W.; Zhong, W.-Z.; Yin, Z.-W. Growth Mechanism and Growth Habit of Oxide Crystals. J. Cryst. Growth 203, 1-2 (1999): 186-196.

[90] Laudise, R. A.; Ballman, A. A. Hydrothermal Synthesis of Zinc Oxide and Zinc Sulfide. J. Phys. Chem. 64, 5 (1960): 688-691.

[91] Li, W.-J.; Shi, E.-W.; Zhong, W.-Z.; Yin, Z.-W. Growth Mechanism and Growth Habit of Oxide Crystals. J. Cryst. Growth 203 (1999): 186-196.

[92] Rajamathi, M.; Seshadri, R. Oxide and Chalcogenide Nanoparticles from Hydrothermal/Solvothermal Reactions. Curr. Opin. Solid State Mat. Sci. 6, 4 (2002): 337-345.

[93] Klinowski, J.; Barrie, P. J., Recent Advances in Zeolite Science. Amsterdam, 1990.

[94] Verdon, E.; Devalette, M.; Demazeau, G. Solvothermal Synthesis of Cerium Dioxide Microcrystallites: Effect of the Solvent. Mater. Lett. 25 (1995): 127-131.

[95] Barbieri, F.; Cauzzi, D.; De Smet, F.; Devillers, M.; Moggi, P.; Predieri, G.; Ruiz, P. Mixed-Oxide Catalysts Involving V, Nb and Si Obtained by a Non-Hydrolytic Sol-Gel Route: Preparation and Catalytic Behaviour in Oxidative Dehydrogenation of Propane. Catal. Today 61, 1-4 (2000): 353-360.

[96] Pârvulescu, V.; Ruwet, M.; Grange, P.; Pârvulescu, V. I. Preparation, Characterisation and Catalytic Behaviour of Cobalt-Niobia Catalysts. J. Mol. Catal. A: Chem. 135, 1 (1998): 75-88.

[97] Kominami, H.; Inoue, M.; Inui, T. Formation of Niobium Double Oxides by the Glycothermal Method. Catal. Today 16, 3-4 (1993): 309-317.

[98] Maurer, S. M.; Ko, E. I. Structural and Acidic Characterization of Niobia Aerogels. J. Catal. 135 (1992): 125-134.

[99] Pinna, N.; Antonietti, M.; Niederberger, M. A Novel Nonaqueous Route to V_2O_3 and Nb_2O_5 Nanocrystals. Colloid Surface Physicochem. Eng. Aspect. 250 (2004): 211-213.

[100] Feldmann, C.; Jungk, H.-O. Polyol-Mediated Preparation of Nanoscale Oxide Particles. Angew. Chem. Intl. 40 (2001): 359-362.

[101] Liete, E. R.; Vila, C.; Bettini, J.; Longo, E. Synthesis of Niobia Nanocrystals with Controlled Morphology. J. Phys. Chem. B 110 (2006): 18088-18090.

[102] Leontidis, E. Hofmeister Anion Effects on Surfactant Self-Assembly and the Formation of Mesoporous Solids. Curr. Opin. Colloid Interface Sci. 7 (2002): 81-91.

[103] Niez, K.; Yang, P.; Somorjai, G. A. Sol-Gel Synthesis of Ordered Mesoporous Alumina. Chem. Commun. 1-3 (2005): 1986-1987.

[104] Newalkar, B. L.; Komarneni, S. Control over Microporosity of Ordered Microporous-Mesoporous Silica SBA-15 Framework under Microwave-Hydrothermal Conditions: Effect of Salt Addition. Chem. Mater. 13, 12 (2001): 4573-4579.

[105] Yu, J.; Shi, J.-L.; Chen, H.-R.; Yan, J.-N.; Yan, D.-S. Effect of Inorganic Salt Addition During Synthesis on Pore Structure and Hydrothermal Stability of Mesoporous Silica. Micropor. Mesopor. Mater. 46 (2001): 153-162.

[106] Alexandridis, P.; Holzwarth, J. F. Differential Scanning Calorimetry Investigation of the Effect of Salts on Aqueous Solution Properties of an Amphiphilic Block Copolymer (Poloxamer). Langmuir 13, 23 (1997): 6074-6082.

[107] Grosso, D.; Soler-Illia, G.; Babonneau, F.; Sanchez, C.; Albouy, P. A.; Brunet-Bruneau, A.; Balkenenende, A. R. Highly Organized Mesoporous Titania Thin Films Showing Mono-Oriented 2D Hexagonal Channels. Adv. Mater. 13, 14 (2001): 1085-1090.

[108] Rosatto, S. S.; Sotomayor, P. T.; Kubota, L. T.; Gushikem, Y. SiO_2/Nb_2O_5 Sol-Gel as a Support for HRP Immobilization in Biosensor Preparation for Phenol Detection. Electrochimica Acta 47 (2002): 4451-4458.

[109] Bagshaw, S. A. Modification of [M]-MSU-X Mesoporous Silicate Pore Morphology by Post-Synthesis Treatment. Chem. Comm. (1999): 271-272.

[110] Shimizu, Y.; Jono, A.; Hyodo, T.; Egashira, M. Preparation of Large Mesoporous SnO_2 Powder for Gas Sensor Application. Sens. Actuators B 108, 1-2 (2005): 56-61.

[111] Jiu, J.; Kurumada, K.-I.; Tanigaki, M. Preparation of Nanoporous ZnO Using Copolymer Gel Template. Mater. Chem. Phys. 81 (2003): 93-98.

[112] Sagar, P.; Shishodia, P. K.; Mehra, R. M. Influence of pH Value on the Quality of Sol-Gel Derived ZnO Films. Appl. Surf. Sci. 253 (2007): 5419-5424.

[113] Mondelaers, D.; Vanhoyland, G.; Van den Rul, H.; D'Haen, J.; Van Bael, M. K.; Mullens, J.; Van Poucke, L. C. Synthesis of ZnO Nanopowder via an Aqueous Acetate-Citrate Gelation Method. Mater. Res. Bull. 37 (2002): 901-914.

[114] Liu, Z.; Jin, Z.; Li, W.; Qiu, J. Preparation of ZnO Porous Thin Films by Sol-Gel Method Using PEG Template. Mater. Lett. 59 (2005): 3620-3625.

[115] Song, H.; Rioux, R. M.; Hoefelmeyer, J. D.; Komor, R.; Niesz, K.; Grass, M.; Yang, P.; Somorjai, G. A. Hydrothermal Growth of Mesoporous SBA-15 Silica in the Presence of PVP-Stabilized Pt Nanoparticles: Synthesis, Characterization, and Catalytic Properties. J. Am. Chem. Soc. 128 (2006): 3027-3037.

[116] Ning, G.-H.; Zhao, X.-P.; Li, J.; Zhang, C.-Q. Hugely Enhanced Electroluminescence from Mesoporous ZnO Particles. Opt. Mater. 28 (2006): 385-390.

[117] Wang, F.; Liu, R.; Pan, A.; Xie, S.; Zou, B. A Simple and Cheap Way to Produce Porous ZnO Ribbons and their Photovoltaic Response. Mater. Lett. 61 (2007): 4459-4462.

[118] Li, M.; Liu, X.-l.; Cui, D.-l.; Xu, H.-y.; Jiang, M.-h. Preparation of ZnO Bulk Porous Nanosolids of Different Pore Diameters by a Novel Solvothermal Hot Press (STHP) Method. Mater. Res. Bull. 41 (2006): 1259-1265.

[119] Wagner, T.; Waitz, T.; Roggenbuck, J.; Froba, M.; Kohl, C.-D.; Tiemann, M. Ordered Mesoporous ZnO for Gas Sensing. Thin Solid Films 515 (2007): 8360-8363.

[120] Huang, M. H.; Mao, S.; Feick, H.; Yan, H.; Wu, Y.; Kind, H.; Weber, E.; Russo, R.; Yang, P. Room-Temperature Ultraviolet Nanowire Nanolasers. Science 292 (2001): 1897-1899.

[121] Wang, X.; Summers, C. J.; Wang, Z. L. Large-Scale Hexagonal-Patterned Growth of Aligned ZnO Nanorods for Nano-optoelectronics and Nanosensor Arrays. Nano Lett. (2004): 423-426.

[122] Scher, E. C.; Manna, L.; Alivisatos, A. P. Shape Control and Applications of Nanocrystals. Philos. Trans. R. Soc. London, Ser. A 361 (2003): 241-257.

[123] Wei, H.; Wu, Y.; Lun, N.; Hu, C. Hydrothermal Synthesis and Characterization of ZnO Nanorods. Mater. Sci. Eng. A 393 (2005): 80-82.

[124] Ni, Y.-H.; Wei, X.-W.; Hong, J.-M.; Ye, Y. Hydrothermal Preparation and Optical Properties of ZnO Nanorods. Mater. Sci. Eng. B 121 (2005): 42-47.

[125] Rensmo, H.; Keis, K.; Lindstrom, H.; Sodergren, S.; Solbrand, A.; Hagfeldt, A.; Lindquist, S. E.; Wang, L. N.; Muhammed, M. High Light-to-Energy Conversion Efficiencies for Solar Cells Based on Nanostructured ZnO Electrodes. J. Phys. Chem. B 101 (1997): 2598-2601.

[126] Dem'yanets, L. N.; Li, L. E.; Uvarova, T. G.; Mininzon, Y. M.; Briskina, C. M.; Zhilicheva, O. M.; Titkov, S. V. Hydrothermal Synthesis and Spectroscopic Properties of Crystalline ZnO Powders and Films. Inorg. Mater. 40, 11 (2004): 1173-1180.

[127] Li, Z.; Xie, Y.; Xiong, Y.; Zhang, R.; He, W. Reverse Micelle-assisted Route to Control Diameters of ZnO Nanorods by Selecting Different Precursors. Chem. Lett. 32, 8 (2003): 760-762.

[128] Sakahara, S.; Ishida, M.; Anderson, M. A. Visible Luminescence and Surface Properties of Nanosized ZnO Colloids Prepared by Hydrolyzing Zinc Acetate. J. Phys. Chem. B 102, 50 (1998): 10161-10175.

[129] Chen, Y.; Bagnall, D. M.; Koh, H.; Park, K.; Hiraga, K.; Zhu, Z.; Yao, T. Plasma Assisted Molecular Beam Epitaxy of ZnO on c-Plane Sapphire: Growth and Characterization. J. Appl. Phys. 84 (1998): 3912-3918.

[130] Yang, Y.; Chen, H.; Zhao, B.; Bao, X. Size Control of ZnO Nanoparticles via Thermal Decomposition of Zinc Acetate Coated on Organic Additives. J. Cryst. Growth 263 (2004): 447-453.

[131] Arii, T.; Kishi, A. The Effect of Humidity on Thermal Process of Zinc Acetate. Thermochim. Acta 400 (2003): 175-185.

[132] Zhao, X.; Zheng, B.; Li, C.; Gu, H. Acetate-Derived ZnO Ultrafine Particles Synthesized by Spray Pyrolysis. <u>Powder Tech.</u> 100 (1998): 20-23.

[133] Berntsen, N.; Gutjahr, T.; Loeffler, L.; Gomm, J. R.; Seshadri, R.; Tremel, W. A Solvothermal Route to High-Surface-Area Nanostructured MoS_2. <u>Chem. Mater.</u> 15 (2003): 4498-4502.

[134] Patzke, G. R.; Krumeich, F.; Nesper, R. Oxidic Nanotubes and Nanorods - Anisotropic Modules for a Future Nanotechnology. <u>Angew. Chem., Int. Ed.</u> 41 (2002): 2446-2461.

[135] Lee, J.-S.; Choi, S.-C. Solvent Effect on Synthesis of Indium Tin Oxide Nano-Powders by a Solvothermal Process. <u>J. Eur. Ceram. Soc.</u> 25, 14 (2005): 3307-3314.

[136] Zhang, J.; Sun, L.; Yin, J.; Su, J.; Liao, C.; Yan, C. Control of ZnO Morphology via a Simple Solution Route. <u>Chem. Mater.</u> 14 (2002): 4172-4177.

[137] Hu, Z.; Oskam, G.; Searson, P. C. Influence of Solvent on the Growth of ZnO Nanoparticles. <u>J. Colloi. Interf. Sci.</u> 263 (2003): 454-460.

[138] Pesika, N. S.; Hu, Z.; Stebe, K. J.; Searson, P. C. Quenching of Growth of ZnO Nanoparticles by Adsorption of Octanethiol. <u>J. Phys. Chem. B</u> 106 (2002): 6985-6990.

[139] Pasche, S.; De Paul, S. M.; Voros, J.; Spencer, N. D.; Textor, M. Poly(L-lysine)-*graft*-poly(ethylene glycol) Assembled Monolayers on Niobium Oxide Surfaces: A Quantitative Study of the Influence of Polymer Interfacial Architecture on Resistance to Protein Adsorption by ToF-SIMS and in Situ OWLS. <u>Langmuir</u> 19 (2003): 9216-9225.

[140] Ye, B.; Trudeau, M.; Antonelli, D. M. Synthesis and Electronic Properties of Potassium Fulleride Nanowires in a Mesoporous Niobium Oxide Host. <u>Adv. Mater.</u> 13, 1 (2001): 29-33.

[141] Gratzel, M. Mesoporous Oxide Junctions and Nanostructured Solar Cells. <u>Curr. Opin. Colloid Interface Sci.</u> 4, 4 (1999): 314-321.

[142] Arshak, K.; Morris, D.; Arshak, A.; Korostynska, O.; Kaneswaran, K. Development of Oxide Thick Film Capacitors for a Real Time Pressure Monitoring System. <u>Mater. Sci. Eng. C</u> 27, 5-8 (2007): 1406-1410.

[143] Obara, K.; Iwasaki, K.; Matushima, S.; Hirose, T.; Shioga, M.; Suemoto, Y. Surface Reactions and Structures of Niobium Oxide Superfine Particles. <u>Catal. Today</u> 28, 1-2 (1996): 183-189.

[144] Chaneliere, C.; Autran, J. L.; Devine, R. A. B.; Balland, B. Tantalum Pentoxide (Ta_2O_5) Thin Films for Advanced Dielectric Applications. <u>Mater. Sci. Eng. R.</u> 22, 6 (1998): 269-322.

[145] Uekawa, N.; Kudo, T.; Mori, F.; Wu, Y. J.; Kakegawa, K. Low-Temperature Synthesis of Niobium Oxide Nanoparticles from Peroxo Niobic Acid Sol. <u>J. Colloid Interface Sci.</u> 264, 2 (2003): 378-384.

[146] Schmitt, M.; Heusing, S.; Aegerter, M. A.; Pawlicka, A.; Avellaneda, C. Electrochromic Properties of Nb_2O_5 Sol–Gel Coatings. <u>Sol. Energ. Mater. Sol. Cell.</u> 54, 1-4 (1998): 9-17.

[147] Sharma, P. K.; Varadan, V. V.; Varadan, V. K. Porous Behavior and Dielectric Properties of Barium Strontium Titanate Synthesized by Sol-Gel Method in the Presence of Triethanolamine. <u>Chem. Mater.</u> 12 (2000): 2590-2596.

[148] Lazarouk, S.; Katsouba, S.; Demianovich, A.; Stanovski, V.; Voitech, S.; Vysotski, V.; Ponomar, V. Reliability of Built In Aluminum Interconnection with Low-e Dielectric based on Porous Anodic Alumina. <u>Solid State Electron.</u> 44 (2000): 815-818.

[149] Cho, W.; Saxena, R.; Rodriguez, O.; Achanta, R.; Plawsky, J. L.; Gill, W. N. Effects of Sintering on Dielectric Constants of Mesoporous Silica. <u>J. Non-Cryst. Solid</u> 350 (2004): 336-344.

[150] Zaima, S.; Furuta, T.; Koide, Y.; Yasuda, Y.; Iida, M. Conduction Mechanism of Leakage Current in Ta_2O_5 Films on Si Prepared by LPCVD. <u>J. Electrochem. Soc.</u> 137 (1990): 2876-2879.

[151] Cho, S.-D.; Lee, J.-Y.; Paik, K.-W. Effects of Particle Size on Dielectric Constant and Leakage Current of Epoxy/Barium Titanate ($BaTiO_3$) Composite Films for Embedded Capacitors. <u>International Symposium on Electronic Materials and Packaging</u> (2001): 63-68.

[152] Mohamed, M. M.; Mekkawy, I. Electrical and Chemical Characteristics of Nano-Meter Gold Encapsulated in Mesoporous and Microporous Channels and Cages of FSM-16 and Y Zeolites. <u>J. Phys. Chem. Solid</u> 64 (2003): 299-306.

[153] Gimon-Kinsel, M. E.; Balkus, K. J. Pulsed Laser Deposition of Mesoporous Niobium Oxide Thin Films and Application as Chemical Sensors. <u>Micropor. Mesopor. Mater.</u> 28, 1 (1999): 113-123.

[154] White, N. M.; Tumer, J. D. Thick-Film Sensors: Past, Present and Future. <u>Meas. Sci. Technol.</u> 8 (1997): 1-20.

[155] Guidi, V.; Butturi, M. A.; Carotta, M. C.; Cavicchi, B.; Ferroni, M.; Malagu, C.; Martinelli, G.; Vincenzi, D.; Sacerdoti, M.; Zen, M. Gas Sensing through Thick Film Technology. Sens. Actuators B 84 (2002): 72-77.

[156] Baraton, M.-I.; Merhari, L.; Ferkel, H.; Castagnet, J.-F. Comparison of the Gas Sensing Properties of Tin, Indium and Tungsten Oxides Nanopowders: Carbon Monoxide and Oxygen Detection. Mater. Sci. Eng. C 19 (2002): 315-321.

[157] Kellner, R.; Mermet, J.-M.; Otto, M.; Valcarcel, M.; Widmer, H. M., Analytical Chemistry: A modern approach to analytical science. 2nd ed.; Wiley-VCH: Weinheim, p 1047, 2004.

[158] Cao, X.; Lan, X.; Zhao, C.; Shen, W.; Yao, D. Porous ZnS/ZnO Microspheres Prepared Through the Spontaneous Organization of Nanoparticles and their Application as Supports of Holding CdTe Quantum Dots. Mater. Res. Bull. (2007): In Press.

[159] Liqiang, J.; Yichun, Q.; Baiqi, W.; Shudan, L.; Baojiang, J.; Libin, Y.; Wei, F.; Honggang, F.; Jiazhong, S. Review of Photoluminescence Performance of Nano-Sized Semiconductor Materials and its Relationships with Photocatalytic Activity. Sol. Energ. Mater. Sol. Cell. 90 (2006): 1773-1787.

[160] Bae, C. H.; Park, S. M.; Ahn, S.-E.; Oh, D.-J.; Kim, G. Y.; Ha, J. S. Sol-Gel Synthesis of Sub-50 nm ZnO Nanowires on Pulse Laser Deposited ZnO Thin Films. Appl. Surf. Sci. 253 (2006): 1758-1761.

[161] Li, D.; Haneda, H. Morphologies of Zinc Oxide Particles and their Effects on Photocatalysis. Chemosphere 51 (2003): 129-137.

[162] Brunauer, S.; Emmett, P. H.; Teller, E. Adsorption of Gases in Multimolecular Layers. J. Am. Chem. Soc. 60 (1938): 309-319.

[163] Melosh, N. A.; Lipic, P.; Bates, F. S.; Wudl, F.; Stucky, G. D.; Fredrickson, G. H.; Chemlka, B. F. Molecular and Mesoscopic Structures of Transparent Block Copolymer-Silica Monoliths. Macromolecules 32 (1999): 4332-4342.

[164] Zhang, W.; Glomski, B.; Pauly, T. R.; Pinnavaia, T. J. A New Nonionic Surfactant Pathway to Mesoporous Molecular Sieve Silicas With Long Range Framework Order. Chem. Comm. (1999): 1803-1804.

[165] Guo, C.; Liu, H. Z.; Chen, J. Y. A Fourier Transform Infrared Study of The Phase Transition in Aqueous Solutions of Ethylene Oxide-Propylene Oxide Triblock Copolymer. Colloid. Polym. Sci. 277 (1999): 376-381.

[166] Fontell, K.; Khan, A.; Lindström, B.; Maciejewska, D.; Puang-Ngern, S. Phase Equilibria and Structures in Ternary Systems of a Cationic Surfactant (C_{16}TABr or (C_{16}TA)$_2$SO$_4$), Alcohol, and Water. <u>Colloid Polym. Sci.</u> 269, 7 (1991): 727-742.

[167] Storch, S.; Bretinger, H.; maier, W. F. Characterization of Micro- and Mesoporous Solids by Physisorption Methods and Pore-Size Analysis. <u>Appl. Catal. A: Gen.</u> 174 (1998): 137-146.

[168] Klein, L. C., <u>Sol-Gel Technology for Thin Films, Fibers, Preforms, Electronics, and Specialty Shapes.</u> Noyes Publications: New Jersey, p 392, 1988.

[169] Metelkina, O.; Hüsing, N.; Pongratz, P.; Schubert, U. Effects of the Post-Synthesis Treatment on the Structural Properties of Alumina-Doped Zirconia. <u>J. Non-Cryst. Solids</u> 285, 1-3 (2001): 64-70.

[170] Grudzien, R. M.; Grabicka, B. E.; Jaroniec, M. Effective Method for Removal of Polymeric Template from SBA-16 Silica Combining Extraction and Temperature-Controlled Calcination. <u>J. Mater. Chem.</u> 16 (2006): 819-823.

[171] Schafer, H.; Gruehn, R.; Schulte, F. The Modifications of Niobium Pentoxide. <u>Angew. Chem. Intl.</u> 5 (1966): 40-52.

[172] Grader, G. S.; Hazan, Y. D.; Bravo-Zhivotovskii, D.; Shter, G. E. Effect of Aging on Nonhydrolytic Alumina Xerogels. <u>Journal of Sol-Gel Science and Technology</u> 10 (1997): 127-137.

[173] Kubota, N. Effect of Impurities of the Growth Kinetics of Crystals. <u>Cryst. Res. Technol.</u> 36, 8-10 (2001): 749-769.

[174] Ciesia, U.; Froba, M.; Stucky, G. D.; Schuth, F. Highly Ordered Porous Zirconias from Surfactant-Controlled Syntheses: Zirconium Oxide-Sulfate and Zirconium Oxo Phosphate. <u>Chem. Mater.</u> 11 (1999): 227-234.

[175] Nair, P.; Nair, J.; Raj, A.; Maeda, K.; Mizukami, F.; Okubo, T.; Izutsu, H. Critical Nuclei Size Effect in the Densification of Nanostructured Niobia Ceramics. <u>Mater. Res. Bullet.</u> 34, 2 (1999): 225-231.

[176] Lewandowska, A. E.; Ban˜ares, M. A. In situ TPR/TPO-Raman Studies of Dispersed and Nano-scaled Mixed V-Nb Oxides on Alumina. <u>Catal. Today</u> 118, 3-4 (2006): 323-331.

[177] de Araujo, E. B.; de Paiva, J. A. C.; Freitas, J. A., Jr.; Sombra, A. S. B. Raman and Infrared Spectroscopy Studies of LiNbO$_3$ in Niobate Glass-Ceramics. <u>J. Phys. Chem. Solids</u> 59, 5 (1998): 689-694.

[178] Huang, B. X.; Wang, K.; Churchb, J. S.; Li, Y.-S. Characterization of Oxides on Niobium by Raman and Infrared Spectroscopy. Electrochim. Acta 44 (1999): 2571-2577.

[179] Riess, G. Micellization of Block Copolymers. Prog. Polym. Sci. 28 (2003): 1107-1170.

[180] Moulik, S. P. Micelles: Self-Organized Surfactant Assemblies. Curr. Sci. 71, 5 (1996): 368-376.

[181] Blin, J. L.; Su, B. L. Tailoring Pore Size of Ordered Mesoporous Silicas Using One or Two Organic Auxiliaries as Expanders. Langmuir 18 (2002): 5303-5308.

[182] Okabe, A.; Niki, M.; Fukushima, T.; Aida, T. A Simple Route to Bimodal Mesoporous Silica via Tetrafluoroborate Ion-Mediated Hydrophobic Transformation of Template Micellar Surface. J. Mater. Chem. 15 (2005): 1329-1331.

[183] Antonietti, M.; Berton, B.; Goltner, C.; Hentze, H.-P. Synthesis of Mesoporous Silica with Large Pores and Bimodal Pore Size Distribution by Templating of Polymer Latices. Adv. Mater. 10, 2 (1998): 154-159.

[184] Yao, J.; Wang, H.; Chan, K.-Y.; Zhang, L.; Xu, N. Incorporating Organic Polymer into Silica Walls: A Novel Strategy for Synthesis of Templated Mesoporous Silica with Tunable Pore Structure. Micropor. Mesopor. Mater. 82 (2005): 183-189.

[185] Xu, C.; Xu, G.; Liu, Y.; Wang, G. A Simple and Novel Route for the Preparation of ZnO Nanorods. Solid State Comm. 122 (2002): 175-179.

[186] Du, J.; Liu, Z.; Huang, Y.; Gao, Y.; Han, B.; Li, W.; Yang, G. Control of ZnO Morphologies via Surfactants Assisted Route in the Subcritical Water. J. Cryst. Growth 280 (2005): 126-134.

[187] Lide, D. R., Handbook of Chemistry and Physics. 81 ed.; CRC Press: Boca Raton, FL, 2000.

[188] Ying, J. Y.; Mehnert, C. P.; Wong, M. S. Synthesis and Applications of Supramolecular-Templated Mesoporous Materials. Angew. Chem. Int. Ed. 38 (1999): 56-77.

[189] McBride, R. A.; Kelly, J. M.; McCormack, D. E. Growth of Well-Defined ZnO Microparticles by Hydroxide Ion Hydrolysis of Zinc Salts. J. Mater. Chem. 13 (2003): 1196-1201.

[190] Vayunandana Reddy, Y. K.; Mergel, D. Frequency and Temperature-Dependent Dielectric Properties of BaTiO$_3$ Thin Film Capacitors Studied by Complex Impedence Spectroscopy. Phys. B Condens. Matter 391, 2 (2007): 212-221.

[191] Oh, S.-T.; Choi, J.-S.; Lee, H.-S.; Lu, L.; Kwon, H.-H.; Song, I. K.; Kim, J. J.; Lee, H.-I. H$_2$O-Controlled Synthesis of TiO$_2$ with Nanosized Channel Structure through in situ Esterification and its Application to Photocatalytic Oxidation. J. Mol. Catal. A: Chem. 267 (2007): 112-119.

[192] Suriye, K.; Praserthdam, P.; Jongsomjit, B. Control of Ti^{3+} Surface Defect on TiO$_2$ Nanocrystal Using Various Calcination Atmospheres as the First Step for Surface Defect Creation and its Application in Photocatalysis. Appl. Surf. Sci. 253 (2007): 3849-3855.

[193] Wang, J.; Gao, L. Hydrothermal Synthesis and Photoluminescence Properties of ZnO Nanowires. Solid State Comm. 132 (2004): 269-271.

[194] Fischer, V.; Stormer, H.; Gerthsen, D.; Stenzel, M.; Zillgen, H.; Ivers-Tiffee, E. Niobium as New Material for Electrolyte Capacitors with Nanoscale Dielectric Oxide Layers. Proceedings of the 7th International Conference on Properties and Applications of Dielectric Materials Nagoya (2003): June 1-5.

APPENDICES

APPENDIX A

CALCULATION OF THE CRYSTALLITE SIZE

Calculation of the crystallite size by Debye-Scherrer equation

The crystallite size was calculated from the f ull width of radian at half maximum of the diffraction peak height of the XRD pa ttern, using the Debye-Scherrer equation.

From Scherrer equation:

$$D = \frac{K\lambda}{\beta \cos \theta} \qquad \text{<A.1>}$$

where
- D = Crystallite size, Å
- K = Crystallite-shape factor = 0.9
- λ = X-ray wavelength, 1.5418 Å for CuKα
- θ = Observed peak angle, degree
- β = X-ray diffraction broadening, radian

The X-ray diffraction broadening (β) is the corrected width of a powder diffraction free from all broadening due to the instrum ent. The α-Alumina was used as a standard sam ple to provide instrum ental broadening data (s ee Figure A.1). The most common correction for the X-ray diffraction broadening (β) can be obtained by using the Warren formula.

Warren formula:

$$\beta = \sqrt{B_M^2 - B_S^2} \qquad \text{<A.2>}$$

where
- B_M = The measured peak width in radians at half peak height.
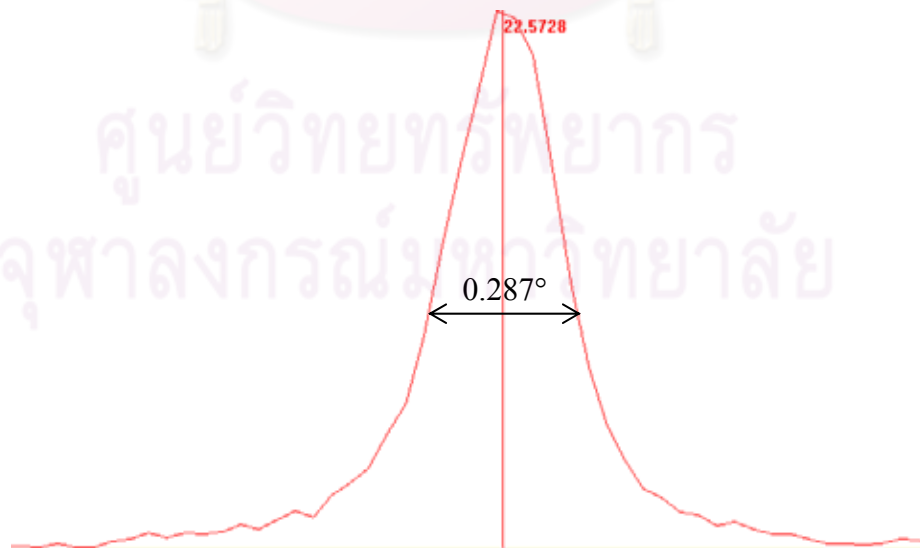- B_S = The corresponding width of the standard material.
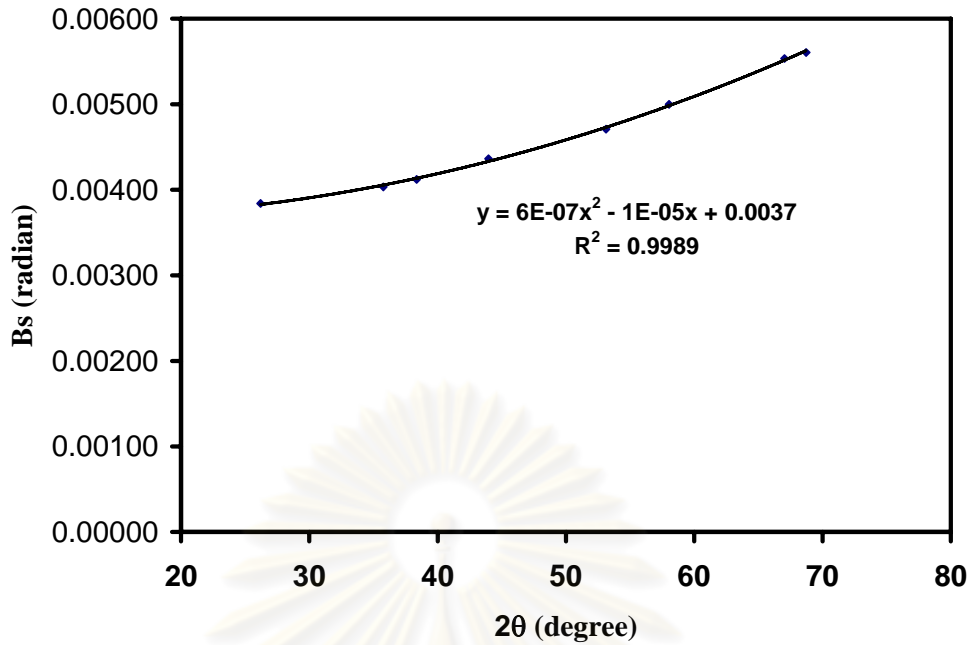
Figure A.1 The plot indicating the value of line broadening due to the
equipment. The data were obtained by using α-alumina as a standard

Example: Calculation of the crystallite size of niobia

An interesting diffraction peak is the (001) plane occurred at the 2θ of 22.6°.

$$Or, \quad \theta \quad = \quad 22.6°/2 \quad = \quad 11.3°$$

Figure A.2 The 001 diffraction peak of niobia for calculation of
the   crystallite size

The half-height width of the (001) diffraction peak = 0.287^o (from Figure A.2)

$$= (2\pi \times 0.287)/360$$

$$= 0.0050 \text{ radian}$$

The corresponding half-height width of peak of α-alumina (data in Figure A.1) at the 2θ of 22.6^o = 0.0038 radian

Hence, the broadening, β = $\sqrt{(0.0050^2 - 0.0038^2)}$, from eq. A.2

$$= 0.0033 \text{ radian}$$

Therefore,

The crystallite size = $\dfrac{0.9 \times 1.5418 \text{ Å}}{0.0033 \times \cos 11.3}$, from eq. A.1

$$= 430 \text{ Å} = 43 \text{ nm.}$$

APPENDIX B

CALCULATION OF RELATIVE DIELECTRIC CONSTANT

Electrodes separated by a non-conductive dielec tric material will s tore a charge when a po tential difference is app lied. Capacitance is defined as th e charge stored per unit potential difference.

Dielectric materials are graded relative to th e dielectric properties of free space, which is said to have a dielectr ic constant (permittivity) of 8.85 x 10^{-12} F/m, or a relative dielectric constant of 1. The total capacity of a sample of dielectric material is a function of the dielectric constant, is proportional to the tota l surface area of the electrodes or plates, and is inversely proportional to the distance between the plates or the dielectric thickness i.e.

$$C = (\varepsilon_o \varepsilon_r A) / d \qquad\qquad B.1 > <$$

where C = Capacitance in Farads, F

ε_o = The dielectric constant for free space, 8.85 x 10^{-12} F/m

ε_r = Relative dielectric constant (also referred to as K)

A = Area of the electrode plates (dielectric area)

d = Dielectric thickness

When the d ielectric material is a p ellet compact, the d ielectric area (A) is equal to the diameter of the pellet, and the dielectric thickness (d) is the thickness of the pellet. The pellet is pla ced in betw een the two electro de plates of the electric meter that generate potential difference (voltage) under dif ferent frequency of the alternative current, and the capacitance (C) is recorded.

For example,

The powder niobia pellet of diameter 13 mm, and thickness of 0.9 mm;

A = π x $(13 \times 10^{-3})^2$ / 4 = 1.327 x 10^{-4} m^2

d = 0.9 x 10^{-3} m.

The capacitance read at frequency at 500 kHz is 28 x 10^{-12} F.

Hence, relative dielectric constant of niobia,

$$\varepsilon_r \quad = \quad \frac{(28 \times 10^{-12}) \times (0.9 \times 10^{-4})}{(8.85 \times 10^{-12}) \times (1.327 \times 10^{-4})} \quad , \text{from eq. B.1}$$

$$= \quad 21.5$$

ศูนย์วิทยทรัพยากร
จุฬาลงกรณ์มหาวิทยาลัย

APPENDIX C

OPERATING CONDITIONS FOR GAS CHROMATOGRAPHY

The gas stream on the inlet and outlet of photocatalytic ethylene oxidation reaction were analyzed by the gas chromatograph having operating conditions as summarized in Table C1.

**Table C1** Operating conditions of gas chromatograph

Gas Chromagraph	SHIMADZU GC-14B
Detector	FID
Column	VZ10
Carrier gas	H_2 (99.999%)
Carrier gas flow (ml/min)	30 cc/min
Column temperature	
- initial (^{o}C)	70
- final (^{o}C)	70
Injector temperature (^{o}C)	100
Detector temperature (^{o}C)	150
Current (mA)	-

APPENDIX D

THE ADDITIONAL DATA OF DIELECTRIC MEASUREMENT

The magnified pictures of the represen tative pellets used in the die lectric measurment are shown in Figure D.1. It could be possible that the obtained capacitance read might be affected by th e variable packing density or grai n boundaries of the pellet under the pelletization process.
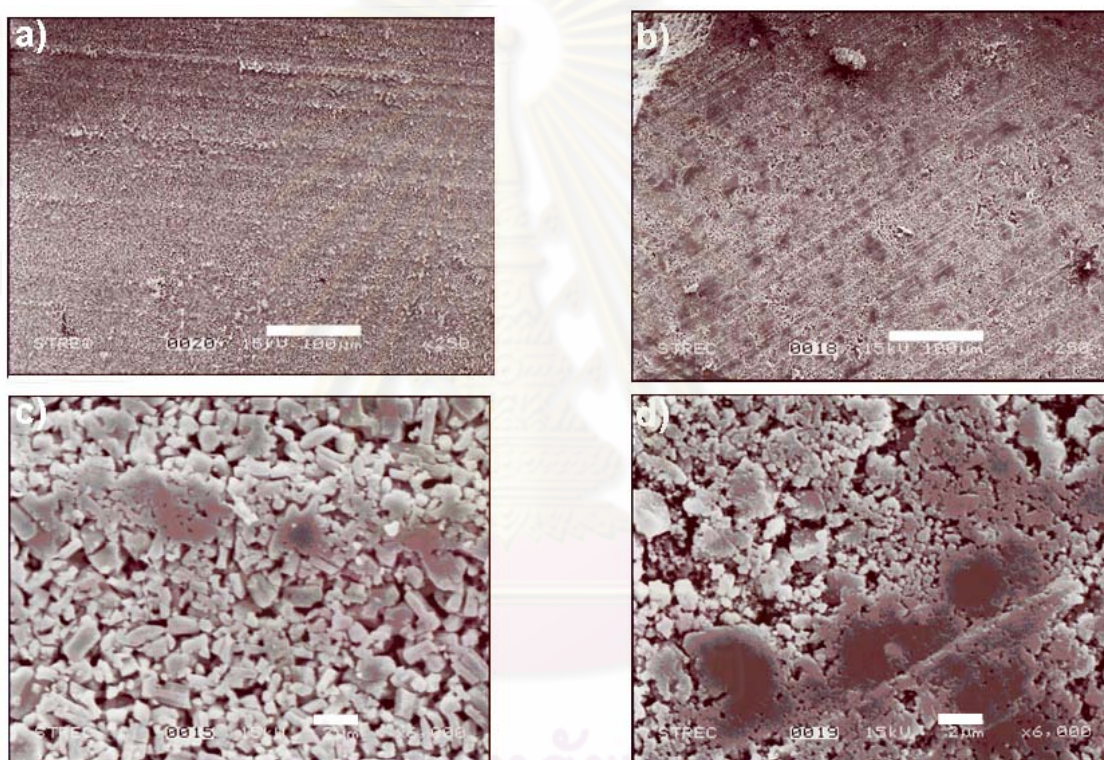
Figure D.1 SEM images taken from top surface of the pellet made from the powder of niobium pentoxide, Aldrich (a and c), and the synthesized F-c1-2dDM-A, calcined at 500°C (b and d). a) and b) are low magnifications, and c) and d) are higher magnifications.

APPENDIX E

LIST OF PUBLICATIONS

International Publications

1) Sirachaya Kunjara Na Ayudhya, Parawee Tonto, Okorn Mekasuwandumrong, Varong Pavarajarn, and Piyasan Praserthdam, "Solvothermal Synthesis of ZnO with Various Aspect Ratios Using Organic Solvents", Crystal Growth & Design, 6, 2466-2450 (2006).

2) Sirachaya Kunjara Na Ayudhya, Apinan Soottitantawat, Piyasan Praserthdam, and Chairit Satayaprasert, "Effect of Aging on the Properties of Mesoporous Niobium Oxide", Materials Chemistry and Physics, *In Press*.

3) Sirachaya Kunjara Na Ayudhya, Piyasan Praserthdam, Michael E. Grass, Gabor A. Somorjai, Apinan Soottitantawat and Chairit Satayapraserth, "Influence of Dialysis on the Formation and Structure of Mes oporous Niobium Oxide from Niobium (V) Chloride", Microporous and Mesoporous Materials, *Revised*.

4) Sirachaya Kunjara Na Ayudhya, Michael E. Grass, Gabor A. Somorjai, Piyasan Praserthdam, Okorn Mekasuwandumrong, Apinan Soottitantawat, "High Temperature Evaporation-Induced Self-Assembly of Ordered Niobium Oxide Mesostructures", *Submitted*.

VITA

Miss Sirachaya Kunjara Na Ayudhya wa s born in Novem ber 19, 1982 in Bangkok, Thailand. She finished high school from Chitralada school, Bangkok in 2000. She received her Bachelor's De gree in Che mical Engineering with 1 st class honor, from the Departm ent of Chem ical Engineering, Chulalongkorn University in 2004. Then she receiv ed the Royal Golden Jubilee Scho larship from the Thailand Research Fund (TRF) and continued studyi ng in Doctoral degree of Che mical Engineering at Chulalongkorn University si nce June 2004. In second year of her doctoral course, she was a visiting scholar to Department of Chemistry, University of California, Berkeley, and experienced rese arch life under supervision of Profess or Gabor A. Somorjai. She spent about 8 months there and cam e back to continue her research in Thailand until graduate.